"I'm sciencing as fast as I can!"

- *Professor Farnsworth, Futurama*

University of Alberta

Restoring Walking After Spinal Cord Injury

by

Bradley Jared Holinski

A thesis submitted to the Faculty of Graduate Studies and Research
in partial fulfillment of the requirements for the degree of

Doctor of Philosophy

Biomedical Engineering

Spring 2013
Edmonton, Alberta

This work is dedicated to my mom and dad, who have supported me during my “extended stay” in school.

ABSTRACT

The overall goal of this thesis was to develop a proof-of-principle for a device that might eventually restore walking in people with paraplegia. The thesis consisted of three component technologies each working in conjunction with one another in adult cats. The first component was the state-based control algorithm, which provided a framework to implement more detailed control of locomotion in the future. The goal of this study was to develop a physiologically based algorithm capable of mimicking the biological system to control multiple joints in the lower extremities for producing over-ground walking. The biological central pattern generator (CPG) integrates open and closed loop control to produce over-ground walking. Similarly, the algorithm used combined open and closed loop control of a state-based model of the step cycle. Each state produced different electrical stimulation patterns and activated a different combination of muscles. This study verified that such a controller could generate closed loop bilateral overground walking. The second study implemented a novel type of functional electrical stimulation, intraspinal microstimulation (ISMS), that activated motor networks in the ventral horn of the spinal cord that would remain intact below the lesion level after a spinal cord injury. In addition to producing movements around single joints, ISMS through individual microwires can elicit coordinated multi-joint movements and the resulting contractions are fatigue-resistant. For the first time, we demonstrate sustainable, bilateral over-ground walking using ISMS. The walking proved to be extremely fatigue-resistant with some cats walking for a distance of over 800 m. The third study added natural sensory feedback of both the limb position in space and ground reaction force using recordings of neurons located in the dorsal root ganglia (DRG). The goal of this study was to decode sensory information from the DRG in real

time for control of unilateral ISMS stepping. These predictions were successfully used to activate a closed loop rule that limited backward hyperextension. Each project resulted in a novel accomplishment and produced a deliverable that successfully worked in conjunction with previously developed components toward a neuroprosthetic device to restore walking.

Preface

I would like to thank all the people that were an integral part of my life (for better or worse) throughout my degree. Both pairs of grandparents have been always extremely supportive and proud of me. My aunts and uncles always took great care of me and kept me fed (especially Cecile, Shirley, Don and Joan). I will miss my Uncle Dave taking me out for nice dinners. I also had great friends who kept me fed. I always looked forward to Sunday dim sum with Robin and his parents, Chiu and Patricia. Volleyball was never the same without chicken wings and beer afterwards with Van Soest clan, Jeff and his parents, Rob and Loraine.

I would also like to thank Scott for being pretty funny (the odd time) and Simon who would graciously lose to me in Super Smash Brothers. My longest running friend, Crystal, always watched horror movies with me when I needed a break from lab work.

At the lab, Dirk and Jan were my partners in crime. I'll miss all the good times there and the pranks on Dirk (Dirk was pretty cool for his age). Jan and I always had an unreal time representing Alberta on conferences. More than likely, Jan and I will still get rich together. Lab ski trips were awesome with Liu Shi and Francois (whenever he came). We had some great people come through the lab: Alison, Liz, Ana, and Kevin. Thanks to Dick and Vivian for mentoring me throughout my program.

Finally, I should thank Alessa for being generally an all-round great girlfriend.

Acknowledgements

This work was funded in part by the National Institutes of Health (NIH-NINDS NS44225), the Canadian Institutes of Health Research and Alberta Innovates-Health Solutions. I would like to thank Robert Rolf for all the technical assistance and someone to talk “nerd” with at the lab and Rodney Gramlich for technical assistance. Thanks to Douglas Weber for MotionTracker2D.

TABLE OF CONTENTS

List of Tables

List of Figures

Chapter 1: Introduction

We rely on mobility to accomplish everyday activities. Our society has created technologies and infrastructure to facilitate the movement of people and goods quickly and efficiently through air, over sea, and across land. However, access to this transportation infrastructure usually requires mobility, whether it be boarding an airplane or dropping off a letter in the mailbox. If personal mobility is compromised due to disease or injury, we experience a decrease in independence in our daily lives.

Spinal Cord Injury

As the spine connects the nerve centers in the brain to the peripheral nerves in the rest of the body, a traumatic spinal cord injury (SCI) can interrupt these paths of neural communication. If the neural pathways are completely severed there will be no cortical sensorimotor communication below the lesion. Patient prognosis is based on the initial severity and spinal level of the injury. The level of the injury determines which bodily functions will be interrupted; injuries higher in the spinal cord interrupt more functions than injuries lower down. Injuries in the cervical section of the spinal cord result in tetraplegia and can cause deficiencies in hand function, breathing, bowel and bladder functions, and walking. People with tetraplegia primarily desire restoration of arm and hand function [1, 2]. Trauma in the thoracic or lumbar regions of the spinal cord results in paraplegia, the disruption of lower body functions such as bowel, bladder, and sexual functions and the ability to walk. Restoration of bowel/bladder and sexual functions are of primary concern for people with paraplegia [2, 3]. The restoration of walking function is ranked as the next most important desire. Our research efforts focus on the restoration of walking in people with complete paraplegia. We hope to improve the quality of life of people with paraplegia by increasing their mobility and independence.

Restoring Mobility: Standard of Care

In Canada, SCI has an incidence rate of more than 3000 new cases per year, 56% of which result in paraplegia [4]. SCI primarily affects a younger demographic with longer life expectancies. Current public health policy strives to discharge people with SCI into the community and to provide them with the ability to return to independent lives. This policy began in the 1940s when Sir Ludwig Guttmann realized the importance of treating people with SCI and created the first comprehensive SCI center for medical treatment and rehabilitation in the world [5]. The goal of the original center (and the many created since) was to help injured individuals to achieve a higher quality of life through restored independence. Although no treatments today can offer complete restoration of nervous function, current treatments and a better understanding of the disease have resulted in decreased morbidity and increased life expectancy.

People with severe mobility impairments are often able to locomote using a wheelchair. The first references to the use of wheel chairs to transport disabled people date back to the 3rd century BC in China [6]. The wheelchair (as we know it) was modernized into a lightweight, steel, collapsible chair in 1933 by Harry Jennings and Herbert Everest [7]. Although the basic design remains largely unchanged, recent advances have made the chairs lighter and more efficient. Their metabolic efficiency in transporting people with disabilities is unrivalled by any other intervention. However, wheelchair use is limited by society's infrastructure which was not designed with the wheelchair in mind. The wheelchair encounters curbs, rough surfaces, mud, and a host of other conditions that can challenge, obstruct, and endanger the transport of its passenger. Also, the wheelchair passenger is restricted to a sitting position which can engender a feeling of subservience during conversations with people who are standing. This can unfavourably impact the psychological well-being of a person who is already dealing with an affliction. The seated position also limits reaching and grasping items located on high shelves and increases the risk of secondary health complications, including a susceptibility to pressure ulcers and bone density loss.

Some powered wheelchairs have been designed to address these issues by either elevating the user's seat or by supporting the user in a standing-like position. The iBot, codeveloped by Johnson and Johnson and DEKA Research, raised the height of the user to a level comparable to a standing position. The iBot was the forefather of the Segway, which shared many of the iBot's balancing and stability technologies. The chair was even capable of ascending and descending stairs by rotating its two sets of wheels about each other. Unfortunately, the iBot has been discontinued since 2009. Another chair, the Tek Robotic Mobilization Device (Tek RMD), was developed in Turkey by AMS Mekatronik and utilizes a novel loading mechanism that allows the user to mount the device from the back using a tensioning sling. The chair then hydraulically lifts the user into a standing-like position. This chair is unique in that it does not require the classic transferring procedure, which can be dangerous and difficult for people without sufficient upper body strength or for overweight or elderly people. The Tek RMD was initially released in Turkey and has not yet gained widespread distribution.

Restoring Walking

Walking restoration has proven to be very difficult, largely because of the complexity in the sensorimotor systems involved. Past efforts have not gained commercial footing, partially due to small potential market share, and have languished in the laboratories. However, recently, there has been a renewed effort in both engineered systems and systems that rely on our knowledge of the physiology of walking.

Engineered Approaches to Walking Restoration

Engineering-based approaches designed to restore walking employ minimal biological principles. The simplest systems consist of passive orthosis without powered actuators to move the limbs. These systems are useful in situations where some function remains (after incomplete SCI) or when the system can be augmented with other techniques such as function electrical stimulation (FES). Exoskeletons completely replace components such as muscles, sensory afferents and neural control with motors, artificial sensors, and control algorithms, respectively.

Passive Orthoses

Series-limb orthoses were designed to enhance existing walking performance by minimizing energy losses from collisions with the ground. These devices consist of rods with elastic properties that absorb and release energy during key times in the step cycle. The PowerSkip and the SpringWalker were supposed to augment human running speed and economy of motion. However, the SpringWalker actually increased the metabolic cost of walking by 20% [8]. These devices can increase jump height and have since been adopted for extreme sports and other leisure activities.

Parallel-limb orthoses transfer the body load directly to the contact surface. These devices are worn along the legs (in parallel) and may provide support and stability across multiple joints. They can also reduce the degrees-of-freedom during walking to facilitate device development. Ankle-foot orthoses (AFOs) rigidly support the ankle against flexion or extension and may be used to prevent foot plantar-flexion during the swing phase (which can impair walking). Knee-ankle-foot orthoses add support of the knee joint as well, locking it against flexion during certain states of the gait cycle. This prevents the knee from buckling and the user from collapsing during stance, but allows knee flexion during swing. Hip-knee-ankle-foot orthoses (HKAFO) resist hip adduction and abduction. The reciprocating gait orthosis is a variation of the HKAFO and uses a cable assembly to constrain the motion of one leg with respect to the other. For instance, during the swing phase of one leg, the opposite leg will extend. When these orthoses are used by people with significant mobility deficiencies, they are used in conjunction with a rolling walker. Therefore, in order to stabilize the trunk and support the upper body with the walker, large upper body exertion is required and it limits practical walking ranges [9].

POWERED ORTHOSES

Powered orthoses (or exoskeletons) are used to minimize the metabolic effort of walking and increase walking speeds and ranges. Artificial actuators move the legs either hydraulically, with cable systems, or with direct current (DC) motors. Hydraulic systems are capable of the largest torques, but are heavy due to the hydraulic fluid and they do not represent the properties of muscles. Using a cable system, the stretching properties of muscles are copied and pulling forces are generated similar to muscle contractions. Cable systems can also mimic biarticular muscles (spanning more than one joint) allowing for physiological control of walking.

The majority of exoskeletons use DC motors and even have the ability to provide increased carrying load capacities for the users. As such, they have gained widespread attention from the U.S. military. The Berkeley lower extremity exoskeleton (BLEEX) was one of the first load-bearing wearable exoskeletons that contained its own power source [10]. Sensory information was provided by a multitude of sensors, including 16 accelerometers and eight joint angle encoders to provide information about each leg joint [11]. A foot switch and load distribution sensor provided additional information about ground contact. The BLEEX has since transitioned into the eLegs by Berkley Bionics for restoration of walking in populations with mobility impairments.

Some devices have specifically targeted the needs of the mobility impaired. The Vanderbilt exoskeleton uses four motors to provide assistive torques at the hip and knee bilaterally. Ankle joints are controlled by a passive AFO worn in conjunction with the exoskeleton. Published peer-reviewed material is sparse for exoskeletons. However, initial trials were published for parallel bar walking by a person with complete paraplegia. Quintero et al. showed a walking speed of 0.22 m/s and with the current battery lasting for one hour, the walking range would be approximately 0.8 km [12]. Unlike the Vanderbilt exoskeleton, Argo Medical's ReWalk is already available for purchase. It is similarly designed using DC motors to move the legs. It is controlled by a wireless wrist mounted unit and requires balancing with a set of crutches. The ReWalk can help a person with SCI go up and down stairs. A recent pilot study with six SCI volunteers showed no adverse health effects and only minor fatigue. Walking ranges were limited to around 100 m [13].

In Japan, the HAL-5 has been ambitiously developed to restore both upper and lower limb functionality [14]. In addition to the standard DC motor actuation and a host of sensors (including potentiometers, ground reaction force, a gyroscope, and accelerometers), the HAL-5 can receive intention signals from electromyography (EMG) electrodes on the legs. EMG electrodes evaluate and record the electrical activity produced by skeletal muscles. Therefore, the HAL-5 can augment insufficient motor function in the event of an incomplete SCI, although it may take up to two months to optimally calibrate EMG control for specific users [15]. Battery life is estimated at approximately 160 minutes [8].

Exoskeletons are currently one of the most promising interventions for restoring walking after injury. However, the current technology has limitations. Actuators can be noisy and unsightly, and can generate limited torques inefficiently. Perhaps the solution relies on electroactive polymers that change size and shape when stimulated by an electric field and can thus mimic muscle force generation [16]. Both passive and powered orthoses must be custom built for each user, increasing production time and cost. The orthosis must be strong and lightweight. These properties often require exotic materials such as titanium and carbon fibre that make pricing prohibitive. The Bionics REX from New Zealand began international sales in 2011 and currently retails for 150,000 NZD. One of the greatest limitations for powered exoskeletons is power usage. Current performance is limited by battery capacity and the weight of batteries and orthosis.

Biologically Inspired Solutions

Through millions of years of evolution, the body has developed robust control systems to successfully transverse through a variety of terrains. Even after injury, the body retains some latent functionality. By offloading some engineering legwork onto retained functions, we may be able to restore functionality sooner than with purely engineered solutions. Understanding and emulating biological systems may our best chance to restore practical walking function.

Central Pattern Generator

The biological control systems we are trying to emulate are very complex. All cyclical movements in the body (e.g., breathing, chewing, walking) originate from an oscillating neural circuit named the central pattern generator (CPG). Detailed network structures in two invertebrates, lamprey and Xenopus tadpole, have illustrated mechanisms regarding CPG swimming function and modulation [17, 18]. However, less is known about the neural circuitry of the walking CPG in vertebrates. It is known that the CPG is capable of rhythmic activity independent of supraspinal centers or sensory feedback. Also, it can be activated and maintained by tonic descending excitation from the midbrain locomotor region (MLR), which presumably equates to the desire to walk [19]. Experiments in both man [20, 21] and spinalized cat (cats that have undergone spinal transections that interrupt nerve signals to the legs) [22] have shown that many independent CPGs can vary their rates independently when each leg walks with a unique cadence. Transverse sectioning at different spinal levels has localized the walking CPG to a distribution in the lumbar-sacral spinal cord (between L3-S1) in cats [23]. Rostral regions have a greater capacity for rythmogenesis than caudal locations in isolation, implying a gradient of rythmogenesis capabilities [24]. Dorsal-ventrally, there is little disagreement that all CPG components in the mammal are located in the ventral horn of the spinal cord [25, 26]. Also, there is little disagreement that the CPG consists of two main components: intrinsic timing and sensory feedback.

Intrinsic Timing

Initially, Sherrington discovered that reflex stepping can be elicited in chronic spinalized cats, implying that locomotor movements could be produced from spinal centers [27, 28]. Later, Brown proposed a neuronal model to explain the alternating activation of flexor and extensor motor pools (intrinsic timing) [29]. This model consisted of two half-centers (populations of excitatory interneurons) being excited by a common excitatory drive and coupled with reciprocal inhibition. Oscillations between half-centers were caused by the eventual fatigue of the active half-center. Initially, views were divided regarding whether movements resulted from reflex chains or some intrinsic timing [30, 31]. In the 1970s it was identified that simultaneous intrinsic timing and sensory feedback were important [32].

The first spinal circuitry with these predicted properties was discovered by Lundberg et al. after administration of a noradrenergic precursor called L-DOPA produced bursts of alternating flexor and contralateral extensor responses upon stimulation of flexor reflex afferents [33, 34]. However, normal locomotor activity patterns were not seen until sensory information was added to the preparations [35].

Real locomotion was first produced in spinalized decerebrate (the cerebral cortex and the nuclei situated in front of the base of the subcortex have been surgically removed) cats which were administered clonidine (a noadrenergic receptor agonist) and received simultaneous sensory input from treadmill walking [36]. The cats adapted to the belt speed. Later, load-bearing treadmill walking (after training) was shown in chronic spinalized cats without drug administration [37, 38].

More complex models are currently being used to explain a number of new experimental observations [39]. When synaptic inhibition is blocked, synchronized oscillations remain [24, 35, 40]. This implies that the half-centers have endogenous rhythm without the need for the reciprocal inhibitory coupling fatigue mechanism. This inhibitory coupling is likely important for proper locomotion patterns with alternating stepping. Two-layer CPG models of varying complexities have been proposed comprised of a rhythm generating layer and a pattern formation layer [39, 41-44]. The pattern formation layer activates synergistic motor pools according to incoming sensory information.

Sensory Feedback

Sensory feedback modifies the activation patterns and timings of the CPG in response to changing conditions during walking. The effects of sensory input are gated to a specific state within the step cycle [45, 46]. Sensory feedback can modify the magnitudes of burst activity [47-49]. It can also affect the onset and offset of states within the step cycle. In spinalized cats, sensory control of the stepping components coordinated walking on a treadmill to different belt speeds [50]. There are a large variety of sensory modalities present in the body. Of these, there are a few well studied proprioceptive inputs that influence timings during the walking cycle such as hip angle, ground reaction force, and cutaneous contact. In chronic spinalized cats, hip extension exceeding a critical angle caused the stance to swing transition [51]. Grillner et al. showed that feedback from proximal muscles played a role in adapting timing patterns. Force sensing through Golgi tendon organs was critical for the stance-to-swing transition, as well [52]. An increased loading on the ankle extensors will increase activation of the extensors resulting in positive feedback and preventing the onset of swing. Conversely, unloading ankle extensors will cause a transition to swing. Cutaneous receptors can detect collisions with the dorsum of the foot and increase activation of the knee flexion to overcome an obstacle [53, 54]. Timing changes have not been observed in humans possibly due to the negative consequences of suddenly switching phases during bipedal gait [55].

Evidence for a Human CPG

Possible evidence for CPGs in humans was reported in 1950 by Kuhn after witnessing involuntary spontaneous activity below the level of a spinal lesion [56]. However, it was not clear with technologies available then whether the lesion was complete. The most convincing evidence for a human CPG comes from application of electrical stimulation to the dorsal side of the spinal cord below the lesion. Many groups have witnessed bursts of EMG activity (which can resemble gait) in the lower limb muscles of people with complete (total loss of sensorimotor function of the legs) spinal cord injury [57, 58]. Evidence for a human CPG is somewhat circumstantial, but definitely suggests a neural circuit similar to what has been discovered in other species, although it is harder to activate and may have an increased reliance on supraspinal centers.

Muscles

Muscle tissue can be classified as skeletal, cardiac, or smooth. Skeletal muscles are striated, usually under conscious control, and used in voluntary movement. Cardiac and smooth muscles operate involuntarily in the heart and walls of internal organs (e.g., stomach, bladder, and blood vessels), respectively. Skeletal muscles are made of repeating contractile elements (sarcomeres) that produce force when activated. The number of parallel sarcomeres determines the amount of force produced. Within these contractile elements are protein filaments called actin and myosin that slide past one another. Myosin is a thick filament that contains a head that binds to actin. Adenosine triphosphate (ATP) also binds to the head of myosin and provides the metabolic energy for contraction. Muscles can be activated electrically or neurologically. When a stimulus is converted to a mechanical response it is called excitation-contraction coupling [59]. When activated, muscle cells produce electrical potentials that can be recorded as electromyography (EMG). As more of the muscle becomes activated, more muscle fibers produce action potentials at varying rates and amplitudes, producing typical EMG waveforms.

There are two main types of skeletal muscle fibers: type 1 and type 2. Type 1 muscles produce less force through aerobic respiration, but are more fatigue resistant. They are used for long duration functions such as breathing or standing. Type 2 muscles can generate large amounts of force but fatigue quickly. Type 2 muscles are used for lifting heavy loads or sprinting.

Muscles undergo physiological changes after spinal cord injury. After loss of voluntary motor function, muscle fibers below the lesion transform from slow twitch to fast twitch due to inactivity [60, 61]. Additionally, the muscle fibers atrophy when they are not used. Over time, the muscles of the lower limbs are almost completely converted into fast twitch. Even with frequent electrical stimulation, movements have little endurance. However, by using functional electrical stimulation (FES) for intense exercise, it is possible to convert some fast twitch fibers into slower twitch fibers resulting in a more-normal muscle composition [62].

Interfacing to the Body

Electrodes are the interface between electronics and the body. Electrodes convert electronic current in the device into ionic current in the body and vice versa depending on whether they are stimulating or recording. Each function, stimulating and recording, has purpose-built electrodes.

Stimulation

The usefulness of neuroprosthetic devices relies on safe electrode operation [63]. Charge is injected into the tissue through electrodes at the electrode-tissue interface. Electron flow is converted into ionic flow in the tissue through either capacitive or faradic reactions. Capacitive reactions are more desirable because no chemical species are created or consumed during the charge transfer. Faradic reactions allow for higher levels of charge transfer but involve electrons traversing the interface, which either oxidizes or reduces chemical species. If the chemical species remain close or adhere to the electrode, the reaction can be reversed during the next charge phase [64]. If the species repeatedly diffuse away from the interface, they can change the environment of the tissue causing damage. Specifically, charge build-up leads to chemical reactions that cause changes in tissue pH and the formation of gases and other compounds [65, 66]. Noble metals such as Pt and Pt-Ir alloys confine the faradic reaction to the electrode surface and are called pseudocapacitive because the reaction can easily be reversed [63]. Poly(ethylenedioxythiophene) or PEDOT is a new conducting polymer that has the possibility to modify the surface with active chemical compounds to increase its charge capacity and biocompatibility [67]. Carbon nanotubes have high surface area, can transfer large amounts of charge, and can also have their surface chemically modified [68, 69].

Current is delivered in pulses, with a typical pulse waveform having either one or two phases with many variations [65]. Typically, the first phase is cathodal and can be followed by an anodal phase in a biphasic waveform. The total amount of charge in each phase is determined by the duration of the phase, pulse width, and the amplitude of the current. The pulses are applied at a frequency that varies depending on the species and tissue type being stimulated. In humans the stimulation frequency can range from > 20 Hz for stimulating muscle contractions to 130 Hz for deep brain stimulation [70, 71]. The minimum threshold of charge density can vary from less than 1 $\mu C/cm^2$ for intrafasicular electrodes in the cat to > 100 $\mu C/cm^2$ in the human retina [72, 73]. Current theory suggests that safe stimulation levels for penetrating microelectrodes in the brain should not exceed 2 nC/phase (800 $\mu C/cm^2$) [74].

Surface Electrodes

Surface electrodes deliver current through the surface of the skin to excite underlying tissue. They can be applied quickly, are less invasive, and are generally safer than penetrating microelectrodes. However, they are the less tissue specific and require larger currents due to the current dissipation throughout the layers of tissue. High current amplitudes might result in discomfort for the user as cutaneous pain afferents become activated. Surface electrodes cannot reliably activate deep muscles and nerves.

Implanted Electrodes

Implantable electrodes are placed directly in contact with excitable tissue (often through surgery). They can target specific tissues, including deep muscles, and need to produce little current due to their close proximity to the target tissue. If the implanted electrodes are percutaneous, their leads may be a source of failure or infection. The design of implanted electrode systems is complicated. They have to withstand long durations in the body without electrode corrosion or mechanical failure. Often these systems require wireless control and power to operate within the body. New technologies, such as the Stim-Router, are able to transcutaneously transmit the current required to stimulate a nerve through a capacitive link on either side of the skin [75]. The Stim-Router has been recently tested in a human volunteer to activate hand function. Nerve cuff electrodes (electrodes within a flexible silicon band) are easier to implant as they wrap around the nerve and do not penetrate the epineurium. However, they may damage the nerve due to swelling from surgery even with good fit [76]. Some microelectrode array implantations use pneumatic insertion with a controlled pulse of highly pressurized air. Upon implantation, the sharpened electrode tips cut through and displace tissue causing some inflammation and cell death [77].

Recording

Neural signals are recorded as voltage changes caused by ion movements in the extracellular environment. Recorded action potentials typically range from 50 μV to over 700 μV in the central nervous system [78, 79]. Recording electrode impedance measured at 1 kHz is typically 50 kohm to 1 Mohm, but will vary after implantation as the connective tissue sheath forms. Although after implantation, impedance has been shown to increase, it does not necessarily lead to a reduction in recording quality [65, 80]. The lack of stable single unit recordings has led to the pursuit of algorithms based on information from multiunit recordings.

Recording Electrodes

Low impedance electrodes can also be used for recording electrical signals from the body [63]. Sources of electrical signals include muscles (electromyography, EMG) or nerves (electroneuography, ENG). Again, there are implantable and nonimplantable electrodes for recording with pros and cons similar to those of stimulation electrodes. For instance, recording from an implanted electrode can provide specific information about a single neuron or a few neighboring neurons whereas surface recording produces ensemble activity from many spatially distributed sources. The largest difference between recording and stimulation electrodes is the susceptibility of recording electrodes to fail due to tissue encapsulation over time. Currently, the trend is to increase the number of microelectrodes to increase the sampling of neuronal populations. The discussion here focuses on implantable electrodes for single unit recording.

Utah electrode arrays are now recording viable neural signals in the cortex for up to 1000 days [81]. Novel electrode substrates are currently being explored to minimize the mismatch in mechanical properties between the soft tissue and typically rigid electrodes [82]. The two most common implanted microelectrodes are the Utah array and the Michigan Probe. The Utah array has up to 100 electrodes in a bed-of-nails configuration on a silicon substrate [83, 84]. The Michigan Probe uses etching and microfabrication technologies to create a planar electrode with multiple recording sites along the shank [85].

Tissue Response to Implanted Electrodes

Implanted electrodes cause insertion trauma and foreign body responses of the tissue to the electrode or motion of the electrode [86, 87]. Tethering of the electrode array also causes elevated tissue responses [88, 89]. Unique electrode designs have been used to increase the amalgamation between the neurons and the electrode. Some electrodes contain holes through which axons are supposed to grow and neurotropic agents to promote their growth [90, 91]. The holes are also designed to increase stability of the array by holding it in place with connective tissue.

Similar to other foreign body responses, the neural response to an implanted electrode consists of encapsulating the electrode in a tissue sheath. Over time meningeal fibroblasts, macrophages, and reactive astrocytes all form part of the sheath [92]. The sheath is completed as early as six weeks post-implantation and remains for the duration of the implant [77]. The sheath is approximately 50–100 µm thick around the insertion site [93]. Dexamethasone, an anti-inflammatory agent, can control reactive responses around an implanted electrode [94]. The mechanism of recording loss is not clear, but may be due to electrical insulation, reduction in ion diffusion, or increased distance to the neuron [95, 96]. Electrode interfacing remains one the more difficult problems in neuroprosthetics.

Functional Electrical Stimulation (FES)

Functional electrical stimulation (FES) technologies restore limited function. FES can utilize biological functions that remain after injury but are otherwise inaccessible to the injured person. FES uses electrical currents applied into the extracellular space to depolarize the cell membrane of excitable tissues to produce muscle contractions. Most often, stimulation is applied to nerves rather than the muscle itself, which produces more complete activation of the muscle fibers with lower current levels [97]. The strength and duration of the current pulse controls the number of activated nerve fibers. Activation order relies on the diameter of the nerve fiber. Larger diameter nerve fibers are more easily activated by FES. Primary sensory afferents and the motor nerves that innervate Type 2 muscles are the first to be activated. With the recruitment of fast-fatigable motor units, high intensity FES used for restoring walking can cause muscle fatigue after as little as one minute of stimulation [98].

FES can also produce secondary health benefits to the user including increased muscle mass, improvements in cardiovascular health, and increased bone density [62, 99]. FES has been used to restore many impaired functions including arm and hand control, breathing, bladder/bowel function, and standing/walking ability [100-102]. I focus on the applications to restore standing and walking.

FES for Standing and Walking

There are relatively few FES devices for restoring standing and walking functions despite the first recorded functional electrically stimulated standing over 50 years ago [103]. Around the same time, Liberson et al. created the first FES foot drop device to dorsiflex the ankle during the swing phase for people that had weakness after hemiplegia [104]. The majority of FES systems currently in use utilize stimulation or control techniques from these original devices. Unfortunately, most FES walking systems require high energy expenditure from the user and permit only a slow speed of gait and small walking range. Initially it was discovered that patterned stimulation through the flexion withdrawal reflex and the quadriceps could improve hemiplegic gait [105]. Kralj et al. also successfully applied this system to many people with SCI [98]. The microelectronics required for FES devices have steadily become smaller and more powerful, allowing the devices to become more portable and flexible. One of the first uses of multichannel FES to restore walking was in 1979 by Strojnik et al., where six channels produced gait patterns in people with complete paraplegia [106]. More recently, the Parastep from Kralj et al. employed the same basic principles with four or six channels of surface stimulation activated by hand switches [107]. The Parastep still requires the user to depend on a walker for stability and an AFO to control the ankle joint. It has been successfully used by over 750 people to stand and to walk short distances. One of the main disadvantages of the Parastep is that surface stimulation does not reach the deep muscles. An attempt to access deeper muscles and improve reliability employed an implanted FES system with percutaneous electrodes [108]. However during daily use, many of the electrodes failed due to lead breakage and development of the system was abandoned. The Cleveland Group is currently testing an implantable system using 16 channels of implanted intramuscular electrodes and a walker for stability. Standing performance is 10 minutes in people with complete SCI and reciprocal gait is possible [109]. Two other implanted devices built by other groups were also abandoned [110, 111].

Hybrid FES systems

Some FES systems use an orthosis to control undesirable movements, limit the degrees of freedom during walking, and provide additional body weight support [9, 109, 112, 113]. Orthoses that additionally support the lower back provide increased trunk stability which may be deficient depending on the level of the SCI. The Parastep is considered a hybrid FES system because it utilizes a pair of AFOs to prevent foot drop. Orthoses have moderately decreased energy expenditure compared to FES alone [9, 114]. However, improvements have not been substantial enough for widespread clinical adoption of the devices.

Spinal Stimulation

Early use of electrical stimulation of the spinal cord focused on alleviating pain and treating multiple sclerosis (MS). Unfortunately, eagerness to live up to expectations produced results that blurred the boundaries of good scientific practice. Part of the difficultly was objectively evaluating the efficacy of spinal FES in alleviating pain and other symptoms associated with MS when the performance criteria were qualitative. Evidence slowly began to mount against the efficacy of these treatments and interest began to wane in the early 1980s [115]. Today's research focuses on obtaining Seligman's fantastical objective of "[playing] the nervous system like some grand, multidimensional instrument (Sherrington's enchanted loom) under prosthetic control" [115]. Slowly, we are realizing Seligman's fantastic goal [115].

A promising form of spinal stimulation is epidural stimulation, where electrical currents are thought to enhance activity of previously silent spared neural circuits or promote plasticity. The main benefit of epidural stimulation is using latent spinal sensorimotor circuitry to control walking. Epidural stimulation in combination with weight bearing treadmill training has been shown to decrease the sense of effort of stepping and increase walking speed in a subject with incomplete SCI [116]. Recently, epidural stimulation has allowed one man with complete absence of motor function to stand, produce locomotor-like movements, and gain some voluntary control of leg movements after treadmill training [117]. Although tonic activation of the spinal cord produced locomotor-like movements, load bearing stepping has not been produced in people with complete SCI. Additionally, more precise control of the different phases of the step cycle would be required to adapt to unique tasks such as stair ascent and decent.

Intraspinal Microstimulation (ISMS)

Intraspinal microstimulation (ISMS) is a form of electrical stimulation that uses fine wires implanted into the ventral horn of the spinal cord to elicit specific movements. The tips of the wires are deinsulated and implanted from the dorsal side of the spinal cord to target the motor pools in the ventral horn. Early work with cats implanted electrodes into the dorsal and intermediate regions and primarily caused flexion withdrawals and paw shakes consistent with sensory perception, but was unable to produce extensor responses [118]. Later, implantation in the ventral horn produced both extensor and flexor responses. In chronically spinalized and acutely implanted cats (after spinalization, cats recovered and were then implanted during a terminal experiment weeks later), low level tonic stimulation caused bilateral stepping movements capable of generating up to 56% of load bearing force [119]. Additionally, tonic stepping speed adapted to varying treadmill speeds implying afferent input is still present during ISMS [120].

According to models, the electrical stimulation directly activates approximately a 1 mm diameter region around the tip [121, 122]. Therefore, each electrode should minimize the overlapping of activation regions (> 2mm separation distance) [123]. However, distances of up to 17 mm rostral and caudal are activated through antidromic conduction of sensory afferents [124]. At lower stimulation amplitudes (< 100 µA) the 1a sensory afferents are activated first [124]. At higher stimulation amplitudes that would be used for walking (> 100 µA), motorneurons, interneurons, and fibers-in-passage are additionally recruited [124]. ISMS is likely activating muscles indirectly through synapses due to the time jitter on activation onset caused by the variable conduction through a synapse [125]. The electrical stimulation is thought to primarily activate axon-hillocks or the cell bodies of neurons [126]. ISMS uses much less (an order of magnitude) current than some other forms of stimulation to produce movements [125].

Although there are examples of applying ISMS to restore bladder function or produce upper limb movements, I focus on its ability to restore walking function [127-129]. By patterning ISMS stimulation across multiple electrodes, sequential muscle activations are assembled into a walking pattern. The wires are implanted in a relatively small region of approximately 3 cm rostral-caudally in cats and 5 cm in humans. Within this region, all movements required for a walking cycle are located. There are a number of proposed benefits to using ISMS which might outweigh the difficulty of successful implantation.

Benefits of ISMS

The first benefit of ISMS is that muscle activation is smoothly graded. Other forms of stimulation have a dependence on distance from the motor point to the electrode which can result in unpredictable force recruitment [130]. As stimulation currents are increased, the force production from activated muscles follows linearly for much of the recruitment curve [131]. Well-developed linear control algorithms could be utilized to control force production. However, maximal twitch forces of single electrodes are between 1.3–73% of the maximal twitch force from whole nerve stimulation [132]. Because whole nerve stimulation activates more axons, an increased number of ISMS electrodes would be required to produce maximum muscular contraction. With tetanic contractions, ISMS force production is similar to nerve cuff stimulation [133].

A second benefit of ISMS is the fatigue resistance of the elicited movements compared with other forms of electrical stimulation. Initial studies on the muscle twitch speed of the lower hind limb muscles showed the possibility of obtaining a natural recruitment order [132]. While natural order is not guaranteed, it is more likely than in other stimulation modalities for some muscles. There are numerous examples of ISMS producing fatigue resistant movements [134]. The relevance of this benefit might depend on the ability of the muscle fiber to transform during electrical stimulation. In rats, Bamford et al. showed that similar numbers of fast-to-slow twitch muscle fiber transformations were caused by ISMS and nerve cuff stimulation [135]. Fatigue resistance can be increased additionally by interleaving the stimulation frequency of electrodes activating a common muscle, but the efficacy of this modification is debatable [123, 136].

Few electrodes can produce all the movements required for bilateral walking. The complete walking cycle was originally thought to require between 100–200 electrodes [136]. Later, Mushahwar et al. successfully demonstrated locomotor-like movements using two electrodes per side in acutely implanted cats [118]. The pairs of electrodes would activate either a flexor or an extensor synergy. Synergies are groups of muscles that when activated produce a co-ordinated multijoint movement [137, 138]. Synergies allow one electrode to simultaneously activate many muscles. The existence of synergistic movements has been verified in chronically implanted cats [139]. Recently, we have used as few as four electrodes per side to produce functional overground walking. However, redundant electrodes are implanted to produce stronger movements with lower currents.

Acute ISMS Development

Initial ISMS research explored the layout of the motor pool maps in the spinal cord. The objective was to locate regions where hind limb muscles could be reliably activated in isolation. The first studies developed coarse mapping by electrophysiolgical means of the main flexors and extensors of the knee and ankle [126]. The first locomotor-like movements were obtained in 2002; bilateral movements were achieved with two electrodes per side [118]. Also, in this study feedback control of a single ankle joint using a proportional-derivative controller was shown. Next, closed loop control of standing was implemented by monitoring joint angles and ground reaction forces to prolong standing duration [134]. ISMS has recently been acutely implanted to restore walking in intact anaesthetized cats for distances of over 800 m. The experiments were terminated at a predefined number of trials but the cats could have walked farther.

In acutely implanted cats anaesthetized with sodium pentabarbitol, decerebration and subsequent removal of anaesthetic did not produce any changes in the force produced by quadriceps [136]. In later papers, however, the issue was debated [126]. One paper reported a significant increase between threshold stimulation currents of the intermediate region in aneasthetized and decerebrate cat preparations [125]. Unfortunately in this paper, after decerebration, movement directions changed resulting in a preponderance of flexion movements.

Chronic ISMS Development

Chronic implantation of ISMS electrodes in cats has proven to be difficult. Following implantation in intact cats, some cats experienced partial paralysis which healed after 2–6 weeks [139]. Over two-thirds of the electrodes chronically implanted retained their initial functions for at least two weeks [139]. During this period it is unclear what happens to motor thresholds. Two studies that employed stainless steel electrodes reported an initial doubling of stimulation thresholds during the first 10 days [118, 139]. However, a more recent study in chronically implanted rats noticed a 50% reduction in threshold after 30 days of implantation with Pt-Ir electrodes [135]. The effect might be species dependent or it might result from differences in electrode material. Chronic implantation did not cause neural die-off over the 30 days although an elevated macrophage and microglia response surrounded 200 µm of the implantation site [135]. During chronic stimulation in both cats and rats, there have been no signs of discomfort or permanent functional deficits [118, 135, 139].

Three cats were spinalized and allowed to recover [140]. A decerebration and implantation was performed weeks later during a terminal experiment. One animal bilaterally stepped on a treadmill for 40 consecutive steps and, later, a control rule was used to initiate the flexion phase. This was the first example of whole limb control during ISMS stepping.

Control

Essentially, we sought to produce a control algorithm than emulated the CPG. The algorithm was intended to have the capability of advancing through walking states according to preset times, but it can also skip states according to sensory information. Guevremont et al. found that the most effective control method to produce overground walking involved a combination of open and closed loop control [141]. Also, sensory feedback contributed significantly to stable walking when central activation levels were low [142]. There are also approaches that further mimic the neural physiology by using integrate-and-fire models of neurons in the control algorithm but they will not be discussed further [143].

Open Loop

The goal of the control algorithm is to reproduce natural sensorimotor performance as closely as possible. Most walking neuroprosthetics like the Parastep use open loop (OL) control to produce stepping once stepping is initiated by the user through push buttons. Open loop control does not respond to feedback and behaves in a preprogramed manner. In the case of state-based control, open loop control will advance through states according to preset timings and is thus easier to implement. However, OL control cannot respond to perturbations in the body (such as muscle fatigue) or in the external environment (such as obstacles). As such, it is less practical for activities of daily life.

Closed Loop

Closed loop control methods can adapt their output to near real time input from sensors. While more difficult to implement, these control methods provide the ability to adapt to perturbations. Most complex walking systems, such as the exoskeletons, make extensive use of closed loop control. In exoskeletons, a large number of sensors are required to provide enough information to control up to 22 degrees of freedom during walking [98]. For example, the BLEEX uses 16 accelerometers and eight joint angle encoders to provide continuous information about each leg joint. New gait phase detection systems using combinations of sensors—gyroscopes for foot angular velocity and multiple force sensors on the foot to produce reliable event detection for control of walking [144]. Often, thresholds are chosen by hand, but machine learning techniques might automate this process [145].

Finite State Control

Finite state control (FSC) simplifies the interpretation and control of many sensors and electrodes, respectively [146]. Each state contains defined behaviour and a deterministic sequence. FSC has since been implemented in many neuroprosthetics to restore walking after SCI [147, 148]. The states can either be manually defined by the engineer or automatically with computer learning [149, 150]. Some improvements to FSC have included fuzzy logic and intention detection. Fuzzy logic might eventually blur the boundaries between states [151]. Additional layers of control might include intention detection [12].

Accurate sensory information is paramount for detecting gait events. Since sensory information is interpreted only in regard to the active state, FSC is more robust to event misdetection and sensory errors. Overall, finite state control has been successfully used to restore function in systems with fluctuations in sensory information and complex outputs [152].

Feedback from Natural Sensors

External sensors such as accelerometers, gyroscopes, potentiometers, and force sensors have disadvantages. They take time to don and doff, they require calibration, and they are unsightly. The next developmental leap in sensory information will come from decoding information from sensory afferents within the body. These natural sensors can provide a host of different sensory modalities, including proprioception. They can be accessed in a variety of locations, including the brain, spinal cord, peripheral nerves, or even muscle. Unfortunately, their signals are usually accessed by invasive means.

Recordings from an implanted nerve cuff on the sural nerve provides sensory information about foot contact with the ground. This information has been used to detect the onset of swing in the ActiGate foot drop stimulator [153]. EMG can also be used to signal muscle activation, but such technologies would only be useful for people with incomplete injuries who are capable of some muscle activation. Additionally, EMG signals from muscles that are above the level of the spinal injury might provide control signals [154, 155].

In monkeys, recordings from the motor and premotor cortex have been used as feedback to compare intended movements with actual arm movements [156]. Further development using monkeys has led to the cortical control of robotic arms and has even allowed people with tetraplegia to control computer cursors [81]. Although excellent work is being done on decoding cortical signals, the signals could only provide intention and not periphery sensing after SCI.

Single Unit Recordings

Spikes and the various sub-bands of field potentials contain information related to the ongoing sensorimotor process of animals. Single units are extracellular recordings of action potentials and are considered major contributors to field potentials [157]. Field potentials can be divided into low (< 2 Hz), medium (2–30 Hz), or high (30–400 Hz) frequency bands [158]. High frequency field potentials contain multiunit activity due to the presence of low frequency components of single units. Earlier studies failed to reach consensus about what was the most informative signal: low frequency field potential in Mehring et al. and multiunit activity in Stark and Abeles [159, 160]. In a more recent study, Bansal et al. (2011) found that single unit recordings were the preferred signal for decoding sensorimotor information to control brain-computer interfaces [161].

SPIKE PROCESSING

Our work has focused on using information from single units. However, before the information is available, two processing steps must be completed: spike sorting and decoding. Spike sorting separates voltages originating from single neurons in spike trains. The spike trains are then processed to deliver sensorimotor information.

Assigning the source of an action potential to a single neuron may be difficult due to high levels of background noise or because other closely located neurons may produce action potentials of similar shape and size [162]. Since neurons in close proximity might not transmit similar information, spike sorting is required for uncontaminated information. The simplest technique to separate an action potential from background noise is to use a threshold to discriminate the larger amplitude of the spike. Although easy to implement, this technique might not achieve adequate discrimination. More advanced sorting methods isolate action potentials based on the shape of the waveform. Feature sorting uses a minimal set of features that yield good discrimination, such as peak-to-peak voltage or duration of the spike [163, 164]. Principle component analysis automates the selection of features to create a set of basis vectors along the directions of the largest variations in the data set [165]. When the action potentials are assigned locations in feature space, clusters of waveforms with similar features will form. Each cluster represents a unique shape and likely originates from a unique neuron. A simple approach to assigning a waveform to a cluster is to minimize the Euclidean distance between the waveform and the mean of the data within that cluster [166]. More complex methods such as Bayesian clustering and classification use statistical methods and can quantify the certainty of correct spike sorting [167]. Smart sorting algorithms can compensate for many recording issues such as electrode drift or non-stationary background noise [162].

The firing rate of spikes carries a significant portion of the neural information compared to precise spike timings [168]. There are a number of methods to accurately calculate firing rates using custom kernels [169, 170]. However, such advanced models have failed to generate large differences in prosthetic decoding performance [168, 171]. To date, most decoding algorithms use a linear mapping between a kinematic parameter and a neural firing rate. The most common methods are population vectors, linear decoders, and Kalman filters [172] [173, 174]. If the parameter does not behave linearly, the neural signals might be discarded, which underutilizes the available data set. Luckily, muscle receptors that provide proprioceptive information behave linearly over a certain range of lengths [175].

Recordings from the Dorsal Root Ganglia

The dorsal root ganglia (DRG) contain the cell bodies of the sensory afferents innervated at a specific spinal level. Initial multisite chronic recording techniques within the DRG were developed by Loeb et al. and Prochazka et al. [176, 177]. The recorded spikes can then be decoded to provide an estimation of the limb endpoint in space, which can be used as feedback during stepping. Recordings from single neurons do not provide adequate information about whole limb proprioception. Initial decoding of proprioceptive afferents was produced from compiling separate recordings [178-180]. Using implanted Utah arrays, we can record from a variety of sensory modalities within a small region.

Ayogi et al. were the first to acutely implant a Utah array into the DRG to record simultaneously from many sensory afferents of anaesthetized intact cats [181]. Later, they postprocessed recordings made during passive limb movements and decoded the hind limb position from collections of neurons in the DRG [173, 182]. Additionally, they showed that limb end point expressed in polar coordinates with respect to the hip was well correlated to firing rates, and thus well represented in the DRG. This is not unique, as recordings from cells in the motor cortex and the dorsal spinocerebellar tract also describe movements in terms of a limb endpoint [183, 184].

Similar techniques were used to decode limb position offline in chronically implanted freely walking cats [185]. Amazingly, a small number of neurons (6–8) could account for over 80% of the variance in limb position [182]. Decoding was also reliable over a range of walking speeds (0.12–0.5 m/s) and was possible in the presence of stimulation artifacts from ISMS.

More complex decoding algorithms have also been tested offline using sensory information from the DRG. A state space decoding algorithm was implemented in DRG recordings and it produced a significant increase in decoding performance for some kinematic parameters but not all [186]. Also, a nonlinear neuro-fuzzy algorithm improved decoding performance while not adding significant computation cost to the linear regression decoding, although initial model learning was more difficult [187].

In addition to implanting for walking feedback, in Bruns et al. recording arrays that contained sensory afferents for the bladder were implanted in the DRG [188]. They were successfully able to identify and linearly correlate single units to bladder pressure. In addition to recording, the DRG may be stimulated to produce somatosensory feedback for a neuroprosthetic device user [189-191].

Dissertation summary and outline

The overall goal of my project was to develop technologies that could be used in a neuroprosthetic device to restore walking in people with paraplegia. The main components of any control system are the controller, the effectors, and the sensors. Our approach sought to utilize physiological principles and design technologies that could interface with the body. My studies developed a new biologically inspired technology for each of the system components. We aimed to be able to implant this neuroprosthetic system in a very small region of the spinal cord during a single surgery.

Chapter 2

The thesis begins by developing a finite state control algorithm that mimics a biological CPG. The control algorithm uses a combination of intrinsic timing and sensory feedback to produce overground walking in an intact anaesthetized cat. It was built to serve as the foundation for the following studies with modular sensory and effector components. The initial sensors were external sensors attached to the hind limb and movements were produced through intramuscular stimulation. This study verified that such a controller could generate closed loop bilateral overground walking.

A version of chapter 2 has been published in the Journal of Neural Engineering. My contributions comprised 80% of the software design and implementation, collection of data during experiments, analyses of data; in addition, I wrote the paper (with the exception of the introduction) and created the figures.

Chapter 3

The next stage in development replaced intramuscular stimulation with a potentially more advantageous technique, intraspinal microstimulation. Again, in a similar experimental setup, the controller (developed in the first study) activated a custom 16-

channel stimulator to produce overground walking. This was the first demonstration of ISMS overground walking to date. The walking proved to be extremely fatigue-resistant with some cats walking for a distance of over 800 m.

Chapter 3 has been targeted toward Nature. My contributions comprised software design and implementation, data collection during experiments, analyses of data; also, I wrote paper and created the figures.

CHAPTER 4

The final stage completely internalized the system. External sensors attached to hind limbs were replaced by recordings from the dorsal root ganglia. As a proof-of-principle, recording arrays were implanted unilaterally in the DRG and the cat unilaterally stepped on either a walkway or a treadmill. Predictions of the limb endpoint in space were made in real time even in the presence of stimulation artifacts from the ISMS. These predictions were successfully used to activate a closed loop rule that limited backward hyperextension.

Chapter 4 has been targeted toward the Journal of Neural Engineering. My contributions comprised software design and implementation, collection of data during experiments, analyses of data, writing the paper, and creating the figures.

CHAPTER 5

The thesis concludes with future directions for a fully implantable neuroprosthetic device and discusses some of the limitations with the current technologies.

References

1. Hanson, R.W. and M.R. Franklin, *Sexual loss in relation to other functional losses for spinal cord injured males.* Arch Phys Med Rehabil, 1976. **57**(6): p. 291-3.

2. Anderson, K.D., Targeting recovery: priorities of the spinal cord-injured population. J Neurotrauma, 2004. **21**(10): p. 1371-83.

3. Brown-Triolo, D.L., et al., Consumer perspectives on mobility: implications for neuroprosthesis design. J Rehabil Res Dev, 2002. **39**(6): p. 659-69.

4. Noonan, V.K., et al., Incidence and prevalence of spinal cord injury in Canada: a national perspective. Neuroepidemiology, 2012. **38**(4): p. 219-26.

5. Ragnarsson, K.T., Functional electrical stimulation after spinal cord injury: current use, therapeutic effects and future directions. Spinal Cord, 2008. **46**(4): p. 255-74.

6. Flaherty, J., Putting the 'whee!' back in 'wheelchair' Wired, 2012.

7. Everest, H.A. and H.C. Jennings, *Folding wheel chair*. 1937: USA.

8. Herr, H., Exoskeletons and orthoses: classification, design challenges and future directions. J Neuroeng Rehabil, 2009. **6**: p. 21.

9. Stein, R.B., et al., Speed and efficiency in walking and wheeling with novel stimulation and bracing systems after spinal cord injury: a case study. Neuromodulation, 2005. **8**(4): p. 264-71.

10. Kazerooni, H. and R. Steger, *The Berkeley lower extremity exoskeleton.* Trans ASME, Journal of Dynamic Systems, Mearsurements, and Control, 2006. **128**: p. 14-25.

11. Ghan, J., R. Steger, and H. Kazerooni, *Control and system identification for the Berkeley lower extremity exoskeleton (BLEEX).* Advanced Robotics, 2006. **20**(9): p. 989-1014.

12. Quintero, H.A., et al., *Feasibility of a Hybrid-FES System for Gait Restoration in Paraplegics.* 2010 Annual International Conference of the Ieee Engineering in Medicine and Biology Society (Embc), 2010: p. 483-486.

13. Zeilig, G., et al., Safety and tolerance of the ReWalk() exoskeleton suit for ambulation by people with complete spinal cord injury: A pilot study. J Spinal Cord Med, 2012. **35**(2): p. 96-101.

14. Suzuki, K., et al., Intention-based walking support for paraplegia patients with Robot Suit HAL. Advanced Robotics, 2007. **21**(12): p. 1441-1469.

15. Guizzo, E. and H. Goldstein, *The rise of the body bots [robotic exoskeletons].* Spectrum, IEEE, 2005. **42**(10): p. 50-56.

16. Biddiss, E. and T. Chau, Dielectric elastomers as actuators for upper limb prosthetics: challenges and opportunities. Med Eng Phys, 2008. **30**(4): p. 403-18.

17. Grillner, S., The motor infrastructure: from ion channels to neuronal networks. Nat Rev Neurosci, 2003. **4**(7): p. 573-86.

18. McLean, D.L., S.D. Merrywest, and K.T. Sillar, The development of neuromodulatory systems and the maturation of motor patterns in amphibian tadpoles. Brain Res Bull, 2000. **53**(5): p. 595-603.

19. Eidelberg, E., J.G. Walden, and L.H. Nguyen, *Locomotor control in macaque monkeys.* Brain, 1981. **104**(Pt 4): p. 647-63.

20. Dietz, V., *Spinal cord pattern generators for locomotion.* Clin Neurophysiol, 2003. **114**(8): p. 1379-89.

21. Yang, J.F., et al., Infant stepping: a window to the behaviour of the human pattern generator for walking. Can J Physiol Pharmacol, 2004. **82**(8-9): p. 662-74.

22. Forssberg, H., et al., *The locomotion of the low spinal cat. II. Interlimb coordination.* Acta Physiol Scand, 1980. **108**(3): p. 283-95.

23. Grillner, S. and P. Zangger, *On the central generation of locomotion in the low spinal cat.* Exp Brain Res, 1979. **34**(2): p. 241-61.

24. Kiehn, O., *Locomotor circuits in the mammalian spinal cord.* Annu Rev Neurosci, 2006. **29**: p. 279-306.

25. Dai, X., et al., Localization of spinal neurons activated during locomotion using the c-fos immunohistochemical method. J Neurophysiol, 2005. **93**(6): p. 3442-52.

26. Tresch, M.C. and O. Kiehn, Coding of locomotor phase in populations of neurons in rostral and caudal segments of the neonatal rat lumbar spinal cord. J Neurophysiol, 1999. **82**(6): p. 3563-74.

27. Sherrington, C.S., *Observations on the scratch-reflex in the spinal dog.* J Physiol, 1906. **34**(1-2): p. 1-50.

28. Sherrington, C.S., Flexion-reflex of the limb, crossed extension-reflex, and reflex stepping and standing. J Physiol, 1910. **40**(1-2): p. 28-121.

29. Brown, T.G., Studies in the physiology of the nervous system XXVIII. Absence of algebraic equality between the magnitudes of central excitation and effective central inhibition given in the reflex center of a single limb by the same reflex stimulus. Q J Exp Physiol, 1924(14): p. 1-23.

30. Gray, J., *Physiological mechanisms of animal behavior.* Cambridge University Press, Cambridge, 1950.

31. Holst, E.V., *On the nature of order in the central nervous system.* The behavioral physiology of animals and man: the collected papers of Erich von Holst, 1973. **1**: p. 3-32.

32. Grillner, S., Locomotion in vertebrates: central mechanisms and reflex interaction. Physiol Rev, 1975. **55**(2): p. 247-304.

33. Jankowska, E., et al., The effect of DOPA on the spinal cord. 5. Reciprocal organization of pathways transmitting excitatory action to alpha motoneurones of flexors and extensors. Acta Physiol Scand, 1967. **70**(3): p. 369-88.

34. Jankowska, E., et al., The effect of DOPA on the spinal cord. 6. Half-centre organization of interneurones transmitting effects from the flexor reflex afferents. Acta Physiol Scand, 1967. **70**(3): p. 389-402.

35. Rossignol, S., R. Dubuc, and J.P. Gossard, *Dynamic sensorimotor interactions in locomotion.* Physiol Rev, 2006. **86**(1): p. 89-154.

36. Forssberg, H. and S. Grillner, *The locomotion of the acute spinal cat injected with clonidine i.v.* Brain Res, 1973. **50**(1): p. 184-6.

37. Forssberg, H., S. Grillner, and J. Halbertsma, *The locomotion of the low spinal cat. I. Coordination within a hindlimb.* Acta Physiol Scand, 1980. **108**(3): p. 269-81.

38. Barbeau, H. and S. Rossignol, *Recovery of locomotion after chronic spinalization in the adult cat.* Brain Res, 1987. **412**(1): p. 84-95.

39. McCrea, D.A. and I.A. Rybak, Modeling the mammalian locomotor CPG: insights from mistakes and perturbations. Prog Brain Res, 2007. **165**: p. 235-53.

40. Beato, M. and A. Nistri, Interaction between disinhibited bursting and fictive locomotor patterns in the rat isolated spinal cord. J Neurophysiol, 1999. **82**(5): p. 2029-38.

41. Koshland, G.F. and J.L. Smith, Paw-shake responses with joint immobilization: EMG changes with atypical feedback. Exp Brain Res, 1989. **77**(2): p. 361-73.

42. Burke, R.E., A.M. Degtyarenko, and E.S. Simon, Patterns of locomotor drive to motoneurons and last-order interneurons: clues to the structure of the CPG. J Neurophysiol, 2001. **86**(1): p. 447-62.

43. Rybak, I.A., et al., Modelling spinal circuitry involved in locomotor pattern generation: insights from deletions during fictive locomotion. J Physiol, 2006. **577**(Pt 2): p. 617-39.

44. Rybak, I.A., et al., Modelling spinal circuitry involved in locomotor pattern generation: insights from the effects of afferent stimulation. J Physiol, 2006. **577**(Pt 2): p. 641-58.

45. McCrea, D.A., et al., Disynaptic group I excitation of synergist ankle extensor motoneurones during fictive locomotion in the cat. J Physiol, 1995. **487 (Pt 2)**: p. 527-39.

46. Angel, M.J., et al., Group I extensor afferents evoke disynaptic EPSPs in cat hindlimb extensor motorneurones during fictive locomotion. J Physiol, 1996. **494 (Pt 3)**: p. 851-61.

47. Gorassini, M.A., et al., Corrective responses to loss of ground support during walking. I. Intact cats. J Neurophysiol, 1994. **71**(2): p. 603-10.

48. Stein, R.B., J.E. Misiaszek, and K.G. Pearson, *Functional role of muscle reflexes for force generation in the decerebrate walking cat.* J Physiol, 2000. **525 Pt 3**: p. 781-91.

49. Donelan, J.M. and K.G. Pearson, Contribution of force feedback to ankle extensor activity in decerebrate walking cats. J Neurophysiol, 2004. **92**(4): p. 2093-104.

50. Shurrager, P.S. and R.A. Dykman, *Walking spinal carnivores.* J Comp Physiol Psychol, 1951. **44**(3): p. 252-62.

51. Grillner, S. and S. Rossignol, On the initiation of the swing phase of locomotion in chronic spinal cats. Brain Res, 1978. **146**(2): p. 269-77.

52. Duysens, J. and K.G. Pearson, Inhibition of flexor burst generation by loading ankle extensor muscles in walking cats. Brain Res, 1980. **187**(2): p. 321-32.

53. Forssberg, H., S. Grillner, and S. Rossignol, *Phasic gain control of reflexes from the dorsum of the paw during spinal locomotion.* Brain Res, 1977. **132**(1): p. 121-39.

54. Forssberg, H., Stumbling corrective reaction: a phase-dependent compensatory reaction during locomotion. J Neurophysiol, 1979. **42**(4): p. 936-53.

55. Hultborn, H. and J.B. Nielsen, *Spinal control of locomotion--from cat to man.* Acta Physiol (Oxf), 2007. **189**(2): p. 111-21.

56. Kuhn, R.A., Functional capacity of the isolated human spinal cord. Brain, 1950. **73**(1): p. 1-51.

57. Dimitrijevic, M.R., Y. Gerasimenko, and M.M. Pinter, *Evidence for a spinal central pattern generator in humans.* Ann N Y Acad Sci, 1998. **860**: p. 360-76.

58. Shapkova, E.Y. and E.D. Schomburg, Two types of motor modulation underlying human stepping evoked by spinal cord electrical stimulation (SCES). Acta Physiol Pharmacol Bulg, 2001. **26**(3): p. 155-7.

59. Sandow, A., *Excitation-contraction coupling in muscular response.* Yale J Biol Med, 1952. **25**(3): p. 176-201.

60. Peckham, P.H., J.T. Mortimer, and E.B. Marsolais, Alteration in the force and fatigability of skeletal muscle in quadriplegic humans following exercise induced by chronic electrical stimulation. Clin Orthop Relat Res, 1976(114): p. 326-33.

61. Lieber, R.L., Comparison between animal and human studies of skeletal muscle adaptation to chronic stimulation. Clin Orthop Relat Res, 1988(233): p. 19-24.

62. Davis, G.M., N.A. Hamzaid, and C. Fornusek, Cardiorespiratory, metabolic, and biomechanical responses during functional electrical stimulation leg exercise: health and fitness benefits. Artif Organs, 2008. **32**(8): p. 625-9.

63. Cogan, S.F., *Neural stimulation and recording electrodes.* Annu Rev Biomed Eng, 2008. **10**: p. 275-309.

64. Brummer, S.B. and M.J. Turner, Electrochemical considerations for safe electrical stimulation of the nervous system with platinum electrodes. IEEE Trans Biomed Eng, 1977. **24**(1): p. 59-63.

65. Merrill, D.R., M. Bikson, and J.G. Jefferys, *Electrical stimulation of excitable tissue: design of efficacious and safe protocols.* J Neurosci Methods, 2005. **141**(2): p. 171-98.

66. Rose, T.L. and L.S. Robblee, Electrical stimulation with Pt electrodes. VIII. Electrochemically safe charge injection limits with 0.2 ms pulses. IEEE Trans Biomed Eng, 1990. **37**(11): p. 1118-20.

67. Cui, X., et al., In vivo studies of polypyrrole/peptide coated neural probes. Biomaterials, 2003. **24**(5): p. 777-87.

68. Wang, X., et al., Carbon nanotube-DNA nanoarchitectures and electronic functionality. Small, 2006. **2**(11): p. 1356-65.

69. Banerjee, S., M.G. Kahn, and S.S. Wong, *Rational chemical strategies for carbon nanotube functionalization.* Chemistry, 2003. **9**(9): p. 1898-908.

70. Benabid, A.L., et al., Acute and long-term effects of subthalamic nucleus stimulation in Parkinson's disease. Stereotact Funct Neurosurg, 1994. **62**(1-4): p. 76-84.

71. Popovic, M.R., et al., Functional electrical therapy: retraining grasping in spinal cord injury. Spinal Cord, 2006. **44**(3): p. 143-51.

72. Mahadevappa, M., et al., *Perceptual thresholds and electrode impedance in three retinal prosthesis subjects.* IEEE Trans Neural Syst Rehabil Eng, 2005. **13**(2): p. 201-6.

73. Nannini, N. and K. Horch, *Muscle recruitment with intrafascicular electrodes.* IEEE Trans Biomed Eng, 1991. **38**(8): p. 769-76.

74. McCreery, D.B., T.G. Yuen, and L.A. Bullara, Chronic microstimulation in the feline ventral cochlear nucleus: physiologic and histologic effects. Hear Res, 2000. **149**(1-2): p. 223-38.

75. Gan, L.S., et al., First permanent implant of nerve stimulation leads activated by surface electrodes, enabling hand grasp and release: the stimulus router neuroprosthesis. Neurorehabil Neural Repair, 2012. **26**(4): p. 335-43.

76. Agnew, W.F., et al., Effects of prolonged electrical stimulation of the central nervous system. In: Neural Prosthesis: Fundamental Studies. 1990, Englewood Cliffs, NJ: Prentice Hall.

77. Polikov, V.S., P.A. Tresco, and W.M. Reichert, *Response of brain tissue to chronically implanted neural electrodes.* J Neurosci Methods, 2005. **148**(1): p. 1-18.

78. Rousche, P.J. and R.A. Normann, Chronic recording capability of the Utah Intracortical Electrode Array in cat sensory cortex. J Neurosci Methods, 1998. **82**(1): p. 1-15.

79. Nicolelis, M.A., Brain-machine interfaces to restore motor function and probe neural circuits. Nat Rev Neurosci, 2003. **4**(5): p. 417-22.

80. Suner, S., et al., Reliability of signals from a chronically implanted, silicon-based electrode array in non-human primate primary motor cortex. IEEE Trans Neural Syst Rehabil Eng, 2005. **13**(4): p. 524-41.

81. Simeral, J.D., et al., Neural control of cursor trajectory and click by a human with tetraplegia 1000 days after implant of an intracortical microelectrode array. J Neural Eng, 2011. **8**(2): p. 025027.

82. Kim, D.H., et al., Dissolvable films of silk fibroin for ultrathin conformal bio-integrated electronics. Nat Mater, 2010. **9**(6): p. 511-7.

83. Campbell, P.K., et al., A silicon-based, three-dimensional neural interface: manufacturing processes for an intracortical electrode array. IEEE Trans Biomed Eng, 1991. **38**(8): p. 758-68.

84. Jones, K.E., P.K. Campbell, and R.A. Normann, *A glass/silicon composite intracortical electrode array.* Ann Biomed Eng, 1992. **20**(4): p. 423-37.

85. Vetter, R.J., et al., Chronic neural recording using silicon-substrate microelectrode arrays implanted in cerebral cortex. IEEE Trans Biomed Eng, 2004. **51**(6): p. 896-904.

86. Edell, D.J., et al., Factors influencing the biocompatibility of insertable silicon microshafts in cerebral cortex. IEEE Trans Biomed Eng, 1992. **39**(6): p. 635-43.

87. Merrill, D.R. and P.A. Tresco, *Impedance characterization of microarray recording electrodes in vitro.* Conf Proc IEEE Eng Med Biol Soc, 2004. **6**: p. 4349-52.

88. House, P.A., et al., Acute microelectrode array implantation into human neocortex: preliminary technique and histological considerations. Neurosurg Focus, 2006. **20**(5): p. E4.

89. Kim, Y.T., et al., Chronic response of adult rat brain tissue to implants anchored to the skull. Biomaterials, 2004. **25**(12): p. 2229-37.

90. Kipke, D.R., et al., Silicon-substrate intracortical microelectrode arrays for long-term recording of neuronal spike activity in cerebral cortex. IEEE Trans Neural Syst Rehabil Eng, 2003. **11**(2): p. 151-5.

91. Kam, L., et al., Selective adhesion of astrocytes to surfaces modified with immobilized peptides. Biomaterials, 2002. **23**(2): p. 511-5.

92. Schmidt, S., K. Horch, and R. Normann, *Biocompatibility of silicon-based electrode arrays implanted in feline cortical tissue.* J Biomed Mater Res, 1993. **27**(11): p. 1393-9.

93. Szarowski, D.H., et al., *Brain responses to micro-machined silicon devices.* Brain Res, 2003. **983**(1-2): p. 23-35.

94. Spataro, L., et al., Dexamethasone treatment reduces astroglia responses to inserted neuroprosthetic devices in rat neocortex. Exp Neurol, 2005. **194**(2): p. 289-300.

95. Liu, X., et al., Histological and physiological effects of the central auditory prosthesis: surface versus penetrating electrodes. Hear Res, 1997. **114**(1-2): p. 264-74.

96. Roitbak, T. and E. Sykova, Diffusion barriers evoked in the rat cortex by reactive astrogliosis. Glia, 1999. **28**(1): p. 40-8.

97. Peckham, P.H., *Principles of electrical stimulation.* Top Spinal Cord Inj Rehabil, 1999(5): p. 1-5.

98. Thrasher, T.A. and M.R. Popovic, Functional electrical stimulation of walking: function, exercise and rehabilitation. Ann Readapt Med Phys, 2008. **51**(6): p. 452-60.

99. Nightingale, E.J., et al., *Benefits of FES gait in a spinal cord injured population.* Spinal Cord, 2007. **45**(10): p. 646-57.

100. Keith, M.W., et al., Implantable functional neuromuscular stimulation in the tetraplegic hand. J Hand Surg Am, 1989. **14**(3): p. 524-30.

101. Brindley, G.S., et al., Sacral anterior root stimulators for bladder control in paraplegia: the first 50 cases. J Neurol Neurosurg Psychiatry, 1986. **49**(10): p. 1104-14.

102. Kim, J.H., et al., Diaphragm pacing: histopathological changes in the phrenic nerve following long-term electrical stimulation. J Thorac Cardiovasc Surg, 1976. **72**(4): p. 602-8.

103. Kantrowitz, A., *Electronic Physiological Aids.* Maimonides Hospital: Brooklyn, New York, 1960: p. 4-5.

104. Liberson, W.T., et al., Functional electrotherapy: stimulation of the peroneal nerve synchronized with the swing phase of the gait of hemiplegic patients. Arch Phys Med Rehabil, 1961. **42**: p. 101-5.

105. Krajl, A., A. Trnkoczy, and R. Acimovic, *Improvement of locomotion in hemiplegic patients with multichannel stimulation.* Proc Conf of Human Locomotor Engineering, Sussex, England, 1971: p. 60-68.

106. Strojnik, P., A. Kralj, and I. Ursic, Programmed six-channel electrical stimulator for complex stimulation of leg muscles during walking. IEEE Trans Biomed Eng, 1979. **26**(2): p. 112-6.

107. Brissot, R., et al., Clinical experience with functional electrical stimulation-assisted gait with Parastep in spinal cord-injured patients. Spine (Phila Pa 1976), 2000. **25**(4): p. 501-8.

108. Marsolais, E.B. and R. Kobetic, Implantation techniques and experience with percutaneous intramuscular electrodes in the lower extremities. J Rehabil Res Dev, 1986. **23**(3): p. 1-8.

109. Kobetic, R., et al., Development of hybrid orthosis for standing, walking, and stair climbing after spinal cord injury. J Rehabil Res Dev, 2009. **46**(3): p. 447-62.

110. Rushton, D.N., et al., Lumbar root stimulation for restoring leg function: results in paraplegia. Artif Organs, 1997. **21**(3): p. 180-2.

111. Davis, R., J. Patrick, and A. Barriskill, Development of functional electrical stimulators utilizing cochlear implant technology. Med Eng Phys, 2001. **23**(1): p. 61-8.

112. Solomonow, M., et al., Reciprocating gait orthosis powered with electrical muscle stimulation (RGO II). Part II: Medical evaluation of 70 paraplegic patients. Orthopedics, 1997. **20**(5): p. 411-8.

113. Solomonow, M., et al., Reciprocating gait orthosis powered with electrical muscle stimulation (RGO II). Part I: Performance evaluation of 70 paraplegic patients. Orthopedics, 1997. **20**(4): p. 315-24.

114. Marsolais, E.B. and B.G. Edwards, Energy costs of walking and standing with functional neuromuscular stimulation and long leg braces. Arch Phys Med Rehabil, 1988. **69**(4): p. 243-9.

115. Seligman, L.J., *Electrical stimulation of the spinal cord: a CRITICAL review.* Pacing & Clinical Electrophysiology, 1987. **10**(1 Part 2): p. 176-179.

116. Carhart, M.R., et al., Epidural spinal-cord stimulation facilitates recovery of functional walking following incomplete spinal-cord injury. IEEE Trans Neural Syst Rehabil Eng, 2004. **12**(1): p. 32-42.

117. Harkema, S., et al., Effect of epidural stimulation of the lumbosacral spinal cord on voluntary movement, standing, and assisted stepping after motor complete paraplegia: a case study. Lancet, 2011. **377**(9781): p. 1938-47.

118. Mushahwar, V.K., et al., *Intraspinal micro stimulation generates locomotor-like and feedback-controlled movements.* IEEE Trans Neural Syst Rehabil Eng, 2002. **10**(1): p. 68-81.

119. Mushahwar, V.K., L. Guevremont, and R. Saigal, *Could cortical signals control intraspinal stimulators? A theoretical evaluation.* IEEE Trans Neural Syst Rehabil Eng, 2006. **14**(2): p. 198-201.

120. Guevremont, L., et al., Locomotor-related networks in the lumbosacral enlargement of the adult spinal cat: activation through intraspinal microstimulation. IEEE Trans Neural Syst Rehabil Eng, 2006. **14**(3): p. 266-72.

121. Yeomans, J., P. Prior, and F. Bateman, Current-distance relations of axons mediating circling elicited by midbrain stimulation. Brain Res, 1986. **372**(1): p. 95-106.

122. Bagshaw, E.V. and M.H. Evans, Measurement of current spread from microelectrodes when stimulating within the nervous system. Exp Brain Res, 1976. **25**(4): p. 391-400.

123. Tai, C., et al., Multimicroelectrode stimulation within the cat L6 spinal cord: influences of electrode combinations and stimulus interleave time on knee joint extension torque. IEEE Trans Rehabil Eng, 2000. **8**(1): p. 1-10.

124. Gaunt, R.A., et al., Intraspinal microstimulation excites multisegmental sensory afferents at lower stimulus levels than local alpha-motoneuron responses. J Neurophysiol, 2006. **96**(6): p. 2995-3005.

125. Mushahwar, V.K., et al., Movements generated by intraspinal microstimulation in the intermediate gray matter of the anesthetized, decerebrate, and spinal cat. Can J Physiol Pharmacol, 2004. **82**(8-9): p. 702-14.

126. Mushahwar, V.K. and K.W. Horch, Selective activation of muscle groups in the feline hindlimb through electrical microstimulation of the ventral lumbo-sacral spinal cord. IEEE transactions on rehabilitation engineering : a publication of the IEEE Engineering in Medicine and Biology Society, 2000. **8**(1): p. 11-21.

127. Moritz, C.T., et al., Forelimb movements and muscle responses evoked by microstimulation of cervical spinal cord in sedated monkeys. J Neurophysiol, 2007. **97**(1): p. 110-20.

128. Gaunt, R.A. and A. Prochazka, *Control of urinary bladder function with devices: successes and failures.* Prog Brain Res, 2006. **152**: p. 163-94.

129. Tai, C., et al., Bladder and urethral sphincter responses evoked by microstimulation of S2 sacral spinal cord in spinal cord intact and chronic spinal cord injured cats. Exp Neurol, 2004. **190**(1): p. 171-83.

130. Grandjean, P.A. and J.T. Mortimer, *Recruitment properties of monopolar and bipolar epimysial electrodes.* Ann Biomed Eng, 1986. **14**(1): p. 53-66.

131. Bamford, J.A., C.T. Putman, and V.K. Mushahwar, Intraspinal microstimulation preferentially recruits fatigue-resistant muscle fibres and generates gradual force in rat. J Physiol, 2005. **569**(Pt 3): p. 873-84.

132. Mushahwar, V.K. and K.W. Horch, *Muscle recruitment through electrical stimulation of the lumbo-sacral spinal cord.* IEEE Trans Rehabil Eng, 2000. **8**(1): p. 22-9.

133. Snow, S., K.W. Horch, and V.K. Mushahwar, *Intraspinal microstimulation using cylindrical multielectrodes.* IEEE Trans Biomed Eng, 2006. **53**(2): p. 311-9.

134. Lau, B., L. Guevremont, and V.K. Mushahwar, Strategies for generating prolonged functional standing using intramuscular stimulation or intraspinal microstimulation. IEEE Trans Neural Syst Rehabil Eng, 2007. **15**(2): p. 273-85.

135. Bamford, J.A., K.G. Todd, and V.K. Mushahwar, *The effects of intraspinal microstimulation on spinal cord tissue in the rat.* Biomaterials, 2010. **31**(21): p. 5552-63.

136. Mushahwar, V.K. and K.W. Horch, Proposed specifications for a lumbar spinal cord electrode array for control of lower extremities in paraplegia. IEEE Trans Rehabil Eng, 1997. **5**(3): p. 237-43.

137. Tai, C., et al., Multi-joint movement of the cat hindlimb evoked by microstimulation of the lumbosacral spinal cord. Exp Neurol, 2003. **183**(2): p. 620-7.

138. Giszter, S.F., F.A. Mussa-Ivaldi, and E. Bizzi, *Convergent force fields organized in the frog's spinal cord.* J Neurosci, 1993. **13**(2): p. 467-91.

139. Mushahwar, V.K., D.F. Collins, and A. Prochazka, Spinal cord microstimulation generates functional limb movements in chronically implanted cats. Exp Neurol, 2000. **163**(2): p. 422-9.

140. Saigal, R., C. Renzi, and V.K. Mushahwar, *Intraspinal microstimulation generates functional movements after spinal-cord injury.* IEEE Trans Neural Syst Rehabil Eng, 2004. **12**(4): p. 430-40.

141. Guevremont, L., J.A. Norton, and V.K. Mushahwar, Physiologically based controller for generating overground locomotion using functional electrical stimulation. J Neurophysiol, 2007. **97**(3): p. 2499-510.

142. Yakovenko, S., V. Gritsenko, and A. Prochazka, *Contribution of stretch reflexes to locomotor control: a modeling study.* Biol Cybern, 2004. **90**(2): p. 146-55.

143. Vogelstein, R.J., et al., *A Silicon Central Pattern Generator Controls Locomotion in Vivo.* IEEE Trans Biomed Circuits and Systems, 2008(23): p. 212-222.

144. Pappas, I.P., et al., *A reliable gait phase detection system.* IEEE Trans Neural Syst Rehabil Eng, 2001. **9**(2): p. 113-25.

145. Hansen, M., M.K. Haugland, and T. Sinkjaer, *Evaluating robustness of gait event detection based on machine learning and natural sensors.* IEEE Trans Neural Syst Rehabil Eng, 2004. **12**(1): p. 81-8.

146. Tomovic, R. and R.B. Mcghee, *A Finite State Approach to Synthesis of Bioengineering Control Systems.* Ieee Transactions on Human Factors in Electronics, 1966. **Hfe7**(2): p. 65-&.

147. Granat, M., et al., The use of functional electrical stimulation to assist gait in patients with incomplete spinal cord injury. Disabil Rehabil, 1992. **14**(2): p. 93-7.

148. Franken, H.M., et al., *Cycle-to-cycle control of swing phase of paraplegic gait induced by surface electrical stimulation.* Medical & Biological Engineering & Computing, 1995. **33**(3 Spec No): p. 440-51.

149. Mazurek, K.A., et al., Feed forward and feedback control for over-ground locomotion in anaesthetized cats. J Neural Eng, 2012. **9**(2): p. 026003.

150. Kirkwood, C.A., B.J. Andrews, and P. Mowforth, *Automatic detection of gait events: a case study using inductive learning techniques.* Journal of Biomedical Engineering, 1989. **11**(6): p. 511-6.

151. Skelly, M.M. and H.J. Chizeck, *Real-time gait event detection for paraplegic FES walking.* IEEE Trans Neural Syst Rehabil Eng, 2001. **9**(1): p. 59-68.

152. Sweeney, P.C., G.M. Lyons, and P.H. Veltink, *Finite state control of functional electrical stimulation for the rehabilitation of gait.* Medical & Biological Engineering & Computing, 2000. **38**(2): p. 121-6.

153. Burridge, J.H., et al., Phase II trial to evaluate the ActiGait implanted drop-foot stimulator in established hemiplegia. J Rehabil Med, 2007. **39**(3): p. 212-8.

154. Kuiken, T.A., et al., Targeted muscle reinnervation for real-time myoelectric control of multifunction artificial arms. JAMA, 2009. **301**(6): p. 619-28.

155. Graupe, D., K.H. Kohn, and S. Basseas, Above- and below-lesion EMG pattern mapping for controlling electrical stimulation of paraplegics to facilitate unbraced walker-assisted walking. Journal of Biomedical Engineering, 1988. **10**(4): p. 305-11.

156. Georgopoulos, A.P., et al., On the relations between the direction of two-dimensional arm movements and cell discharge in primate motor cortex. J Neurosci, 1982. **2**(11): p. 1527-37.

157. Sigala, N. and N.K. Logothetis, Visual categorization shapes feature selectivity in the primate temporal cortex. Nature, 2002. **415**(6869): p. 318-20.

158. Bansal, A.K., et al., Decoding 3D reach and grasp from hybrid signals in motor and premotor cortices: spikes, multiunit activity, and local field potentials. J Neurophysiol, 2012. **107**(5): p. 1337-55.

159. Stark, E. and M. Abeles, *Predicting movement from multiunit activity.* J Neurosci, 2007. **27**(31): p. 8387-94.

160. Mehring, C., et al., Inference of hand movements from local field potentials in monkey motor cortex. Nat Neurosci, 2003. **6**(12): p. 1253-4.

161. Bansal, A.K., et al., Relationships among low-frequency local field potentials, spiking activity, and three-dimensional reach and grasp kinematics in primary motor and ventral premotor cortices. J Neurophysiol, 2011. **105**(4): p. 1603-19.

162. Lewicki, M.S., A review of methods for spike sorting: the detection and classification of neural action potentials. Network, 1998. **9**(4): p. R53-78.

163. Simon, W., The Real-Time Sorting of Neuro-Electric Action Potentials in Multiple Unit Studies. Electroencephalogr Clin Neurophysiol, 1965. **18**: p. 192-5.

164. Schmidt, E.M., *Computer separation of multi-unit neuroelectric data: a review.* J Neurosci Methods, 1984. **12**(2): p. 95-111.

165. Adamos, D.A., E.K. Kosmidis, and G. Theophilidis, *Performance evaluation of PCA-based spike sorting algorithms.* Comput Methods Programs Biomed, 2008. **91**(3): p. 232-44.

166. Hartigan, J.A., *Clustering algorithms [by] John A. Hartigan*. Wiley series in probability and mathematical statistics. Appliedprobability and statistics. 1975: New York, Wiley [1975].

167. Li, Z., et al., Adaptive decoding for brain-machine interfaces through Bayesian parameter updates. Neural Comput, 2011. **23**(12): p. 3162-204.

168. Chestek, C.A., et al., *Neural prosthetic systems: current problems and future directions.* Conf Proc IEEE Eng Med Biol Soc, 2009. **2009**: p. 3369-75.

169. Shinomoto, S. and S. Koyama, *A solution to the controversy between rate and temporal coding.* Stat Med, 2007. **26**(21): p. 4032-8.

170. Ahrens, M.B., L. Paninski, and M. Sahani, *Inferring input nonlinearities in neural encoding models.* Network, 2008. **19**(1): p. 35-67.

171. Cunningham, J.P., et al., Methods for estimating neural firing rates, and their application to brain-machine interfaces. Neural Netw, 2009. **22**(9): p. 1235-46.

172. Georgopoulos, A.P., A.B. Schwartz, and R.E. Kettner, *Neuronal population coding of movement direction.* Science, 1986. **233**(4771): p. 1416-9.

173. Stein, R.B., et al., Encoding mechanisms for sensory neurons studied with a multielectrode array in the cat dorsal root ganglion. Can J Physiol Pharmacol, 2004. **82**(8-9): p. 757-68.

174. Li, Z., et al., *Unscented Kalman filter for brain-machine interfaces.* PLoS One, 2009. **4**(7): p. e6243.

175. Terzuolo, C.A. and Y. Washizu, Relation between stimulus strength, generator potential and impulse frequency in stretch receptor of Crustacea. J Neurophysiol, 1962. **25**: p. 56-66.

176. Prochazka, A., R.A. Westerman, and S.P. Ziccone, *Discharges of single hindlimb afferents in the freely moving cat.* J Neurophysiol, 1976. **39**(5): p. 1090-104.

177. Loeb, G.E., M.J. Bak, and J. Duysens, Long-term unit recording from somatosensory neurons in the spinal ganglia of the freely walking cat. Science, 1977. **197**(4309): p. 1192-4.

178. Loeb, G.E., J.A. Hoffer, and W.B. Marks, Activity of spindle afferents from cat anterior thigh muscles. III. Effects of external stimuli. J Neurophysiol, 1985. **54**(3): p. 578-91.

179. Prochazka, A. and M. Gorassini, *Ensemble firing of muscle afferents recorded during normal locomotion in cats.* J Physiol, 1998. **507 (Pt 1)**: p. 293-304.

180. Jones, K.E., J. Wessberg, and A.B. Vallbo, *Directional tuning of human forearm muscle afferents during voluntary wrist movements.* J Physiol, 2001. **536**(Pt 2): p. 635-47.

181. Aoyagi, Y., et al., Capabilities of a penetrating microelectrode array for recording single units in dorsal root ganglia of the cat. J Neurosci Methods, 2003. **128**(1-2): p. 9-20.

182. Stein, R.B., et al., Coding of position by simultaneously recorded sensory neurones in the cat dorsal root ganglion. J Physiol, 2004. **560**(Pt 3): p. 883-96.

183. Bosco, G. and R.E. Poppele, *Proprioception from a spinocerebellar perspective.* Physiol Rev, 2001. **81**(2): p. 539-68.

184. Nicolelis, M.A., *Actions from thoughts.* Nature, 2001. **409**(6818): p. 403-7.

185. Weber, D.J., et al., Limb-state feedback from ensembles of simultaneously recorded dorsal root ganglion neurons. J Neural Eng, 2007. **4**(3): p. S168-80.

186. Wagenaar, J.B., V. Ventura, and D.J. Weber, *State-space decoding of primary afferent neuron firing rates.* J Neural Eng, 2011. **8**(1): p. 016002.

187. Rigosa, J., et al., Neuro-fuzzy decoding of sensory information from ensembles of simultaneously recorded dorsal root ganglion neurons for functional electrical stimulation applications. J Neural Eng, 2011. **8**(4): p. 046019.

188. Bruns, T.M., R.A. Gaunt, and D.J. Weber, *Estimating bladder pressure from sacral dorsal root ganglia recordings.* Conf Proc IEEE Eng Med Biol Soc, 2011. **2011**: p. 4239-42.

189. Gaunt, R.A., J.A. Hokanson, and D.J. Weber, Microstimulation of primary afferent neurons in the L7 dorsal root ganglia using multielectrode arrays in anesthetized cats: thresholds and recruitment properties. J Neural Eng, 2009. **6**(5): p. 55009.

190. Weber, D.J., et al., Limb-state information encoded by peripheral and central somatosensory neurons: implications for an afferent interface. IEEE Trans Neural Syst Rehabil Eng, 2011. **19**(5): p. 501-13.

191. Bourbeau, D.J., et al., A computational model for estimating recruitment of primary afferent fibers by intraneural stimulation in the dorsal root ganglia. J Neural Eng, 2011. **8**(5): p. 056009.

Chapter 2: Feed Forward and Feedback Control for Over-Ground Locomotion in Anesthetized Cats

K A Mazurek[1*], B J Holinski[2*], D G Everaert[3], R B Stein[2,3], R Etienne-Cummings[1], and V K Mushahwar[3,4]

A version of this chapter was published in Journal of Neural Engineering 2012 Apr;9(2):026003.

[1]Department of Electrical and Computer Engineering, Johns Hopkins University, Baltimore, MD, USA

[2]Department of Biomedical Engineering, University of Alberta, Alberta, Canada

[3]Centre for Neuroscience, University of Alberta, Canada

[4]Deparment of Cell Biology, University of Alberta, Alberta, Canada

[*]*KA Mazurek and BJ Holinski contributed equally as first authors.*

Introduction

The ability to walk is developed at an early age in most legged species. In vertebrates, a specific pattern of alternating activation of flexor and extensor muscles is generated through the spinal cord to provide sufficient force and appropriate movements necessary for locomotion (Brown, 1914). During walking, lower limb movements must be coordinated to produce patterns of swing and stance while maintaining balance. The principal mechanisms underlying the generation and control of locomotion have been studied in detail in animals such as cats (Grillner, 1985; Conway *et al.*, 1987; Burke *et* *al.*, 2001; Hiebert and Pearson, 1999; Prilutsky *et al.*, 1996; Grillner and Zangger, 1979) and lampreys (Grillner and Matsushima, 1991; Islam *et al.*, 2006; Mentel *et al.*, 2006; Archambault *et al.*, 2001).

The spinal central pattern generators (CPG), located in the cervical and lumbar enlargements, are responsible for the bilateral rhythmic outputs activating flexor and extensor muscles in the upper and lower extremities (Yamaguchi, 2004). Other important locomotor centres are located in the midbrain locomotor region. CPGs controlling functions such as swallowing and breathing are also located in the brain stem (Dick *et al.*, 1993). The CPG controlling locomotion in the lower extremities is thought to be located in the lumbosacral region of the spinal cord where descending signals from the brain as well as afferent feedback are integrated to generate muscle activation patterns observed during walking (Kiehn, 2006). The CPG utilizes feed forward control (defined as open loop control) using predefined timing values to establish a timing pattern (McCrea and Rybak, 2007). Spinal and supraspinal centres process the sensory feedback signals to adjust the output of the CPG (defined as closed loop control). This feedback allows the CPG to adjust its output based on external (e.g. environmental) and internal (e.g. fatigue) perturbations. Support for the existence of the CPG comes from the observations of rhythmic walking movements after low thoracic spinalization in cats and after spinal cord injury (SCI) in humans (Hultborn and Nielsen, 2007).

Individuals with SCI may lose the ability to walk due to damaged neural communication between the brain and locomotor CPG. People with incomplete SCI retain some residual neural connections and often may be able to walk with impairments. If the SCI is complete, the individual loses all functionality and control of the lower extremities. Attempts have been made to restore locomotion through functional electrical stimulation (FES) (Kobetic *et al.*, 1997; Thrasher and Popovic, 2008). The systems available restore only limited standing and gait function, and require user input to determine the stimulation patterns. In addition, the systems do not contain sensory feedback to respond to changes in the environment.

The proposed control algorithm in this work applied a complex state-system to produce feedback controlled locomotion patterns across several joints. The application of state-based control for walking neuroprostheses was first proposed by Tomovic and Mcghee (1966), a few years after Mealy and Moore published some of the first state-based automata (Mealy, 1955). Since Tomovic and Mcghee, state-based control, while common in other fields of engineering, has only been implemented with limited state spaces or with single joint control in walking neuroprostheses (Crago *et al.*, 1996). Recent work by Quintero et al. (2010) has shown that state-based control of quadriceps stimulation and orthoses can restore walking by using 4 states to sequentially activate the legs. Currently, most state-based FES walking systems do not utilize sensory feedback (Sweeney *et al.*, 2000). In addition to a larger state space and multi-joint sensory feedback control, the controller developed as part of the present work can be reconfigured to elicit several types of locomotion using the same framework (eg. running).

Other locomotion controllers have been developed which attempt to restore complete gait function by emulating the functionality of the CPG (Guevremont *et al.*, 2007b). The goal of such systems is to restore locomotion while requiring minimal conscious effort to operate and generate sufficient forces to support body weight. The controller designed by Guevremont *et al* (2007a) used IF-THEN statements to determine the intramuscular stimulation (IMS) patterns in selected hind limb muscles of cats. Open loop *or* closed loop control were implemented individually for determining the transition between a swing and stance state. Open loop control used intrinsic timing as feed forward control to determine the swing and stance state transitions. Closed loop control used sensory feedback information to perform these same transitions. Each control paradigm had its limitations, and a combined controller was briefly tested and showed promising results for producing safe over-ground walking. Prochazka *et al* (2002) demonstrated the utility of open and closed loop control during locomotion in their computer model of a cat. Sensory feedback was also shown to be important in computer simulations of stepping (Ekeberg and Pearson, 2005). Another controller implemented by Vogelstein *et al* (2008) configured a silicon neural network to emulate functions of the CPG by controlling the movements of several hind limb joints. This controller only used closed loop control to determine transitions between swing and stance but was one of the first neuromorphic devices to instantiate a functional CPG *in vivo*. Although it was successful at restoring locomotion in an anaesthetized cat, the controller would occasionally become trapped in undesirable states during stance and swing transitions which effectively stopped the over-ground walking. These limitations again emphasized the need for a combined open and closed loop controller and led to the development of the present system which features a larger and more comprehensive state system for precision rule-based control.

Therefore, the goal of this study was to develop a physiologically-based control algorithm capable of using intrinsic timing and sensory feedback to control multiple joints in the lower extremities for producing safer over-ground walking than that obtained with an open loop controller. Such a controller was deemed successful if it produced a sufficient level of load bearing force, maintained natural ranges of motion, and successfully traversed an over-ground walkway. The algorithm can easily be translated into a silicon chip capable of using a variety of input and output modalities of which certain components have been implemented (Mazurek *et al.*, 2010; Mazurek and Etienne-Cummings, 2011). This paper describes the proposed locomotion control algorithm and the results of its implementation *in vivo*. The locomotion controller allowed for comparing two configurations: an open loop controller and a hybrid-CPG controller. The success of each controller depended on its ability to restore over-ground walking while overcoming internal and external perturbations. We hypothesized that the hybrid-CPG would produce more successful over-ground trials compared to the open loop controller. Additionally, the hybrid-CPG controller might generate more steps with adequate load bearing force and these steps would have more natural ranges-of-motion. Direct comparisons of the efficacy of the controllers were made through analysis of parameters such as body weight support, walking speed, and limb kinematics.

METHODS

LOCOMOTION CONTROL ALGORITHM

The locomotion control algorithm was designed as a framework for configuring different implementations of open and closed loop control to shape the output stimulation waveforms. The algorithm consisted of three main components: the control logic, the sensory rules, and the stimulation output. These three components are depicted in figure 2-1.

The control logic (figure 2-1A) contained a programmable state system where transitions between each state were intrinsically timed (in the form of timing rules). The control logic activated multiple joints (ankle, hip, and knee) in the lower extremities in an appropriate pattern to generate walking movements and supportive forces. Sensory information (figure 2-1B) adjusted the transitions between certain states and ensured the correct state was active based on the position of the lower limbs. The 'active state' was defined as the state that the control logic was currently executing. Each state contained information about which sensory rules were enabled during that phase of the step cycle. The algorithm was configured to have *M* sensory rules where the limit of the value of *M* was constrained to the resources available in the system (such as the number of sensory signals, resources for digitizing the signals, etc.). Associated with each rule (timing or sensory) was a 'destination state' which would become the new 'active state' if that rule were activated (figure 2-1A). The rules were organized in a predetermined priority to ensure proper state transitions in the event that two rules were activated simultaneously.

The stimulation output waveforms (figure 2-1C) allowed for increases or decreases in muscle activity by modulating amplitudes after each state transition. Each state corresponded to a specific set of stimulation parameters for all output stimulation channels. These parameters included whether the channel was active or inactive, the stimulation amplitude, the pulse width, and the stimulation frequency. The control logic produced the output stimulation waveform according to the parameter values associated with the active state. These changing waveforms aimed to activate different muscle groups at varying stimulation levels as observed during normal locomotion. The output stimulation channels were activated in parallel to reduce potential delays that may be introduced during serial activation of different sites (muscles).

The stability of such a controller was directly related to the configuration of the state system. An unstable controller would demonstrate oscillations between states based on uncertain inputs. This was preventable in the algorithm by appropriately setting the sensory and timing rules to ensure that transitions could only be made in a certain direction. In addition, the timing rules allowed for the controller to transition between states in the event that sensory feedback was insufficient.

Implemented Controller

We implemented two forms of the locomotion control algorithm (open loop and hybrid-CPG) to produce over-ground walking in adult cats. The pre-determined state system was the same for both controllers and was developed from known biological descriptions of the cat step cycle as described in figure 2-2. Each state corresponded to a specific combination of movements of both hind legs. The initial state generated double stance in both legs to produce standing and weight support, and the remaining 8 states (states 2-9) consisted of a symmetrical step cycle. In past experiments the step cycle for each hind leg was divided into two states representing swing and stance (Guevremont *et al.*, 2007a). The step cycle in the present work used four sub-states (F, E1, E2, E3) as previously defined in humans (Nilsson *et al.*, 1985) and cats (Goslow *et al.*, 1973) which enabled the representation of more detailed changes in muscle activation and movements during walking.

The swing portion of the step cycle consisted of lifting and moving the leg forward (F). The stance phase followed by extending the knee to place the foot on the ground (E1), activating the knee and ankle extensor muscles for weight support (E2), and adding the activation of hip extensors and increasing the activation in ankle extensors to produce propulsive force and forward progression of the body (Yang and Winter, 1985). The relative duration of each sub-state to the total step period could be adjusted for different gaits and is thought to be controlled by intrinsic timing circuits located within the spinal cord (Grillner, 1985; McCrea and Rybak, 2008; Yakovenko, 2011). In the present work, the durations of these sub-states for each leg were 20%, 20%, 20%, and 40% of the total step period (for F, E1, E2, and E3, respectively) for the intrinsic timing rules. The walking cycle duration was set to 1.5 s for both the open loop and hybrid-CPG controllers to resemble adult cats walking at slow to moderate speeds. The timing of the phases of the hybrid-CPG controller could be modified as necessary based on sensory input. In order to maintain controller stability, measures were taken to ensure that the controller did not enter states that would unload both legs (such as double flexion, F). Also, when sensory feedback was activated, sensory information would only be interpreted within the context of a specific state. The open loop controller advanced through the states shown in figure 2-2 using the preset timing rules. For the hybrid-CPG, the additional sensory feedback rules were translated into three specific IF-THEN statements. These rules monitored the ground reaction forces (GRF) and range of backward extension which governed the transition from swing-to-stance (E1 to E2), the transition from stance-to-swing (E3 to F), and fatigue compensation rule. The purpose of the rules was to adapt the walking cycle to different perturbations. Sensory signals were recorded from accelerometers, gyroscopes, and force plates, and were processed every 31ms corresponding to the update period of the controller. The accelerometers (located on the foot and shank) and gyroscopes (located on the foot) provided information about limb angle while the force plates provided information about the GRF of each leg. The diagram in figure 2-2 depicts how certain sensory rules were enabled for certain states and disabled for others.

For both the open loop and hybrid-CPG controllers, intramuscular stimulation (IMS) was controlled to activate hip, knee or ankle flexor and extensor muscles of the hind limbs according to the 'active state' of the control logic. Stimulation amplitudes were set to generate the desired movement and force. The initial amplitude of stimulation for the hip, knee and ankle flexor and extensor muscles in each leg was based on observation of the evoked movements and the level of force generated. Initially, the minimal level of stimulation capable of producing weight-bearing and propulsive forces during the E2 and E3 phases was chosen for the hip, knee and ankle extensor muscles. Stimulation amplitudes for the flexor muscles were chosen to produce adequate upward and forward movements of the hind limb. This balanced combination of stimulation channels generated the synergistic movements necessary to evoke over-ground walking. Table 2-1 specifies which leg movements were associated with each sub-state of the step cycle. Note that the same flexor or extensor muscle (stimulation channel) could be active for multiple states in both controllers but the amplitude of activation varied between states. Upon transitioning between states, the stimulation amplitudes from the old active state were ramped to the amplitudes set in the new active state (over 93 ms). This resulted in a shaped stimulation waveform resembling natural electromyographic recordings (EMG) of muscle activation (Guevremont *et al.*, 2007a).

STANCE-TO-SWING RULE

The transition from stance-to-swing occurred when the leg generating the propulsive force extended backwards and was no longer in a supportive position. The rule was implemented using the following **IF-THEN** statement:

IF limb angle from integrated gyroscope < threshold

THEN transition from state E3 to state F

Swing-to-Stance Rule

The swing phase of the step cycle was considered to be completed when the leg had adequately moved forward as determined by the limb angle (relative to the hip). When the limb angle exceeded a pre-determined threshold, the E1 state was terminated. This rule was implemented using the following **IF-THEN** statement:

IF limb angle from accelerometer > threshold

THEN transition from state E1 to state E2

Fatigue Compensation Rule

Over time it was visually observed that the supportive force generated by the hind limbs declined due to muscle fatigue. The purpose of the fatigue rule was to adjust the stimulus amplitude to the extensor muscles to ensure that the cat could propel itself adequately across the walkway. The level of the supportive force was continuously monitored and if the peak force dropped below a certain threshold during the E3 phase, the rule was enabled and acted to increase the amplitude of stimulation to the knee extensor muscle by 30% in the subsequent E2 state. The increase in stimulation amplitude was maintained for the remainder of the trial (i.e., until the cat traversed the walkway). The reason for monitoring E3 and changing E2 instead of only monitoring E2 across steps was because of the physiological delay (approximately 60 – 80ms) between the onset of stimulation and force generation. This rule was implemented using the following **IF-THEN** statement:

IF max(ipsilateral force during E3) < threshold

THEN increase stimulation amplitudes of all subsequent E2 by *x*%

The value of *x* was typically 30%.

Animal Preparation

For detailed animal preparation please see Guevremont *et al* (2007a). All experimental procedures were approved by the University of Alberta's Animal Care and Use committee. The cats were anesthetized using isoflurane inhalation and subsequently transitioned to sodium pentobarbital. The cat remained under anaesthesia for the duration of the experiment. Pairs of stimulation electrodes were inserted percutaneously into 8 muscles of each leg [tibialis anterior, gastrocnemius, vastus medialis, vastus lateralis, rectus femoris, sartorius (anterior compartment), semitendinosus, and semimembranosus (anterior compartment)]. The cat was then transferred to an instrumented walkway and partially suspended in a cart-mounted sling. Due to the experimental setup, the sling supported 75% of the cat's weight (head, trunk, and abdomen). Therefore, 12.5% of body weight was considered full load bearing support for a single hind limb. The mass of the cart and the equipment on it was offset by a pulley system (unloading between 400-600g, ~5% of the combined cat and cart weight) to reduce the effect of static friction. The unloading was initially chosen by applying incremental weights to the pulley system until the cart began to move even without muscle activation. The chosen pulley weight was 100g less than the unloading level at which the cart moved without muscle activation.

The walkway contained a variable friction profile to which the control rules had to accommodate. The friction around the middle section of the walkway was less than that at the beginning or endpoint (figure 2-3).

Stimulation and Sensors

Walking patterns were produced by direct bipolar electrical stimulation of the target muscles using trains of biphasic charge-balanced pulses (62 Hz, up to 20 mA, 100 µs) in a similar fashion to that described in Guevremont *et al* (2007a). The electrodes were pairs of 34AWG sterilized 9-strand stainless steel Cooner wire (Cooner Wire Inc., Chatsworth, CA, USA), Teflon insulated except for 3 to 4 mm exposure at the tips. The distance between the tips within a muscle was approximately 1cm and the AC resistance was approximately 1 kΩ. The wires were positioned near the motor points according to anatomy reference guides. Location was verified using 1 sec stimulation trains and electrodes were readjusted if necessary. This typically resulted in maximal threshold currents of 2 – 3 mA, and maximal force generation was achieved with amplitudes of 6 – 8 mA, thus leaving ample room for increases in stimulation amplitude (up to 20 mA) during the course of the experiment. This process ensured that electrode placement was not the reason for failed trials in any of the experiments. Stimulation was produced by a parallel command stream using a National Instruments DAC (PCI-67xx Series, National Instruments Corp., Austin, TX, USA) connected to modified EMS-6500 stimulators (Electrostim Medical Services, Tampa, FL). The parallel command stream was created in real time by the two controller algorithms. Amplitudes were chosen to recreate estimates of the continuously graded EMG patterns as observed by Goslow *et al* (1973) and provide adequate forward propulsion. Muscles were grouped according to a common function or synergy as described in table 2-1.

Accelerometers and gyroscopes were attached to the hind limbs for recording signals appropriate for triggering sensory rule transitions. Tri-axial accelerometers were fixed to both the shank and the foot of each leg (X direction was horizontal in the forward direction of movement, Y direction was vertical). The gyroscopes were placed on each foot proximal to the accelerometers (figure 2-4). The gyroscope signals were integrated to provide foot angle. Due to the drift caused by the integration of the gyroscope signal, the angle signals were reset at the beginning of the stance phase (E2) of each limb. A custom 3.5m-walkway was instrumented with separate force plates for each leg. The downward forces perpendicular to the walkway were used as the GRF. Gyroscope, accelerometer, and GRF recordings were acquired using a Cerebus (Blackrock Microsystems, Salt Lake City, UT, USA) data acquisition system at 1000 samples/s. The data were streamed from Cerebus into Matlab (The MathWorks Inc., Natick, MA, USA) to be processed in real time by custom written software. All gyroscope, accelerometer, and force data were recorded for each trial and a moving average filter with a window length of 120 ms was applied to smooth the signals for use in the sensory rules.

Reflective markers were placed on the right hind limb of the cat to indicate the iliac crest, hip, knee, ankle, and metatarsophalangeal joints. The positions of these markers were used to delineate joint position and leg movement, but were not applied to any sensory feedback rules. The length of the walkway was captured by a high speed JVC (JVC Americas Corp., Wayne, NJ, USA) camcorder (120 frames/sec) positioned 4.5 m away from the midpoint of the walkway with the lens parallel to the walkway.

Experimental Procedures

Before testing either the open loop or hybrid-CPG controller, appropriate stimulation amplitudes were established for the different step cycle sub-states in each limb. For a typical cat, the amplitudes for each channel (and muscle) across a walking cycle. One such example is shown in figure 2-5. Sometimes muscles could not be reliably isolated and those stimulation channels were disabled (vastus medialis and semitendinosus for the cat amplitudes in figure 2-5). Once these values were deemed appropriate for generating the desired functional movements and forces, the open loop controller was tested to generate over-ground walking. During these trials, the sensory signals from the accelerometers, gyroscopes, and force plates were recorded and analysed to determine appropriate threshold values to apply to the feedback rules in the hybrid-CPG controller. Upon determining these thresholds, the hybrid-CPG controller was tested to produce over-ground walking. A total of 7 experiments were conducted with 5 cats (male or female, 3.5kg – 4.4 kg).

Data Analysis

Upon completion of trials with both the open loop and hybrid-CPG controllers, the recorded data from accelerometers, gyroscopes, and force plates were compared between controllers. A trial was considered successful if the cat began <10 cm from the start of the walkway and walked at least 75% across the length of the walkway (resulting in a total distance of at least 2.24 m). For each successful trial, the force and length of each step was analyzed to determine which controller produced a greater proportion of successful steps. The minimal load bearing force during any point of the stance phase had to exceed 12.5% of body weight (due to our setup) to ensure the knees would not buckle. The step also could not be longer than 20 cm with reference to the hip ensuring a physiologically realistic range of motion by similar sized cats (3 kg) walking at approximately 0.20 m/s (Halbertsma, 1983). With our experimental setup, a stride length exceeding 20 cm was an indication of excessive backward extension of the hind limb at the end of the stance phase resulting in a loss of supportive force and/or slipping of the foot. The percentage of successful steps within trials where the cat walked over 75% of the walkway length was used to judge the effectiveness of each controller configuration in producing walking. Marker positions were digitized from the high speed recordings using custom Matlab software (MotionTracker2D) written by Dr. Douglas Weber (University of Pittsburgh, Pittsburgh, PA). Each frame was calibrated using a set of reference markers to correct for offset in the camera angle. Joint angles and limb representations were calculated from the marker locations. Limb angle (vector from the hip to the metatarsophalangeal joint) was measured with respect to the horizontal. The cart was also tracked for position and velocity measurements. Walking speed measurements were calculated by neglecting the first 50 cm of the walkway to prevent variations in static friction from affecting the result. Therefore, walking speed was calculated for an effective distance of 2.2 m.

The beginning of each step was signified by touchdown on the force plate. Each step was analysed for maximal step length and GRF. These values were normalized to each cat to allow for inter-experimental comparisons. Step length was normalized to the distance from the ankle to the metatarsophalangeal joint and vertical GRF was normalized to body mass. Statistical analysis was performed using SPSS (IBM Corporation, Armonk, NY, USA). Differences between population means were tested using the *t*-test when all statistical assumptions were met. Equality of the population variances was assessed with Levene's Test (equal variances assumed if $P>.05$) Normality was tested using the Kolmogorov-Smirnov statistic with a Lilliefors significance correction. If the Lilliefors gave a $P<0.05$, the data were considered non-normal and an

Independent Samples Median Test (a non-parametric test) was used to determine if the groups had significantly different medians.

RESULTS

On average, 18 ± 7 over-ground walking trials (mean ± standard deviation) were obtained per experiment. The controller required 1-12 trials setup trials across all experiments (i.e, 3.7 – 45% of the trials were for setting initial parameters). Setup trials were terminated when the cat was able to traverse the walkway successfully. Across all experiments, 74 trials (out of 113 total trials) produced over-ground walking in which the cat traversed at least 75% of the length of the walkway and were therefore considered successful. Durations for traversing the walkway in the successful trials ranged from 7.66 to 19.2s depending on controller settings (control method, enabled rules, and rule thresholds). The number of trials per experiment was limited by the eventual onset of muscle fatigue which was observed visually through the reduced force production during the trial. Experiments were terminated when the maximal level of safe current delivery (20mA) was reached and insufficient propulsive force was produced to traverse 75% of the length of the walkway.

Of the 39 trials in which the walkway was not traversed, 16 failed due to poor parameter settings, when experimenting with ramping rates and synergy timings, and incorrect sensory thresholds for rule transitions. Most of these issues were easily corrected after detecting the problems in the software or setup. Fatigue and a lack of consistency in elicited movements (eg the paw stepping off of the walkway) were other reasons for failure.

Successful implementation of the sensory rules in the hybrid-CPG controller required selecting the appropriate sensory signals and thresholds. Thresholds were chosen to allow appropriate compensation to the varying walkway friction and muscle fatigue, and to optimize stepping (peak force output and step length). Figure 2-6 shows traces of sensory signals from the right limb. The integrated gyroscope signal contained accurate timing and relative magnitudes of the limb angle compared to recordings from the motion capture system (figure 2-6A-B). For the swing-to-stance transitions, neither the shank accelerometer (X direction) nor the foot accelerometer (X and Y directions) represented the limb angle accurately. During impact events, the accelerometer signal contained multiple threshold crossings within the transition region. Accelerometer signals contained high frequency components that made it difficult to place a threshold that would reliably discriminate the range of limb excursion for the swing-to-stance transitions. Therefore, the gyroscope signals were applied to this rule. Nonetheless, the accelerometer signals were beneficial for swing-to-stance transitions because the foot was suspended in the air prior to the transition which removed some of the high frequency components. This provided reliable thresholds to activate the swing-to-stance rule.

Each rule in the hybrid-CPG controller improved the quality of stepping in response to environmental perturbations when compared to the open loop controller. The stance-to-swing rule influenced the amount of time each leg remained in the E3 sub-state. The swing-to-stance rule shortened the amount of time each leg remained in the F or E1 sub-states. The fatigue compensation rule in the hybrid-CPG controller increased the stimulation amplitude based on the generated GRFs in an effort to increase body weight support.

Effect of Stance-to-Swing Transition on Forward Over-ground Walking

Walking performance varied with the hybrid-CPG controller parameters due to the changing environment (e.g., walkway resistance, muscle fatigue and choice of threshold levels in the sensory signals), thus affecting the activation of individual rules. Therefore, the effects of the sensory rules are presented through specific examples from individual trials.

A comparison of the GRF between trials with the open loop and hybrid-CPG controllers is depicted in figure 2-7. Using the open loop controller, the step cycle period did not adjust to the reduced friction in the centre of the walkway and the cat took longer steps that resulted in an increased backward limb extension. This backward extension also caused a decrease in supportive forces during the push off stage of the step cycle. With the addition of the stance-to-swing transition rule in the hybrid-CPG controller, backward extension of the limb was reduced by up to 13° (figure 2-7A) while maintaining appropriate GRFs (figure 2-7B). *Comparing the sum of the total forces from each leg demonstrated that without the feedback rule, load bearing support dropped to 40% of the desired load bearing level.* With the transition rule in the hybrid-CPG controller, the sum of the GRFs dropped to only 80% of the desired level. While this was lower than the desired full load bearing level (12.5% of body weight), it was a marked improvement over the open loop control. This rule only affected the backward extension during the stance phase of the step cycle and not flexion during the swing phase. The sensory signal used in this rule was ipsilateral foot gyroscope signal representing limb angle.

Effect of Swing-to-Stance Transition

The swing-to-stance transition rule increased the speed of the walking cycle by eliminating excess time spent in the swing sub-states F and E1 (figure 2-8). With the open loop controller, the hip angle had a range of 38°, and consistently reached the end of the range of motion during flexion (figure 2-8A). Since the amount of time spent in flexion was fixed, the leg remained in swing phase (F, E1) for longer than desired. Moreover, the hip angle and timing did not adapt to the variable resistance of the walkway but instead produced movements more suitable for a uniform walkway.

With the addition of the swing-to-stance rule in the hybrid-CPG controller, a more desirable adaptation of the hip angle was achieved and the swing stage was adjusted proportionally to the walkway resistance (figure 2-8B). The range of the hip angle was slightly reduced to 35 degrees but more importantly the E1 duration was often truncated. This is evident in figure 2-8B in the middle of the trial (around 5-10s) during steps over the walkway where the resistance decreased. There was less time holding the limb in flexion due to the ability of the cat to move more easily across the walkway as opposed to the regions with higher resistance. The sensory signal used in this rule was the foot accelerometer signal in the Y direction of the ipsilateral hind limb (e.g. figure 2-6E).

Combined Transition Effects on Forward Over-ground Walking

Stick figure representations and foot trajectories of the right hind limb portray the effect of both transition rules between the open loop and hybrid-CPG controllers (figure 2-9). Less time was spent in the swing portion of the step cycle in the hybrid-CPG controller than the open loop controller. The backward excursions were constrained when the stance-to-swing was activated as observed by the decreased step length (figure 2-9B).

With the hybrid-CPG controller, the joint angle range of the hip slightly decreased and was more comparable to natural movements (Goslow *et al.*, 1973) when sensory feedback was enabled (table 2-2).

Fatigue Compensation Rule

Over the course of multiple trials, muscles fatigued and produced less supportive force. The sensory feedback rules of the hybrid-CPG controller compensated for this internal perturbation to the system. In figure 2-10, the stimulation amplitudes of the left leg remained unchanged from open loop controller amplitudes. However, in the right leg, feedback increased stimulation amplitudes in stance by a predetermined amount (30%) when force dropped below the critical threshold. This resulted in an increase in the GRF of right foot from 0.72 kg (19% of BW) to an average of 0.93 kg (25% of BW) over the next 6 steps. The stimulation amplitudes during the stance phase of the right leg were increased after the vertical dotted activation line on the following step.

Summary of Results

A summary of walking characteristics across the 74 successful trials (18 open loop trials, 56 hybrid-CPG) are presented in table 2-3. Peak step length, average velocity, number of steps and the summation of left and right forces (averaged over time) were determined for each trial. Step cycle duration and peak force were analyzed on a step basis (i.e., all steps for all trials pooled).

The mean (± SD) normalized peak step length was 3.1 units smaller with the hybrid-CPG controller (21.8 ± 7.5, N=56) than with the open loop controller (24.9 ± 8.4, N=18). However, *t* test showed that the difference was not significant (P=.06). The *t* test was appropriate as the Lilliefors test scores for normality were 0.34 and 0.09 respectively for the hybrid-CPG and open loop controller, and the group variances were equal (Levene's Test P=.62).

A nonparametric Independent Samples Median Test showed that the hybrid-CPG controller produced significantly (P=.024) more steps for walking the same distance: median (1st quartile, 3rd quartile) for the number of steps taken by the open loop and hybrid-CPG controllers was respectively 7(6,9) and 9(8,11). The median total supportive force showed an upward trend from the open loop controller generating 15.1 % BW (14.3, 18.7) to 18.4% BW (16.1, 20.0) with the hybrid-CPG controller, however it was not significant (P=.10).

A difference between controllers was also observed in the step cycle duration. The median (1st quartile, 3rd quartile) for step cycle duration was significantly lower (P<.001, Independent Samples Median Test) with the hybrid-CPG controller [1.27 s (1.15, 1.49), N=544 steps] than with the open loop controller [1.48 s (1.48, 1.49), N=134 steps]. Thus with the hybrid-CPG controller the cat walked with shorter step cycle durations but took a higher number of steps. Despite the additional steps taken with sensory feedback, a *t* test showed that the average velocity (0.21 ± 0.05 m/s, N=56, Lilliefors test P>0.5) was not significantly different (P=0.62, equal variances assumed (Levene's Test P=0.2)) from that obtained during the open loop condition (0.22 ± 0.04 m/s, N=18, Lilliefors test P=0.107)

An Independent Samples Median Test did not reveal significant differences between the peak step forces generated by open and hybrid-CPG controllers, respectively [17.1% (14.7, 20.3) and 16.8% (14.8, 20.1) BW (P=.69)]. When evaluating each step based on our success criteria (peak force during stance >12.5% BW and peak step length <20 cm), 49% of open loop steps (65/134) generated adequate force (≥ 12.5% BW) and had a natural step length (≤ 20 cm) while 68% of the hybrid-CPG controller steps were successful (372/544). Periods of double stance were maintained through an overlap of 124 ms between the stance and push off states of the two hind limbs. This overlap allowed the stance limb to build enough supportive force before the extended limb swung forward. Also, the state based control algorithm prevented combinations of sub-states that would produce dangerous walking in either controller, such as a state of simultaneous flexion (F) in both legs that would result in falling.

Discussion

The goal of this study was to develop a physiologically-based control algorithm capable of using open loop and closed loop control of multiple joints in the lower extremities for producing locomotion. Emulating the biological CPG provides a control solution for bipedal walking that is thought to be the most efficient method to date (Berniker *et al.*, 2009). The controller emulated the functionality of the spinal CPG by processing intrinsic and sensory based information to implement detailed descriptions of the walking cycle. The feedback information from external sensors (gyroscopes, accelerometers, force plates) was processed to adjust stimulation amplitudes similar to how the biological CPG adjusts muscle activation during locomotion based on sensory neural signals. The controller adapted the stimulation patterns in response to internal and external perturbations to maintain body support and produce effective over-ground locomotion. In agreement with earlier evidence presented by Guevremont *et al* (2007a), the combination of open loop and closed loop control provided the most functional over-ground walking and the most successful steps. Throughout the regions of least resistance in the walkway, the sensory rules allowed the state transitions in the hybrid-

CPG controller to increase the speed of walking, resulting in decreased step length and preventing excessive extension and loss of load bearing GRFs. Load bearing is a critical measure of safety for a functional walking device as it prevents falling and reduces the dependence on the arms for weight support.

The use of appropriate sensory signals was essential for successful implementation of feedback rules in the hybrid-CPG controller. The gyroscopes were most suited for the stance-to-swing transition rule because they best represented the relative magnitudes and timing information of the limb angle. The main challenge with the gyroscope signals was the drift caused by the integration. Therefore, the signal had to be reset at the onset of every stance phase. More sophisticated methodologies for obtaining limb angle using a combination of accelerometer and gyroscope feedback have been proposed (Dejnabadi *et al.*, 2006). For our purposes, we found that a simple reset worked sufficiently well to control walking.

Each of the sensor types used in this study could be practically translated to future applications. The force plates in the walkway can be replaced by force sensitive resistors in each shoe. This has proven to be a reliable and inexpensive solution in many commercial devices such as the Ness L300 (Bioness, Valencia, CA) and the Odstock dropped foot stimulator (Salisbury District Hospital, U.K.). Other sensory information required by the controller can be provided by a combination of a gyroscope and an accelerometer. Currently, sensor technology is small and readily available (Analog Devices, Norwood, MA).

Previous work has focused on developing a controller capable of walking on a treadmill (Strange and Hoffer, 1999), or stepping in place (Saigal *et al.*, 2004). When stepping in place, Saigal *et al* (2004) found that locomotion driven by FES control using open loop or closed loop control alone was equally successful. However, when the animal must physically propel itself, many new challenges are introduced. The FES generated movements have to produce enough force to propel the animal forward as it ambulates and unstable controller states become of paramount importance. In order to create a functional device that can be eventually translated to the clinic, the control algorithm had to be tested in the demanding environment of over-ground walking.

In a clinical application, the device will have to maintain safe walking with a variety of conditions. In order to do so, the controller should adapt to perturbations using sensory feedback similar to the ways in which the human body relies on sensory input (Rossignol *et al.*, 2006). The walkway used in the present experiments had a variable friction profile that perturbed the operation of the controller. The varying resistance was analogous to walking over variable pitched terrain. During regions of low friction, the cart and cat would have momentum similar to walking downhill. The controller responded by increasing the step frequency (by truncating excess extension and flexion) of the walking to maintain supportive forces.

The hybrid-CPG controller also had to respond to variations in muscle output. Direct activation of the muscles with electrical stimulation has been known to produce rapid fatigue of the activated muscles (Bogey and Hornby, 2007). As muscles fatigue, the preset stimulation amplitudes would no longer suffice. The fatigue compensation rule in this study recognized a gradual decrease in muscle strength over a prolonged period of time and increased stimulation amplitudes to compensate and maintain force production. The fatigue rule was limited by maximal safe stimulation amplitudes. However, this solution did not address differential fatigue where different muscles fatigue at different rates and cause much larger disruptions in a control system (Godfrey *et al.*, 2002). Eventually, the experiments were terminated when safe stimulation limits were reached without producing adequate force. Alternative stimulation methods such as intraspinal microstimulation (ISMS) are more fatigue resistant and require a less demanding fatigue compensation rule (Lau *et al.*, 2007).

The swing-to-stance transition was designed to limit excess time spent in the swing phase to optimize the walking cycle. The rule activates if the leg adequately reaches its range of flexion, thereby eliminating excess swing time and speeding up the walking cycle. As a secondary benefit, the truncated swing phase allowed for more time in contact with the ground and more force overlap between limbs.

The implemented hybrid-CPG controller does have some limitations in its present configuration. Currently, the IF-THEN rule thresholds are set manually by the operator. Incorrect threshold levels can cause the controller to become unstable (often by inappropriately activating rules if the thresholds are prematurely reached). If thresholds are set too leniently, rules never activate compromising the safety and the adaptability of the controller. Moreover, the fatigue compensation rule would prove more effective if adaptive stimulation amplitudes were used across all sub-states rather than only the E2 sub-state as currently implemented. In addition, the effectiveness of the limb angle calculations could be improved through more accurate corrections for high frequency noise (accelerometers) and drift (gyroscopes) in the signals. The controller utilizes a single sensory signal as input to a rule. More complex rules utilizing multiple signals would better emulate the natural control of walking. Nonetheless, the general design of the locomotion control algorithm provides the capabilities to perform these corrections with relative ease through the inclusion of additional states and sensory transitions. By adapting the controller to different stimulation modalities and new sensory inputs, the algorithm could improve walking in a variety of applications.

Conclusions and Future Work

The work presented here demonstrates our ability to create a reconfigurable control algorithm for realizing different stimulation paradigms to create functional walking movements in multiple joints. The implemented hybrid-CPG controller was capable of adapting to different environmental perturbations while maintaining sufficient GRF to support the body weight of the animal. Through the *in vivo* over-ground walking trials, the combination of open and closed loop control produced the most effective walking and most successful steps.

For the next stage in development, we will implement the software algorithm in a hardware-based model using mixed signal VLSI circuitry. The chip will be tested *in vivo* and the results will be compared to those obtained by the software controller. The silicone controller will be flexible enough to allow additional rules and utilize a variety of input and output stages. Moreover, the output will be capable of driving other modalities of functional electrical stimulation. Specifically, we will replace intramuscular stimulation with ISMS and external sensors with recordings from the dorsal root ganglia to allow the internalization of the prosthetic device. Eventually, we hope to develop a compact and fully implantable walking prosthesis.

FIGURES

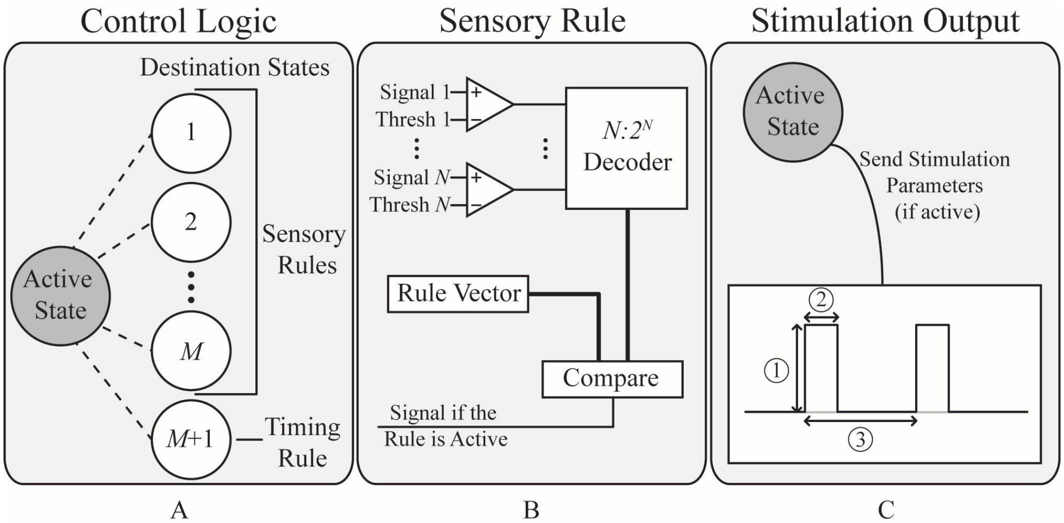

Figure 2-1. Overview of the components of the locomotion control algorithm. (A) The control logic consisted of an active state and several destination states. One of the destination states was specified by the pre-set timing rules while the remaining states were specified by certain sensory rules. (B) Each sensory rule consisted of a number of sensory input signals and programmable thresholds which were decoded and corresponded to specific logic functions. If the output of the comparators matched one of the desired output functions, a signal was passed to the control unit to indicate that the rule was active. (C) Each active state contained information about all stimulation output waveforms and whether each output was active or not. The stimulation (1) amplitude, (2) pulse width, and (3) frequency were all specified by the active state and were adjusted to produce shaped waveforms.

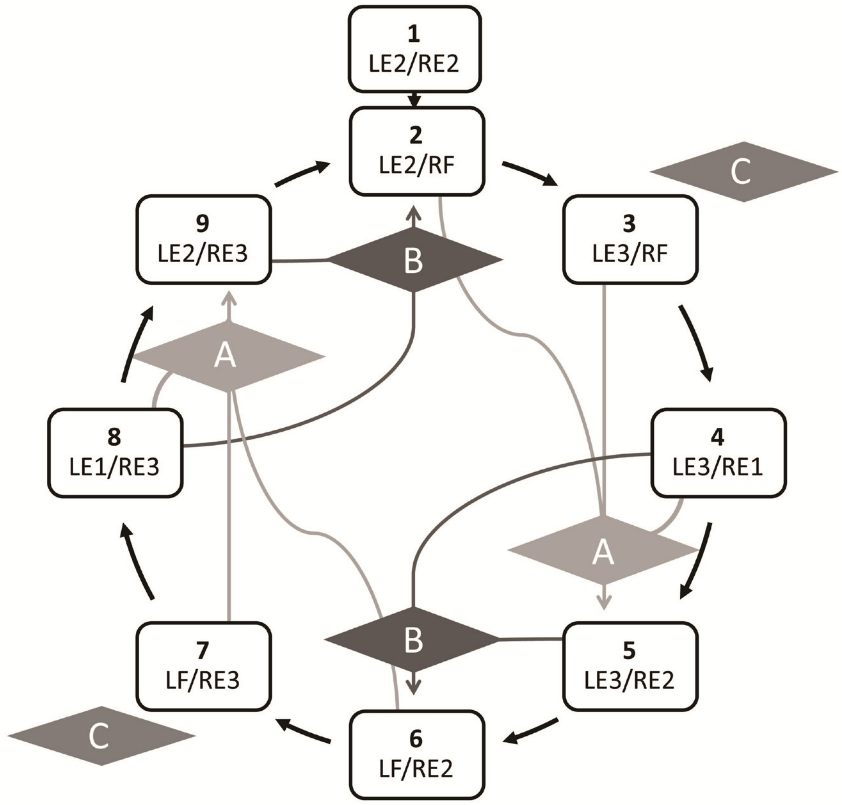

Figure 2-2. Overview of the states for the open loop controller and hybrid-CPG controller. Each controller state represents two sub-states corresponding to a portion of the step cycle in each leg. The sub-state definitions are as follows: F, flexion; E1, foot placement; E2, support; and E3, push-off. The cat enters LE2/RF (state 2 with the left (L) cat leg is in E2 and the right (R) leg is in F) and advances through the step cycle based on preset timing or activated sensory rules. Both controllers begin a trial in double stance (state 1) denoted by LE2/RE2 for the left and right legs, respectively. Black arrows symbolize intrinsically timed transitions used for both controllers. Grey diamonds denote sensory feedback rules and their respective pathways for both legs with the rules as follows: Swing-to-Stance (A), Stance-to-Swing (B), and Fatigue Compensation (C). The sensory rules were only applicable to the hybrid-CPG controller.

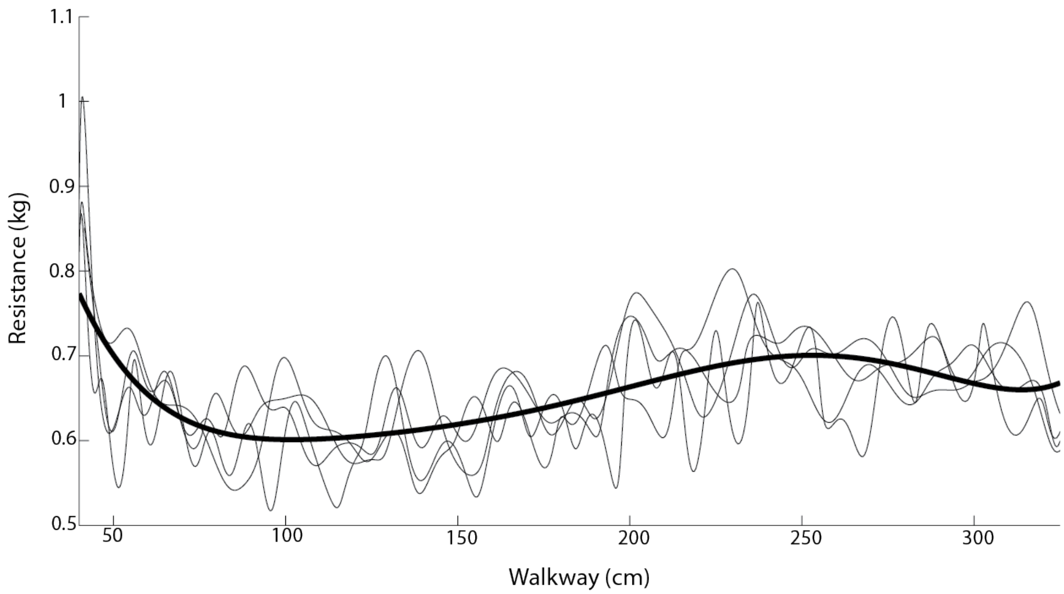

Figure 2-3. Resistance profile of the walkway. The cart was loaded with 5.5kg to represent the combined weight of a cat and equipment during an experiment. The force required to move the cart was measured over 4 trials (light traces) and fitted with a trend line (bold line) to represent the resistance profile of the walkway. The initial peak resistance was required to overcome static friction.

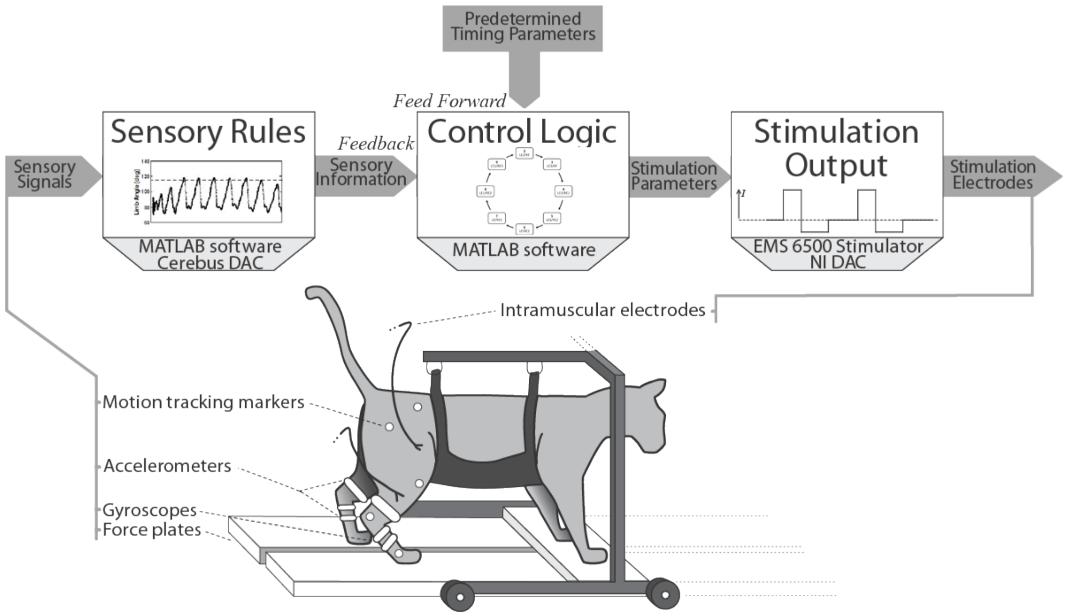

Figure 2-4. Experimental setup. The anesthetized cat was suspended in a cart mounted sling over a walkway and the right hind limb was videotaped for motion tracking. Intramuscular stimulation electrodes activated the hind limbs to propel the cat along the walkway. Sensory feedback was provided by accelerometers, gyroscopes and force plates. These sensory signals were used in the hybrid-CPG controller for different feedback rules based on appropriate threshold values. If activated, the feedback rules overrode the timing rules and allowed the hybrid-CPG controller to adjust the stimulation output. The signals were digitized using a Cerebus (BrainGate Co. LLC, Ponte Verdra Beach, FL, USA) ADC and streamed into custom Matlab (MathWorks Inc., Natick, MA, USA) software which utilized National Instruments (National Instruments Corp., Austin, TX, USA) DAC to send stimulation parameters to modified EMS 6500 stimulators.

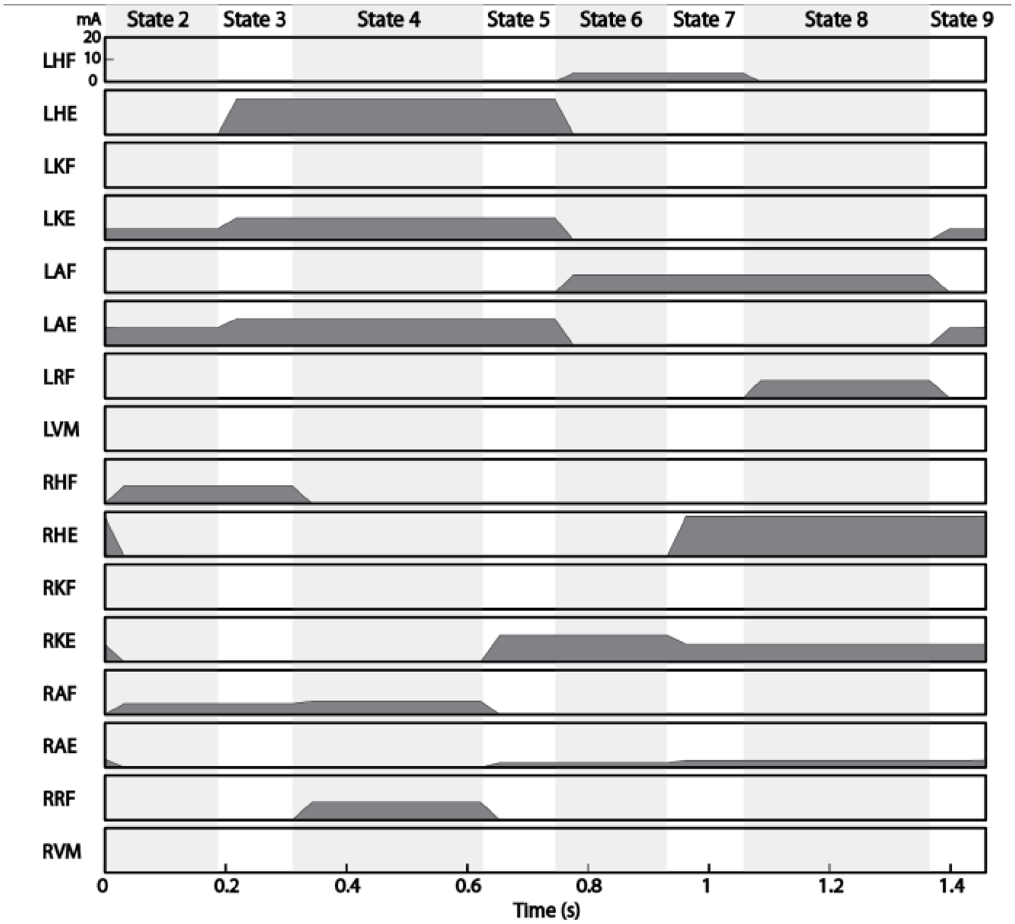

Figure 2-5. Typical stimulation amplitudes across one step cycle. Each channel is shown with its stimulation amplitudes and duration in grey. Some ramping occurs at the onset and offset of a channel's activation. Vertical shading shows the timing and duration of the states within the walking cycle. Vastus medialis and semitendinosus could not be targeted in this animal and have been disabled for the experiment. LHF= left hip flexor= sartorius (anterior compartment), LHE= left hip extensor= semimembranosus (anterior compartment), LKF= left knee flexor= semitendinosus, LKE= left knee extensor= vastus lateralis, LAF= left ankle flexor= tibialis anterior, LAE= left ankle extensor= gastrocnemius, LRF= left rectus femoris, LVM= left vastus medialis. The last 8 channels are the equivalent muscles for the right side.

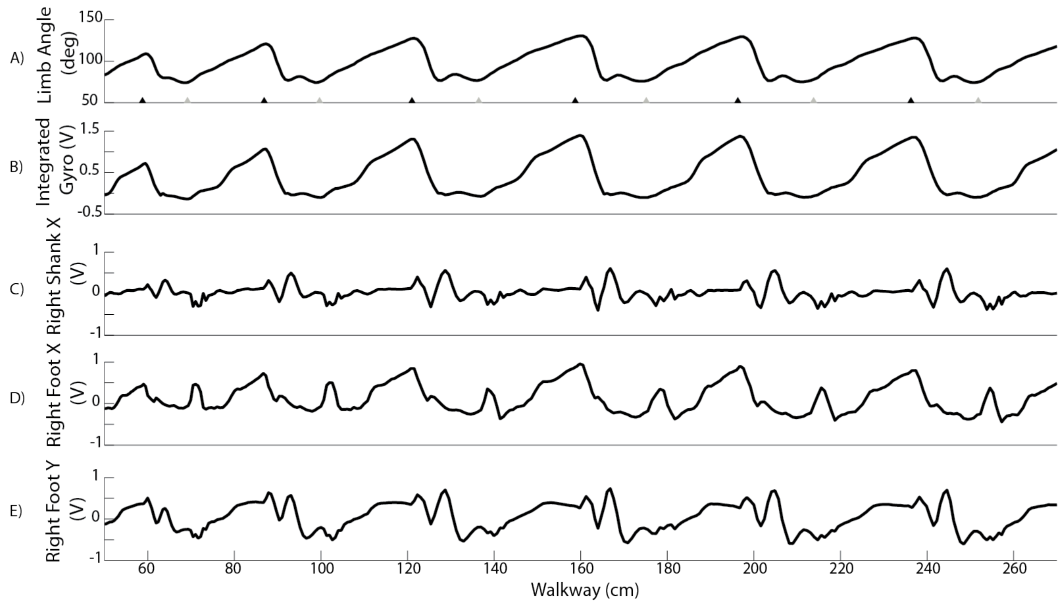

Figure 2-6. Traces of sensory signals from one trial involving the open loop controller. A) Limb angle (vector from the hip to the metatarsophalangeal joint) obtained from video capture. Paw touchdown is shown with grey triangles and lift off is shown with black triangles. B) Integrated gyroscope signal representing the limb angle. (C-E) Accelerometer signals on the shank (X direction) and the foot (X and Y directions).

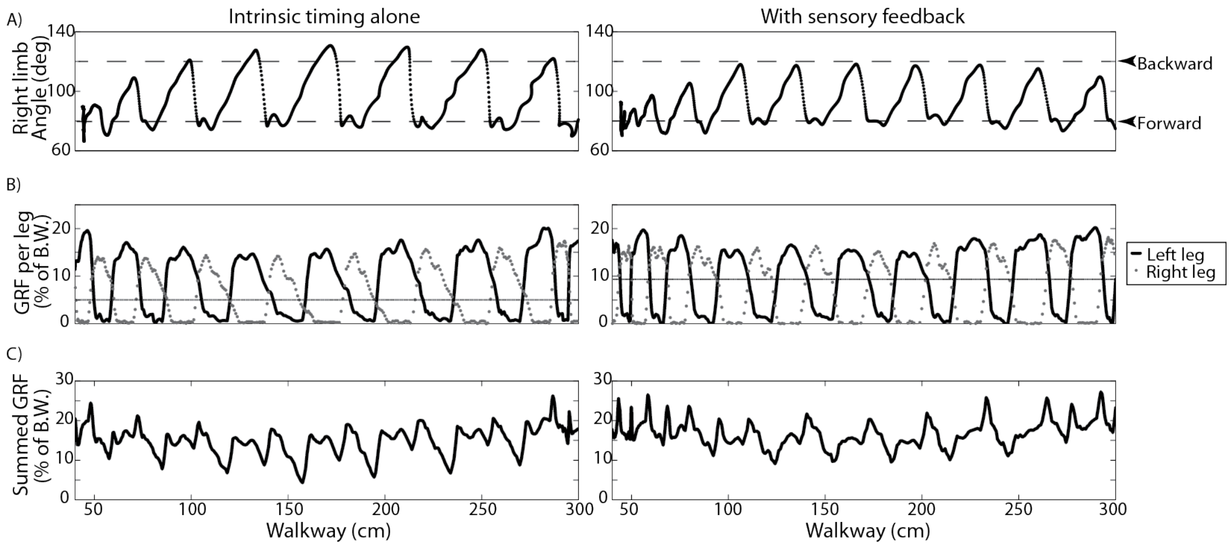

Figure 2-7. Comparison of limb excursion and GRF in trials with the open loop (left) and hybrid-CPG (right) controllers. A) The limb angles of right leg from video capture. Increasing angle corresponds to the leg moving forward; decreasing angle corresponds to the leg moving backward. B) GRF of right and left hind legs where the black trace represents forces from the left leg and the gray trace represents the right leg. C) Summation of GRFs from both hind legs.

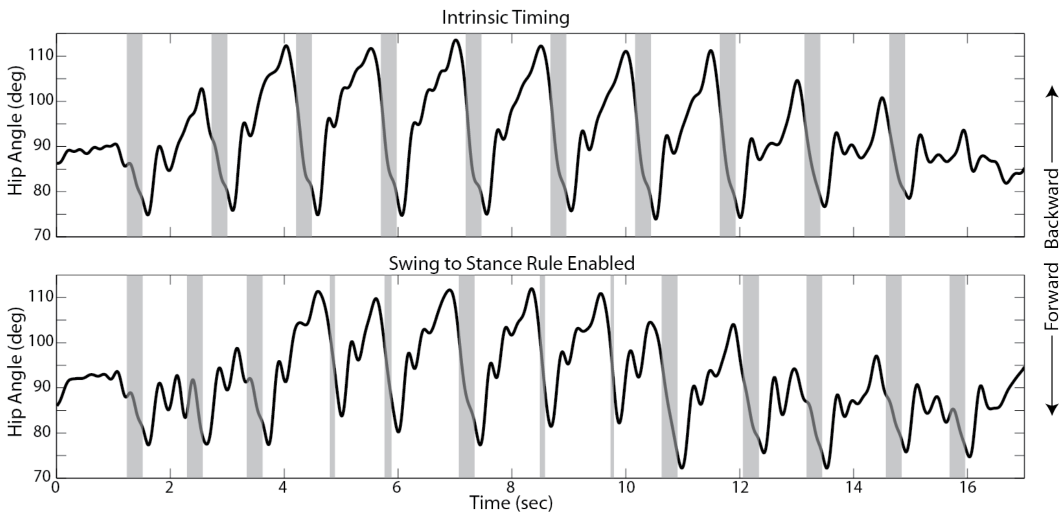

Figure 2-8. Effect of swing-to-stance rule on hip angle. A) Hip angle with open loop control alone from video capture. Swing phases (F and E1) are highlighted in grey. B) Hip angle with the addition of swing-to-stance rule truncates excess swing phase while maintaining proper hip range of motion.

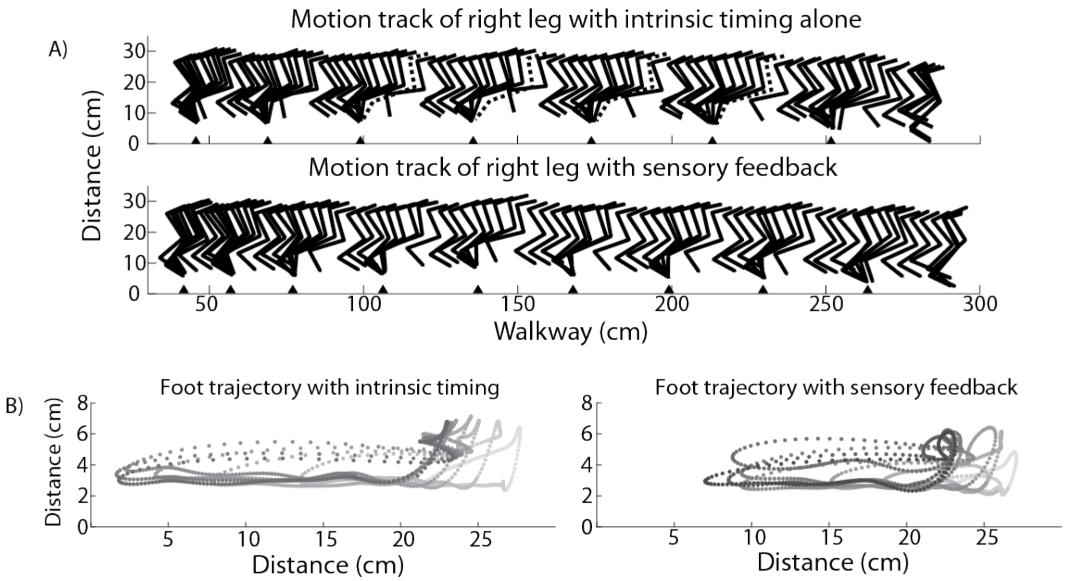

Figure 2-9. Motion tracking data and foot trajectory for trials with and without sensory feedback: A) Stick figure representation of the right hind leg from video capture (direction of movement is towards the right). Black triangles mark the beginning of steps. Upper panel: With open loop control alone, regions of hyperextension are evident. Dotted stick figures show whole leg hyperextension. Lower panel: With sensory feedback the regions of hyperextension are eliminated. B) Foot trajectories of multiple steps overlaid with respect to the hip marker from trials shown in A. Steps are drawn with increasing darkness of grey as the trial progressed. Left panel: Large backward hyperextension without sensory feedback. Right panel: Sensory feedback reduces backward hyperextension.

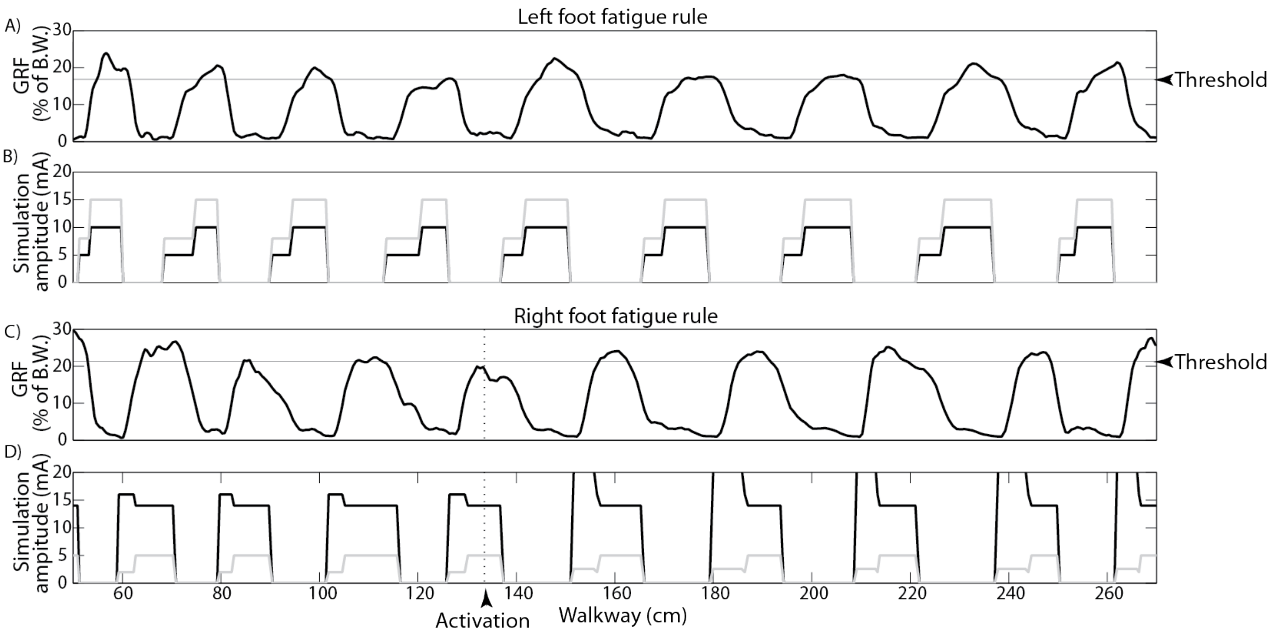

Figure 2-10. Effect of the fatigue compensation rule on force production during a single trial: A) GRF of left hind leg and threshold for activation of the fatigue compensation rule if the supportive force drops below the threshold (grey dashed line) for a prolonged period of time. B) Stimulation amplitudes on two different extensor electrodes (knee in black and ankle in grey) during the stance phase (E2 and E3). C) Similar to A) but for the right hind leg. The black, vertical dashed line shows activation of the rule due to prolonged sub-threshold force production in stance. Force increases to acceptable levels on the remaining steps. D) Similar to B) but stimulation amplitudes for right side extensor electrodes (knee and ankle) increase in E2 by 30% (to a maximum of 20 mA) on steps following rule activation. Only the knee extension received an increase in amplitude because maintaining appropriate posture was difficult when ankle extension was increased during the stance phase.

Table 2-1. Flexor and extensor muscles active during each state of the step cycle.

Step Cycle State	Flexion	Extension
F	Hip, knee, ankle	None
E1	Hip, ankle	Knee
E2	None	Knee, ankle
E3	None	Hip, knee, ankle

Table 2-2. Average joint angles measured during single trials with and without sensory feedback (walking at approximately 0.25m/s). The values were measured in degrees with the ratio of measured joint angles to typical joint angles (walking at 0.67 m/s).

Joint Angle Range (typical)	Open Loop Controller (Ratio)	Hybrid-CPG Controller (Ratio)
Hip (49)	27 (0.55)	24 (0.49)
Knee (38)	43 (1.1)	39 (1.0)
Ankle (45)	96 (2.1)	68 (1.5)

Table 2-3. Summary of 74 trials in which cats walked 75% of the walkway.

Walking Property		Open Loop Controller	Hybrid-CPG Controller	*P*-Values
Trial-Based		*N=18*	*N=56*	
Peak Step Length [a]	*Mean ± SD* [c]	24.9 ± 8.4	21.8 ± 7.5	.06 [e]
Average Velocity	*Mean ± SD* [c]	0.22 ± 0.04 m/s	0.21 ± 0.05 m/s	.62 [e]
Number of Steps [b]	*Median* [d] *(Q1,Q3)*	7 (6, 9)	9 (8, 11)	.024 [f]
Sum of Forces	*Median* [d] *(Q1,Q3)*	15.1% BW (14.3, 18.7)	18.4 % BW (16.1, 20.0)	.10 [f]
Step-Based		*N=134*	*N=544*	
Step Cycle Duration [b]	*Median* [d] *(Q1,Q3)*	1.48 s (1.48, 1.49)	1.27 s (1.15, 1.49)	<.001 [f]
Peak Step Force	*Median* [d] *(Q1,Q3)*	17.1% BW (14.7, 20.3)	17.0 % BW (14.8, 20.1)	.69 [f]
Successful Steps	(%) (success/total)	49% (65/134)	68% (372/544)	

[a] Step length was normalized against the distance from the ankle to the metacarpophalangeal joint.

[b] Significant difference between trials with open loop control alone and with combined open and closed loop control.

[c] The means and standard deviations (SD) are shown for normally distributed data.

[d] The medians and 1st and 3rd quartiles (Q1,Q3) are shown for non-normally distributed data.

[e] Unpaired student's t-test was used for normally distributed data.

[f] Independent Samples Median Test (non-parametric) was used for non-normally distributed data

BW= Body weight

References

Archambault P S, Deliagina T G and Orlovsky G N 2001 Non-undulatory locomotion in the lamprey *Neuroreport* **12** 1803-7

Berniker M, Jarc A, Bizzi E and Tresch M C 2009 Simplified and effective motor control based on muscle synergies to exploit musculoskeletal dynamics *Proc Natl Acad Sci U S A* **106** 7601-6

Bogey R and Hornby G T 2007 Gait training strategies utilized in poststroke rehabilitation: are we really making a difference? *Top Stroke Rehabil* **14** 1-8

Brown T G 1914 On the Nature of the Fundamental Activity of the Nervous Centres; Together with an Analysis of the Conditioning of Rhythmic Activity in Progression, and a Theory of the Evolution of Function in the Nervous System *Journal of Physiology* **48** 18-46

Burke R E, Degtyarenko A M and Simon E S 2001 Patterns of locomotor drive to motoneurons and last-order interneurons: clues to the structure of the CPG *Journal of Neurophysiology* **86** 447-62

Conway B A, Hultborn H and Kiehn O 1987 Proprioceptive input resets central locomotor rhythm in the spinal cat *Experimental Brain Research* **68** 643-56

Crago P E, Lan N, Veltink P H, Abbas J J and Kantor C 1996 New control strategies for neuroprosthetic systems *J Rehabil Res Dev* **33** 158-72

Dejnabadi H, Jolles B M, Casanova E, Fua P and Aminian K 2006 Estimation and visualization of sagittal kinematics of lower limbs orientation using body-fixed sensors *IEEE Trans Biomed Eng* **53** 1385-93

Dick T E, Oku Y, Romaniuk J R and Cherniack N S 1993 Interaction between central pattern generators for breathing and swallowing in the cat *J Physiol* **465** 715-30

Ekeberg O and Pearson K 2005 Computer simulation of stepping in the hind legs of the cat: an examination of mechanisms regulating the stance-to-swing transition *J Neurophysiol* **94** 4256-68

Godfrey S, Butler J E, Griffin L and Thomas C K 2002 Differential fatigue of paralyzed thenar muscles by stimuli of different intensities *Muscle Nerve* **26** 122-31

Goslow G E, Reinking R M and Stuart D G 1973 The cat step cycle: Hind limb joint angles and muscle lengths during unrestrained locomotion *Journal of Morphology* **141** 1-41

Grillner S 1985 Neurobiological bases of rhythmic motor acts in vertebrates *Science* **228** 143-9

Grillner S and Matsushima T 1991 The neural network underlying locomotion in lamprey--synaptic and cellular mechanisms *Neuron* **7** 1-15

Grillner S and Zangger P 1979 On the central generation of locomotion in the low spinal cat *Experimental Brain Research* **34** 241-61

Guevremont L, Norton J A and Mushahwar V K 2007a Physiologically Based Controller for Generating Overground Locomotion Using Functional Electrical Stimulation *Journal of Neurophysiology* **97** 2499-510

Guevremont L, Norton J A and Mushahwar V K 2007b Physiologically based controller for generating overground locomotion using functional electrical stimulation *J Neurophysiol* **97** 2499-510

Halbertsma J M 1983 The stride cycle of the cat: the modelling of locomotion by computerized analysis of automatic recordings *Acta Physiol Scand Suppl* **521** 1-75

Hiebert G W and Pearson K G 1999 Contribution of sensory feedback to the generation of extensor activity during walking in the decerebrate Cat *Journal of Neurophysiology* **81** 758-70

Hultborn H and Nielsen J B 2007 Spinal control of locomotion--from cat to man *Acta Physiol (Oxf)* **189** 111-21

Islam S S, Zelenin P V, Orlovsky G N, Grillner S and Deliagina T G 2006 Pattern of motor coordination underlying backward swimming in the lamprey *Journal of Neurophysiology* **96** 451-60

Kiehn O 2006 Locomotor circuits in the mammalian spinal cord *Annu Rev Neurosci* **29** 279-306

Kobetic R, Triolo R J and Marsolais E B 1997 Muscle selection and walking performance of multichannel FES systems for ambulation in paraplegia *IEEE Trans Rehabil Eng* **5** 23-9

Lau B, Guevremont L and Mushahwar V K 2007 Strategies for generating prolonged functional standing using intramuscular stimulation or intraspinal microstimulation *IEEE Trans Neural Syst Rehabil Eng* **15** 273-85

Mazurek K, Holinski B J, Everaert D G, Stein R B, Mushahwar V K and Etienne-Cummings R 2010 Locomotion Processing Unit *Proceedings of IEEE Biomedical Circuits and Systems Conference (BIOCAS), Paphos, Cyprus*

Mazurek K A and Etienne-Cummings R 2011 Implementation of Functional Components of the Locomotion Processing Unit *Proceedings of IEEE Biomedical Circuits and Systems Conference (BIOCAS), San Diego, California USA*

McCrea D A and Rybak I A 2007 Modeling the mammalian locomotor CPG: insights from mistakes and perturbations *Prog Brain Res* **165** 235-53

McCrea D A and Rybak I A 2008 Organization of mammalian locomotor rhythm and pattern generation *Brain Res Rev* **57** 134-46

Mealy G H 1955 A Method for Synthesizing Sequential Circuits *At&T Tech J* **34** 1045-79

Mentel T, Krause A, Pabst M, El Manira A and Buschges A 2006 Activity of fin muscles and fin motoneurons during swimming motor pattern in the lamprey *European Journal of Neuroscience* **23** 2012-26

Nilsson J, Thorstensson A and Halbertsma J 1985 Changes in leg movements and muscle activity with speed of locomotion and mode of progression in humans *Acta Physiologica Scandinavica* **123** 457-75

Prilutsky B I, Herzog W and Allinger T L 1996 Mechanical power and work of cat soleus, gastrocnemius and plantaris muscles during locomotion: possible functional significance of muscle design and force patterns *Journal of Experimental Biology* **199** 801-14

Prochazka A, Gritsenko V and Yakovenko S 2002 Sensory control of locomotion: reflexes versus higher-level control *Adv Exp Med Biol* **508** 357-67

Quintero H A, Farris R J, Durfee W K and Goldfarb M 2010 Feasibility of a Hybrid-FES System for Gait Restoration in Paraplegics *2010 Annual International Conference of the Ieee Engineering in Medicine and Biology Society (Embc)* 483-6

Rossignol S, Dubuc R and Gossard J P 2006 Dynamic sensorimotor interactions in locomotion *Physiol Rev* **86** 89-154

Saigal R, Renzi C and Mushahwar V K 2004 Intraspinal microstimulation generates functional movements after spinal-cord injury *IEEE Trans Neural Syst Rehabil Eng* **12** 430-40

Strange K D and Hoffer J A 1999 Restoration of use of paralyzed limb muscles using sensory nerve signals for state control of FES-assisted walking *IEEE Trans Rehabil Eng* **7** 289-300

Sweeney P C, Lyons G M and Veltink P H 2000 Finite state control of functional electrical stimulation for the rehabilitation of gait *Med Biol Eng Comput* **38** 121-6

Thrasher T A and Popovic M R 2008 Functional electrical stimulation of walking: function, exercise and rehabilitation *Ann Readapt Med Phys* **51** 452-60

Tomovic R and Mcghee R B 1966 A Finite State Approach to Synthesis of Bioengineering Control Systems *Ieee Trans Hum Fact* **Hfe7** 65-&

Vogelstein R J, Tenore F V G, Guevremont L, Etienne-Cummings R and Mushahwar V K 2008 A Silicon Central Pattern Generator Controls Locomotion in Vivo *IEEE Transactions onf Biomedical Circuits and Systems* **2** 212-22

Yakovenko S 2011 A hierarchical perspective on rhythm generation for locomotor control *Prog Brain Res* **188** 151-66

Yamaguchi T 2004 The central pattern generator for forelimb locomotion in the cat *Prog Brain Res* **143** 115-22

Yang J F and Winter D A 1985 Surface EMG profiles during different walking cadences in humans *Electroencephalography and Clinical Neurophysiology* **60** 485-91

Chapter 3: Intraspinal Microstimulation for Restoring Walking

Introduction

Spinal cord injury is estimated to affect 1.3 million people in the U.S.A.[1] Regaining the ability to walk is a high priority for people with paraplegia that can improve their quality of life.[2,3] Efforts to restore walking after spinal cord injury to date have had limited success.[4-6] Regeneration of the damaged neural pathways through biological bridging approaches may be the ultimate solution to restore walking function, but to date promising results in animals have not yet translated into successful human applications.[5,7,8] In the meantime, the field of biomedical engineering has also developed several approaches to restore walking, including electrical stimulation and exoskeletons. [9-11] Epidural electrical stimulation (in combination with treadmill training) applied to the dorsal surface of the spinal cord improved the rhythm of walking and decreased the sense of effort during walking in a study volunteer with incomplete spinal cord injury. [12,13] More recently, Harkema *et al.* demonstrated some restoration of voluntary leg control in a person with a more severe spinal cord injury by using a combined treatment of rigorous treadmill training and epidural stimulation. [14] However, both of these applications of epidural stimulation produced stepping and locomotor-like patterns but not the strong, weight bearing forces needed for functional walking. Functional electrical stimulation (FES) in which patterned electrical stimuli are applied to the peripheral nervous system (nerves or neuromuscular junctions) has been able to produce sufficient muscle contractions with forces adequate for walking in people with spinal cord injury, while using a walker or crutches to maintain balance. [9,10,15-17]

However, walking distance has been limited to approximately 100 m with current FES systems due to the rapid muscle fatigue associated with peripheral stimulation through surface or implanted electrodes, which tends to stimulate large, fast fatigable muscle fibers first. [9,18] Although the use of FES may provide additional health benefits to the user such as increased muscle mass and strength and improved cardiovascular fitness, the short walking distances have limited the clinical acceptance of FES for walking. [15,19,20]

Alternatively, powered exoskeletons can restore walking by moving the paralyzed legs with motors which allow for coordinated control of multiple joints. [11,21,22] The energy capacity of the batteries powering the motors limits the walking range of powered exoskeletons. [23] The limited walking range along with the bulkiness of the systems limits the usefulness of exoskeletons in daily life.

In this work, we use a novel method of FES to restore walking-like movements called intraspinal microstimulation (ISMS). This approach entails the implantation of a few ultrafine, hair-like wires with exposed tips targeting the ventral horn in the small, lumbosacral region of the spinal cord. Passing minute electrical currents through these wires activates spinal networks below the level of a lesion. We have shown that ISMS through individual wires produces single joint as well as coordinated multi-joint synergistic movements with relatively low current amplitudes. [24-26] Furthermore, ISMS activates the motoneurons trans-synaptically; thus recruiting motor units in a near normal physiological order starting with the small, fatigue resistant muscle fibers. [26] Previous work demonstrated that cats can maintain a weight bearing standing posture for significantly longer durations when muscle contractions are evoked with ISMS than with intramuscular stimulation.[27]

This paper represents the first study in which ISMS was used to generate over-ground walking-like movements. We show the quality and duration of the over-ground walking produced by ISMS in cats during acute (1-day long) experiments. We also show that a single integrated circuit capable of providing control and stimulation, similar to that of a larger desktop system, produced similar outcomes. This work demonstrates the strong potential of ISMS as a means for restoring functional walking after spinal cord injury in the future.

ISMS TARGETS MOTONEURON POOLS IN THE VENTRAL HORN

Microwire electrodes were implanted in 5 cats with the tips targeting the motoneuron pools in the ventral horn of the lumbosacral enlargement of the spinal cord (a 3 cm-long region in cats and 5 cm-long in humans). Functional limb movements have consistently been produced with ISMS through electrodes with tips implanted deep in this portion of the gray matter. [28,29] Even with tips located in the ventral horn, ISMS mainly activates networks of spinal neurons rather than motoneurons directly, and often results in whole-limb extensor or flexor synergies (e.g. hip, knee and ankle extension or flexion combined) [21,23,25] A complete step cycle can typically be produced by stimulating through as few as 4 microwire electrodes per side. Nonetheless, in these experiments, each cat was implanted with a total of 24 microwire electrodes in both sides of the spinal cord (12 per side). The implanted electrode arrays were arranged such that ISMS through each of 3 adjacent electrodes in one side of the cord produced a similar primary synergistic movement in the ipsilateral hind limb (upward, forward, downward or backward). This redundancy improved the reliability of the implant and the repeatability of evoked movements. Due to the availability of 8 stimulation channels for each side of the spinal cord, 2 of the 3 electrodes producing similar synergistic movements were chosen for generating walking patterns in each experiment (except Cat A where a second ankle flexion could not be found, therefore, it was replaced with an additional full limb extensor synergy). Tip locations were verified using magnetic resonance imaging (MRI) of the extracted spinal cords post-mortem. Figure 3-1A summarizes the electrode tip locations with respect to the gray matter. Locations are coloured according to the primary synergistic limb movement elicited by ISMS: hip flexion (forward), ankle flexion (upward), knee extension (downward), and full limb extensor synergy (backward). More information regarding target locations and the layout of the motoneuron pools are published elsewhere.[30-33] On average, 11 of the 16 electrodes used for producing over-ground walking in each cat had tips positioned within the ventral gray matter (Cats A: 15/16, B: 10/16, C: 10/16, D: 8/16, E: 12/16). The tips of all remaining electrodes were within 0.8 mm of the lateral and ventral boundary of the ventral gray. These electrodes probably activated gray matter networks as electrodes models suggest that all electrodes activate approximately a 1mm spherical diameter.[34,35]

ISMS PRODUCED FUNCTIONAL OVER-GROUND WALKING-LIKE MOVEMENTS

Five anaesthetized cats implanted with ISMS microwire electrodes were each suspended partially in a cart-mounted sling that supported their head, forelimbs, trunk and abdomen but allowed free movement of the hind limbs (figure 3-1B). The timing and amplitude of ISMS through pairs of electrodes producing similar upward, forward, downward or backward movements was patterned using a physiologically-based state controller. The controller incorporated flexor-extensor timing elements that mimicked the oscillatory activity of the locomotor central pattern generator (CPG) as well as sensory-driven modulations.[36,37] The goal of the experiments was to produce weight-bearing and propulsive walking-like movements of the hind limbs that are capable of pushing the cat across a 2.9 m-long walkway as many times as possible and up to 300 times. The quality of walking-like movements produced by ISMS was evaluated by comparing the kinematics and kinetics to those of freely walking cats published in the literature. Results from a trial near the end of an experiment at which point the cat (Cat E) had already performed 281 successful trials and "walked" 815 m are shown in figure 3-2. In this trial, the maximal force output that the animal could still produce even after more than 800 m of "walking" was tested by increasing the resistance to the cart. The stimulation amplitudes were increased to the maximal safe limits, which was about 30% higher than during the previous trials without the added cart resistance (average current: 59 μA; pulse width: 290 μs, frequency: 62 Hz). Stick figure representations of the right hind limb at 125 ms intervals produced from video recordings during the trial are shown in figure 3-2A. The stride length ranged from 123 mm to 179 mm depending on the variable resistance between the walkway railings and suspension cart during a given trial. The average stride length for the trial (153 ± 15 mm) was less than the values reported in the literature for freely waking cats (200 mm).[38] The shorter hind limb stride lengths were possibly due to the slower walking speed of 0.12 m/s in our experiment compared to 0.20 m/s for the values reported in the literature (as stride length decreases with walking speed) [38] and the bipedal only (hind limb) "walking" in our experiments. The average peak ground clearance of the paw was 10.3 ± 3.6 mm, which was functional, but less than the 16mm clearance reported for natural walking.[39] The radius and angle of the hind limb segment (vector from hip to metatarsophalangeal

(MTP) joint) plotted over time) are shown in figure 3-2 B-C. The limb angle reached a maximal backward excursion (from forward horizontal, measured clockwise) of 127° which was comparable to the 130° reference value.[40]

In addition to appropriate kinematics, successful over-ground walking requires sufficient supportive and propulsive forces. Figure 3-2D depicts the traces of the left and right supportive forces (vertical). The average peak supportive force generated during the stance phase was 5.2N and 6.0N for the left and right legs, respectively, and the mean vertical force was 3.0N f and 3.7N, respectively. Due to the experimental set-up in which the sling supported the quiescent abdomen, the measured supportive forces reflected the weight bearing level of the hind legs, and not the hindquarters (which include the abdomen). Therefore, while lower than the weight normally supported by the hind quarters of a cat (46% of the bodyweight during quiet stance), the supportive forces produced full weight-bearing of the hind legs during stance. [41] Regions of double stance (both limbs on the ground) allowed for safe transitions from the swing phase of one leg to the other during “walking”, which minimized the risk of falling. The average duration of double stance was 22% of the walking cycle compared to 20% of the walking cycle reported for naturally walking cats at similar speeds.[39] During these regions of double stance, the mean total supportive force was 4.8N. As expected, the propulsive forces (parallel to the direction of walking) for each leg were larger than the supportive forces (figure 3-2E). The peak propulsive forces averaged across all steps taken within this trial reached 12.0N and 14.4N for the left and right legs, respectively. This was adequate for the cat to propel itself and the resistive cart across the walkway.

To evaluate intralimb co-ordination, video recordings of the hind limb joint angles were plotted in angle-angle plots. These graphs depict the intersegmental coupling of joint angles and enable analysis of the consistency of walking-like movements across consecutive steps by calculating the angular component of the coefficient of correspondence (ACC).[42,43] The ACC has a range of 0 to 1 where 0 implies no consistency and 1 is complete consistency between step cycles. Plots of the hip-knee and hip-ankle angle are shown in figure 3-2F with each step shown in a different colour. Angle-angle plots from records of an intact cat freely walking on a treadmill are shown in figure 3-2G (naïve treadmill). The ACC value for hip-knee in Cat E was 0.67 (compared to normal=0.72) and for hip-ankle 0.79 (normal= 0.70), indicating that intralimb coordination was consistent throughout the steps of the trial, and that the consistency was similar to that seen in normal walking. The area of the angle-angle cyclogram represents the conjoint range of joint movements and was 0.49 (normal=1.47) for hip-knee and 1.41 (normal= 1.12) for hip-ankle.[44] The deviations from normal data were due to a decreased hip range and an increased ankle range, which was likely caused by mechanical restrictions of the supporting sling. Overall, ISMS produced co-ordinated multi-joint movements that maintained similar kinematic relationships to that of a freely walking cat, and sufficient forces and limb movements to propel the animal and cart adequately over ground.

ISMS PRODUCED FATIGUE-RESISTANT MOVEMENTS

We next studied the changes in kinematics and kinetics over long periods of walking-like movements to quantify the consistency and rate of change in parameters. Figure 3-3 shows kinematic parameters from Cat E which performed a total of 300 “walking” trials during the experiment. All stimulation parameters were held constant for the first 133 successful trials (385m) of the experiment to evaluate changes due to muscle fatigue.

Linear regression was performed on these 133 trials to determine if there was a significant relationship between trial number and several of the outcome walking variables. The top, middle, and bottom panels of figure 3-3A show the average hip, knee and ankle ranges per trial. Over 385m of walking-like movements, the hip and knee joint ranges did not show a significant correlation with time. However, there was a significant negative relationship between trial number and ankle joint range ($p<.001$, $r^2=.36$), ground clearance ($p<.001$, $r^2=.19$), and stride length ($p<.001$, $r^2=.49$), indicating that these variables decreased in value over time (figure 3-3 B-C). The predicted ankle joint range decreased from 74.8 to 65.0° after 133 trials (a difference of 13%), average ground clearance from 12.6mm to 9.75 mm (23%), and average stride length from 192mm to 161mm (16%).

The angle-angle plots are shown in figure 3-3D for a trial near the beginning and one near the end of the constant stimulation period to evaluate the changes in intralimb coordination. The first panel shows the hip-knee plot with an ACC of 0.58 for the early trial. In the second panel after walking 325m, the ACC is 0.56. Similarly, in figure 3-3E angle-angle plots are shown for the hip-ankle relationship with an ACC of 0.68 for both the early and the late trial. Overall, movements produced by ISMS showed little degradation in multi-joint co-ordination over extended periods of “walking”.

Changes in supportive forces were also analyzed. Figure 3-4 shows the average peak left and right supportive forces (normalized to the average of the first 5 trials) across the entire experiment in Cat E, which included the constant stimulation period, trials with the LPU, and trials with changing stimulation parameters. The supportive forces showed a significant negative relationship with trial number (Left, $r^2=.17$, $p<.001$; Right, $r^2=.16$, $p<.001$) during the constant stimulation trials. Predicted forces showed a 4.8% decrease (from 93.6% to 88.8%) for the left leg, and a 5.7% decrease (from 94.3% to 88.6%) for the right leg with respect to the initial values over a distance of 385m. By linearly extrapolating the force decay, the cat would be able to "walk" for approximately 3000m before the supportive forces would drop to 50% of their initial values. Small increases in stimulation amplitudes restored the force production back to the initial values as shown in Figure 3-4. Thus, in this cat, walking-like movements could be maintained for a total of 300 trials (longest tested) or 835m (> half a mile) with minor modifications to stimulation amplitudes.

Walking-like movements were consistent across cats

An overview of the ISMS stimulation parameters and walking outcomes for all 5 cats is presented in Table 3-1. In the first 2 cats (A and B) the electrodes produced weaker movements. Thus, higher stimulation levels were required that exceeded the reversible charge capacity of the electrodes and limited the number of "walking" trials. The remaining 3 cats (C, D, and E) all "walked" 300 trials across the walkway (maximal tested), of which at least 210 trials were considered successful during post-hoc analyses. These 3 cats "walked" between 609 m and 835m each, and their results were averaged in Table 3-1. The walking outcome variables were averaged either across trials (trial-based) or steps (step-based). Throughout the experiments, stimulation amplitudes were adjusted to ensure successful traversing of the walkway. The 'all' column shows averages of all trials for each experiment The mean values for cat C, D and E for ground clearance and stride length were respectively 9.1 ± 1.5 mm (mean ± SEM) and 128 ± 17.1 mm. Joint angle ranges were consistent between cats with average values of 23 ± 2.0°, 29 ± 0.2°, and 60 ± 5.2° for the hip, knee, and ankle, respectively. Walking-like movements were consistently powerful across cats with average peak supportive forces of 3.5 ± 0.6N and average duration for double stance of 0.8 ± 0.1s. Intralimb coordination, ACC, demonstrated that consistent multi-joint coupling during walking-like movements were obtained across cats (hip-knee: 0.6 ± 0.02, hip-ankle: 0.7 ± 0.04).

For Cats C, D and E, the walking outcome variables were averaged for the 10 first and last 10 successful trials in order to evaluate changes in "walking" capacity over the course of an experiment. Stimulation amplitudes were increased throughout the experiment for flexors (mean: 49 to 74 µA) and extensors (41 to 69 µA). Peak ground clearance and stride length decreased overall from 11 to 7 mm, and from 140 to 126 mm, respectively. Supportive forces increased from the start to the end (3.5 to 4.0 N), likely due to increases in stimulation amplitudes which were applied to maintain weight-bearing and propulsive stepping.

Implementation in an Integrated Circuit

The final objective of this study was to amalgamate the control and stimulation paradigms required for ISMS into an integrated circuit that could operate without intervention from desktop computers. [45,46] This locomotion processing unit (LPU) provided a proof-of-principle for an implantable ISMS device that could eventually translate to clinical use. The core decision making procedure of the LPU contained a programmable, state-based realization of the walking cycle similar to that implemented in software.[36] Each state of the LPU allowed for adjustments in stimulation parameters such as amplitudes and waveforms. Transitions occurred between states based on pre-determined timings or sensory feedback rules with similar capabilities to the software based controller.[36] The output of the LPU applied biphasic, cathodic leading stimulation waveforms through the ISMS electrode array to generate the desired walking-like movements. The LPU contained the software control strategy and stimulation paradigm on a chip, so it could operate as a stand-alone device without intervention from a personal computer. This is advantageous for application in over-ground walking as it provides the recipient with more mobility.

The LPU was tested in Cat E after 150 trials were performed with the full-size system. The LPU produced 42 successful trials (out of 49) equaling a “walking” distance of 121.8m. These successful trials replicated the performance of its software counterpart in producing functional over-ground walking-like movements (see Table 3-1). During these LPU trials, the mean stimulation levels of the flexor and extensor groups were 30.0 ± 3.44μA and 47.1 ± 17.30μA, respectively. This was similar to the corresponding mean stimulation levels with the full-size system (37.1 ± 10.19 μA and 51.3 ± 20.27 μA, respectively). Overall, the LPU produced ranges of movement for the hip, knee, and ankle of 23 ± 1.88°, 29.4 ± 2.29°, and 59.4 ± 4.45°, respectively, which were similar to those produced by the full-size system. The mean supportive forces for walking-like movements with the LPU were larger (2.00 ± 0.39N) than those with the full-size system (1.68 ± 0.35N); however, these higher forces did not translate into increased walking speed (0.13 ± 0.03m/s and 0.16 ± 0.02m/s for the LPU and software controller, respectively). With further adjustments of the stimulation parameters, we believe that comparable walking speeds and angles of motion to that obtained by the full-size system would be possible. Supportive forces during the LPU trials are shown in figure 3-4.

DISCUSSION

Over-ground "walking" in an anesthetized animal of over 835 m with the potential to walk even farther, was produced by ISMS through a few microwire electrodes implanted in each side of the spinal cord. ISMS elicited coordinated multi-joint movements by activating spinal networks which remain intact following spinal cord injury, and produced walking-like movements with similar kinematics to natural walking. Ranges of motion and force production remained relatively constant showing only minor decay over "walking" distances of 835m (average of 4384 steps), and were reproducible over multiple cats. The ISMS amplitudes were on average very low (< 100 µA), and adjustments in these amplitudes could compensate for gradual changes in walking. These exciting findings demonstrate, for the first time, that ISMS may be an effective approach for producing functional, weight-bearing and propulsive walking after spinal cord injury. Walking-like movements over distances that are more than 6 times longer than those achieved with currently available peripheral FES systems can be obtained. [9]

The capacity of ISMS to produce long distances of functional over-ground walking in models of spinal cord injury with long-term ISMS implants remains to be tested. Nonetheless, previous studies demonstrated that a chronic ISMS implant in animal models with intact spinal cords can function properly for 6 months (longest duration tested). [32] Moreover, short-term ISMS implants in animal models with chronic spinal cord injury demonstrated that functional, weight-bearing stepping can be produced.[30] Long-term implants in animal models of chronic spinal cord injury would ensure that ISMS could also reliably produce over ground walking movements and forces over long durations of time. Moreover, in chronically implanted preparations in which recovery from the ISMS implantation surgery would be possible, anesthesia would not be needed during the walking trials, which removes inhibitory effects associated with anesthetic agents and potentially produce even larger forces during walking with ISMS. Previous studies in which anaesthesia was not needed, ISMS was capable of producing supportive forces in excess of 20N during stance. [30,47] This more clinically relevant model may allow lower initial stimulation amplitudes to produce equivalent forces, which would further reduce muscle fatigue and increase walking distances.

The LPU integrated chip system successfully implemented the ISMS as demonstrated by the desktop system. This represented the first time that control strategies capable of using real-time sensory feedback and on board stimulators were miniaturized to a standalone chip and produced similar *in vivo* results to those produced by a full-sized desktop system. This is a key step towards realizing a wearable prosthetic device that can process the necessary sensory information to produce a time changing stimulation pattern for restoring walking. Because ISMS utilizes very low stimulation currents, it lends itself to implementation in an integrated circuit that consumes low power. The LPU consumed an average of 15.3mW during a walking cycle and can eventually be wirelessly powered and controlled through a transcutaneous induction link. With further improvements, such as an increased number of stimulation channels and a smaller device size, an implantable version of the prosthesis may provide a mobile solution for restoring walking in the future. Hopefully soon, ISMS can make the translation from the bench to the bedside and begin improving the quality of life of people with paraplegia.

Supplementary Methods

Implantation

All experimental procedures were approved by the University of Alberta's Animal Care and Use Committee. A total of 5 male intact cats (4.2-5.5 kg) were used in acute, 1 day-long, non-recovery experiments. Cats were anaesthetized with sodium pentobarbital and a laminectomy was performed on vertebrae L4 to L6 to expose spinal cord segments L4-S1. A fine-wire array consisting of 12 electrodes per side was implanted bilaterally (Pt-Ir 80-20%, 50µm diameter, 0.1mm deinsulated tip). The electrode tips were implanted to target the ventral horns of the gray matter. Maps of motoneuron pools were used to target hip and knee flexors, knee extensors and a full limb extensor synergy for each side (3 electrodes per function). [30,31,33,48]

Electrical Stimulation

The 8 electrodes per side producing the best upward, forward, downward and backward limb movements were selected and connected to a 16-channel bench-top current controlled stimulator that delivered trains of charge balanced, biphasic pulses (up to 120 µA, monophasic, 290 µs pulse width, 62 Hz). Stimulation was modified in real-time by a controller capable of adapting the intrinsic timing cycle with sensory feedback.[36] For a subset of 49 trials in Cat E, the best 7 electrodes per side were selected and connected to the LPU that contained an on-board stimulator (approximately 60Hz, 245µs pulse width, biphasic up to 120µA). The stimulation frequency was an approximation as stimulation waveforms were triggered by an integrate-and-fire neuron circuit. The stimulation output was charge balanced by matching the anodic and cathodic phase durations. The LPU's stimulation amplitudes were modified to match the movements generated by the 16 channel stimulator used for the previous "walking" trials of Cat E. For both the desktop-based system and the LPU, the step cycle duration was set to 1.5 s. Four sequential controller states (1 flexion and 3 extension states, E1, E2, and E3) each accounted for 20%, 20%, 20%, and 40%, respectively (See Mazurek et al. for details). [36]

Experimental Procedure

After implantation, the cats were transferred to an instrumented walkway and partially suspended in a cart-mounted sling and maintained under anaesthesia. Motion tracking markers were fixed to the right hind limb to record kinematics with a camcorder positioned 4.5 m away from the midpoint of the walkway with lens parallel to the walkway (120 fps, JVC Americas Corp., Wayne, NJ, USA). Markers were placed on the iliac crest, hip, knee, ankle and metatarsophalangeal joints. Force transducers mounted under the walkway plates captured independent left and right supportive (vertical) and propulsive (horizontal) forces. During the setup trials, appropriate stimulation amplitudes were established for the 4 controller states (flexion, E1, E2, and E3). Once the ISMS parameters for traverse the walkway during setup trials was established (average: 9 setup trials), data collection began and the hind limbs bilaterally propelled the cat and the cart a distance of 2.9m (the walkable length of the walkway). For the majority of the trials, the mass of the cart and equipment on it was offset by a pulley system to reduce the effect of static friction (by pulling the cart forward with about 5-10% of the cat body mass). The controller had the capability to process incoming signals from external sensors (force transducers, accelerometers and gyroscopes) in real time with a moving average filter of 120ms in Matlab (The MathWorks Inc., Natick, MA, USA). Initial experiments were terminated when the cat could no longer traverse the walkway, but as the number of trials greatly increased, experiments were terminated after 300 trials were reached. For 1 cat, the desktop-based controller and data collection hardware were replaced with a stand-alone chip (LPU) for 49 trials in the middle of the experiment.

Immediately following each experiment, the cats which were still deeply anaesthetized, were perfused intracardially with Formalin (4 % formaldehyde). The spinal cord was then extracted with the implanted array in place and imaged using magnetic resonance imaging to determine the location of the electrode tips in relationship to the gray matter.

Outcome measures

A trial was considered successful if the cat traversed the entire length of the walkway (2.9m) within 90 seconds. To account for variations in stepping when "walking" was initiated and terminated within a trial, a 2.2m section in the middle of the walkway was used for analysis. Marker positions were digitized by custom Matlab software written by Dr. Douglas Weber (University of Pittsburgh, Pittsburgh, PA, USA). Each frame was calibrated with a known set of reference markers. All kinematic parameters were calculated from the marker set and filtered using a 3Hz low pass Butterworth filter (10th degree).

The beginning of each step was indicated by touchdown on the force plate. Stepping parameters were determined for each step and averaged across a trial. Ground clearance was recalibrated for each step with respect to the walkway location to minimize tracking error. The coupling of movements between 2 joints was assessed using the angular component of the coefficient of correspondence (ACC), which was calculated according to methods described by Field-Foote *et al.* [43]

FIGURES

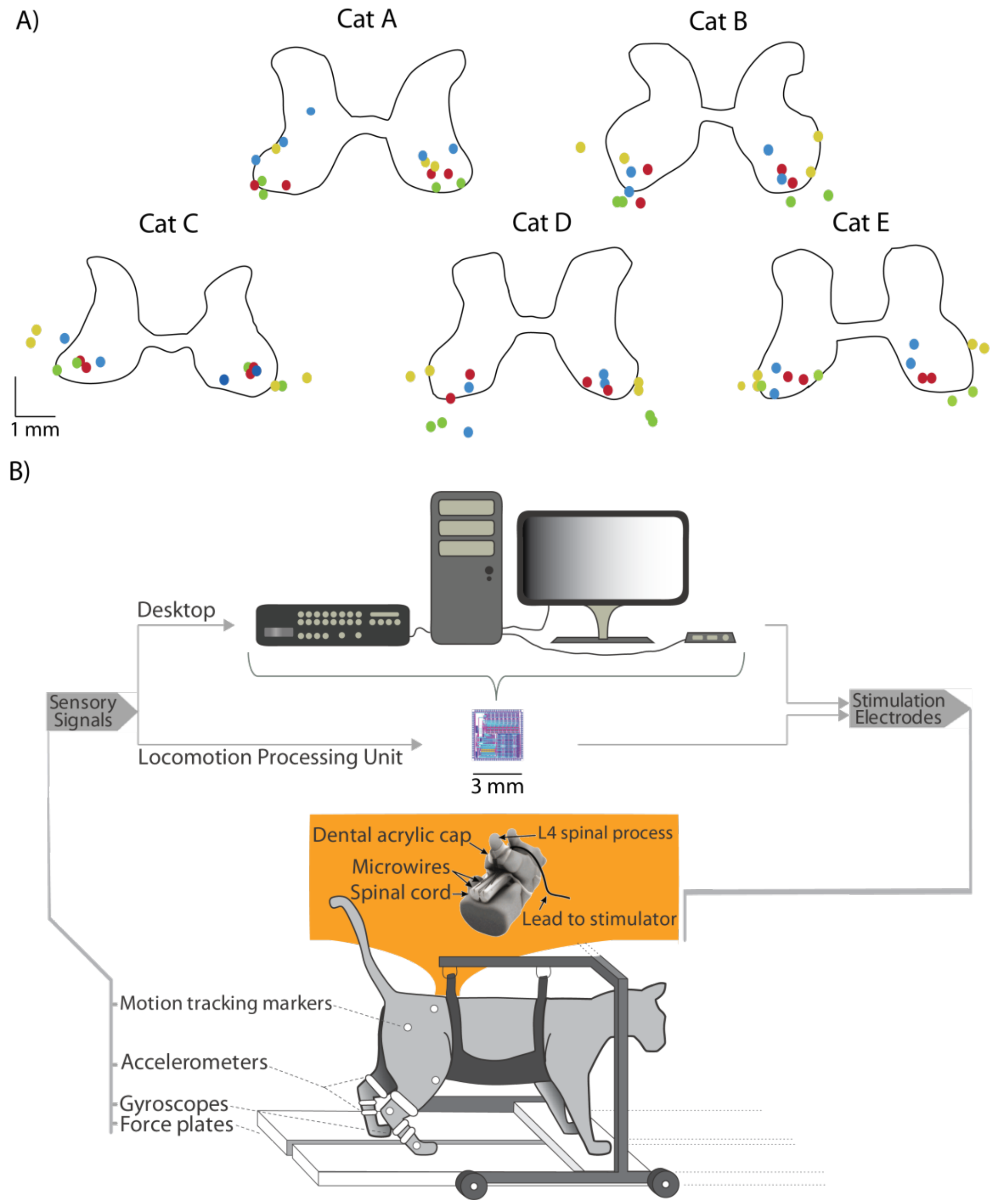

Figure 3-1: Overall setup and implanted electrode locations

A) The tip locations of the 8 electrodes selected for ISMS per side are shown for the 3 cats that walked the largest number of trials. Locations are shown with respect to the grey matter. Green= hip flexion (forward limb movement), yellow= ankle flexion (upward limb movement), red=knee extension (downward limb movement), blue= extensor synergy (backward limb movement).

B) Experimental setup with sensor locations on the suspended cat. An orange insert shows the implant location of the ISMS electrodes. For the majority of trials, “walking” was elicited by a full size computer system. During a subset of trials on Cat E, a compact integrated circuit was used to produce “walking” (LPU).

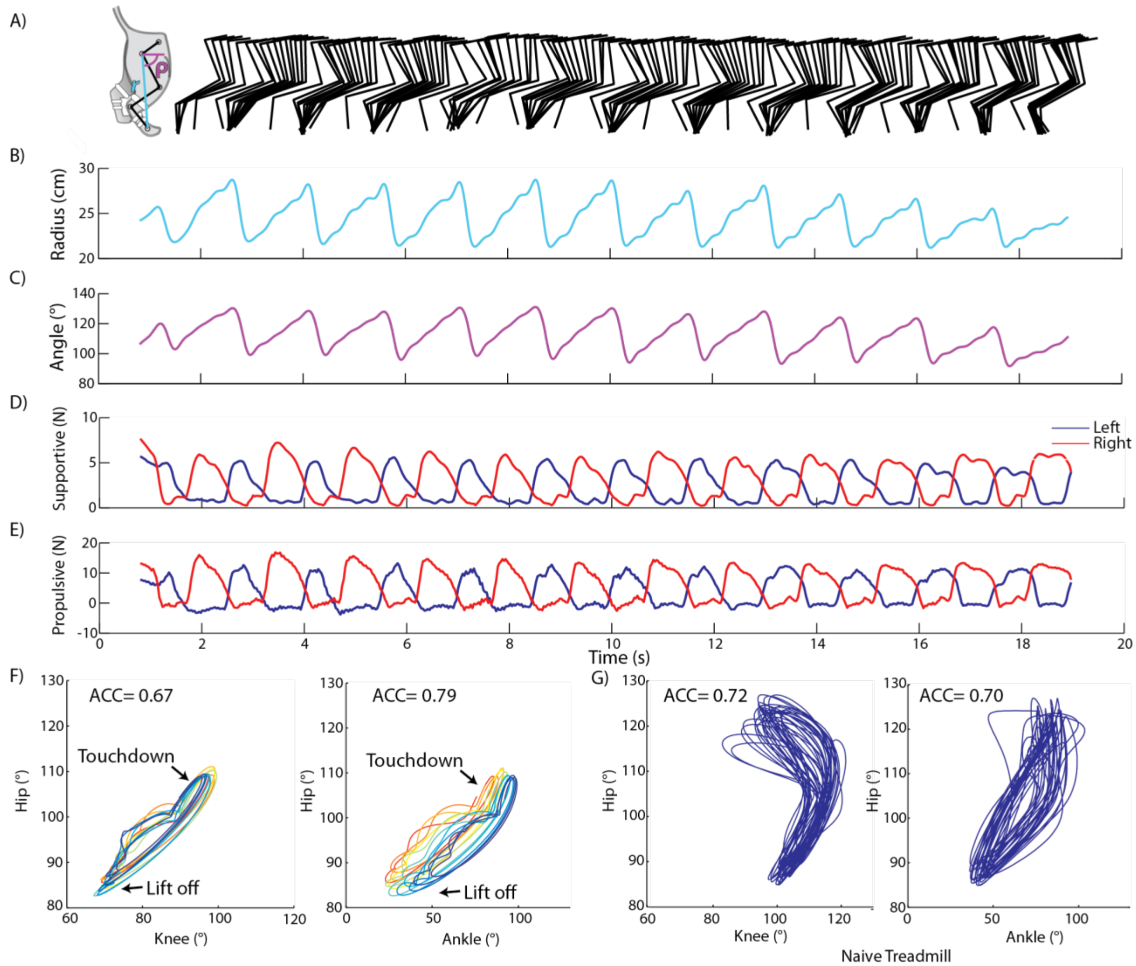

Figure 3-2: ISMS "walking" trial with maximal force production (Cat E)

A) Stick figure representations of the right hind limb are shown every 120ms for the duration of the trial. The hind limb insert shows conventions for kinematic parameters.

B) Distance between the hip marker and the metatarsophalangeal (MTP) joint.

C) Angle of the vector described in B) with respect to forward horizontal, measured clockwise.

D) Supportive (vertical) forces for the left and right hind legs.

E) Propulsive (parallel to direction of walking) forces for left and right hind legs.

F) Angle-angle plots of the hip, knee and ankle joints. Each step is shown in a different colour.

G) Similar to f), angle-angle plots for walking on a treadmill by a naïve (normal) cat.

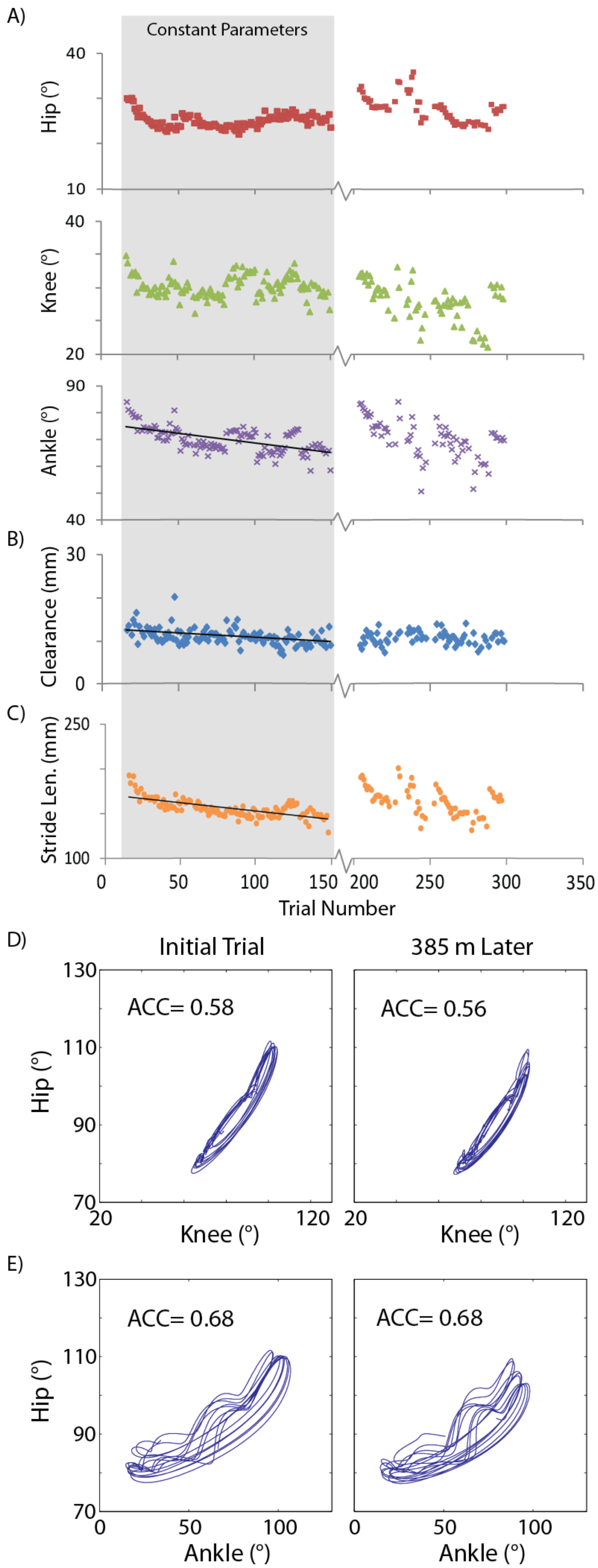
A)
Constant Parameters
Hip (°)
Knee (°)
Ankle (°)
B)
Clearance (mm)
C)
Stride Len. (mm)
Trial Number
D)
Initial Trial
385 m Later
ACC= 0.58
ACC= 0.56
Hip (°)
Knee (°)
E)
ACC= 0.68
ACC= 0.68
Hip (°)
Ankle (°)

Figure 3-3: Kinematics of ISMS-produced "walking" in Cat E throughout the course of the experiment

A) Each panel shows the range of hip, knee or ankle joints, respectively, across trials. For the region shaded in gray, ISMS amplitudes and control parameters were kept constant to track changes in "walking". A linear trend line was fit to this section if the changes were significant. The trials from 150-200 used the LPU.

B) Similar to a) and shows the average peak ground clearance of the paw per trial.

C) Similar to a) and shows the average stride length per trial.

D) Angle-angle plots demonstrating consistency of "walking" at the beginning and end of the constant parameter section for hip-knee relationship.

E) Similar to c), for hip-ankle relationship.

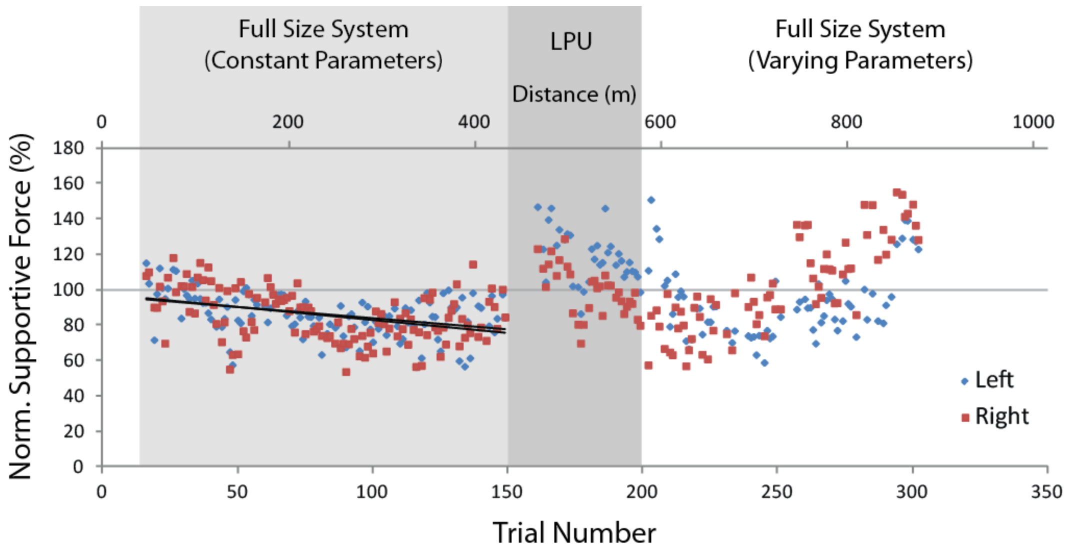

Figure 3-4: Supportive force during ISMS-generated "walking" for Cat E over the course of the experiment (including LPU)

The average peak supportive forces for the left and right legs are shown per trial for the entire experiment in Cat E. Cumulative distance "walked" is displayed above the traces. Forces were normalized to an average of the first 5 trials. Linear trend lines were fitted to the constant parameter trials for each leg to show long term changes. After a slight force recovery due to the time required to converted to the integrated ISMS chip controller, the LPU generated similar forces to those produced using the full size system (darkest shaded region). For the remaining trails, ISMS stimulation amplitudes and control parameters were modified using the full size system.

	Full size system																LPU		Average ± SEM	
	Cat A		Cat B		Cat C				Cat D				Cat E				Cat E		Cats C, D, E	
Experiment-Based																				
Setup Trials	2		22		11				5				11				8			
Successful Trials	65		29		210				288				241				42			
Distance walked (m)	188.5		84.1		609				835.2				698.9				121.8			
	All		**All**		**Start**	**End**	**All**		**Start**	**End**	**All**		**Start**	**End**	**All**		**All**			
Mean Stim. Amp EXT (µA)	82.4	± 11.28	56.8	± 9.98	43	86	71.5	± 15.69	46.2	69.3	56.3	± 16.41	34.5	53	37.1	± 10.19	30	± 3.44	55.0	± 10.0
Mean Stim. Amp FLEX (µA)	100.6	± 38.80	96.6	± 23.80	38.5	80.7	63.7	± 18.37	60.4	83	71.3	± 11.85	49.5	58.8	51.3	± 20.27	47.1	± 17.30	62.1	± 5.8
Trial-Based																				
n Trials	34		15		10	10	146		10	10	128		10	10	192		36		155.3	± 19.1
Velocity (m/s)	0.11	± 0.02	0.044	± 0.01	0.07	0.088	0.075	± 0.02	0.12	0.09	0.12	± 0.02	0.17	0.15	0.16	± 0.02	0.13	± 0.03	0.1	± 0.02
Strides	15.3	± 3.77	33.5	± 4.28	22.1	16.9	20.7	± 5.89	13.2	15.2	13.6	± 3.73	8.9	10.3	9.63	± 1.57	12.6	± 3.23	14.6	± 3.2
Stride-Based																				
n Strides	523		506		221	169	3031		132	152	1752		89	103	1808		453		2197.0	± 417.3
Peak Ground Clearance (mm)	18.5	± 3.96	5.25	± 0.62	12	6.92	9.5	± 6.95	7.54	4.52	6.3	± 1.67	13	10.7	11.5	± 1.74	7.14	± 4.57	9.1	± 1.5
Stride Length (mm)	118	± 18.20	78	± 9.00	101	101	100	± 13.38	141	115	126	± 18.02	178	161	159	± 14.50	129	±12.44	128.3	± 17.1
Hip Range (deg)	28.8	± 3.80	18.2	± 1.62	20.7	20.8	19.8	± 5.51	24.8	23	22.8	± 3.78	28.1	26.5	26.7	± 2.45	23	± 1.88	23.1	± 2.0
Knee Range (deg)	30.7	± 3.99	21.1	± 1.26	25.5	30.7	28.9	± 8.44	26.6	30.6	28.9	± 5.16	31.9	27.3	29.4	± 2.45	29.4	± 2.29	29.1	± 0.2
Ankle Range (deg)	49	± 6.80	33.2	± 4.34	57.1	53	52.1	± 9.23	64.1	53.5	58.9	± 13.93	78.2	67.6	70	± 5.67	59.4	± 4.45	60.3	± 5.2
ACC Hip-Knee	0.65	± 0.09	0.63	± 0.05	0.61	0.68	0.64	± 0.07	0.52	0.69	0.56	± 0.08	0.6	0.68	0.62	± 0.07	0.6	± 0.10	0.6	± 0.02
ACC Hip-Ankle	0.78	± 0.10	0.79	± 0.05	0.75	0.85	0.8	± 0.06	0.65	0.77	0.66	± 0.07	0.72	0.8	0.74	± 0.07	0.73	± 0.07	0.7	± 0.04
Area Hip-Knee (deg^2)	0.44	± 0.07	0.39	± 0.03	0.49	0.62	0.66	± 0.24	0.37	0.49	0.41	± 0.12	0.53	0.46	0.49	± 0.08	0.43	± 0.07	0.5	± 0.1
Area Hip-Ankle (deg^2)	0.85	± 0.12	0.76	± 0.13	1.48	1.51	1.53	± 0.23	1.51	1.25	1.35	± 0.11	1.82	1.45	1.58	± 0.18	1.4	± 0.12	1.5	± 0.1
Step-Based																				
n Steps	1042		1005		445	340	6057		264	317	3495		178	200	3600		888		4384.0	± 837.0
Peak Supportive Force (N)	3.67	± 0.82	3.34	± 0.21	4.12	3.30	3.73	± 0.65	3.72	5.21	4.42	± 1.02	2.72	3.49	2.44	± 0.50	3.08	± 0.75	3.5	± 0.6
Mean Supportive Force (N)	2.49	± 0.45	0.99	± 0.14	2.90	2.31	2.55	± 0.44	2.61	3.52	2.91	± 0.52	1.86	2.16	1.68	± 0.35	2.00	± 0.39	2.4	± 0.4
Force Duration (s)	0.84	± 0.14	0.86	± 0.19	1.13	0.98	1.02	± 0.11	0.74	1.06	0.79	± 0.23	0.79	0.82	0.72	± 0.17	0.86	± 0.17	0.8	± 0.1

Table 3-1: Comparison of "walking" across all cats

Kinematic and force parameters are shown for each cat. Parameters were grouped according to experiment, trial, stride or step. The majority of trials across all cats were collected using the full size system. A subset of trials in Cat E used the LPU. Cats C, D, and E were used for longevity analysis due to the large number of walking trials. An average of the first and last 10 trials were used as the start and end values for each cat. An average across all trials was recorded in the 'all' columns. Mean ± standard deviation unless otherwise stated.

References

1 *One Degree of Separation: Paralysis and Spinal Cord Injury in the United States*, <http://www.christopherreeve.org/atf/cf/%7B3d83418f-b967-4c18-8ada-adc2e5355071%7D/8112REPTFINAL.PDF> (

2 Widerstrom-Noga, E. G., Felipe-Cuervo, E., Broton, J. G., Duncan, R. C. & Yezierski, R. P. Perceived difficulty in dealing with consequences of spinal cord injury. *Arch Phys Med Rehabil* **80**, 580-586, doi:S0003-9993(99)90203-4 [pii] (1999).

3 Brown-Triolo, D. L., Roach, M. J., Nelson, K. & Triolo, R. J. Consumer perspectives on mobility: implications for neuroprosthesis design. *J Rehabil Res Dev* **39**, 659-669 (2002).

4 Prochazka, A., Mushahwar, V. K. & McCreery, D. B. Neural prostheses. *J Physiol* **533**, 99-109, doi:PHY_12138 [pii] (2001).

5 Fouad, K. & Pearson, K. Restoring walking after spinal cord injury. *Prog Neurobiol* **73**, 107-126, doi:10.1016/j.pneurobio.2004.04.003

S0301008204000589 [pii] (2004).

6 Ditunno, J. & Scivoletto, G. Clinical relevance of gait research applied to clinical trials in spinal cord injury. *Brain Res Bull* **78**, 35-42, doi:S0361-9230(08)00312-2 [pii]

10.1016/j.brainresbull.2008.09.003 (2009).

7 Courtine, G. *et al.* Can experiments in nonhuman primates expedite the translation of treatments for spinal cord injury in humans? *Nat Med* **13**, 561-566, doi:nm1595 [pii]

10.1038/nm1595 (2007).

8 Snyder, E. Y. & Teng, Y. D. Stem Cells and Spinal Cord Repair. *New Engl J Med* **366**, 1940-1942, doi:doi:10.1056/NEJMcibr1200138 (2012).

9 Stein, R. B. *et al.* Speed and efficiency in walking and wheeling with novel stimulation and bracing systems after spinal cord injury: a case study. *Neuromodulation* **8**, 264-271, doi:10.1111/j.1525-1403.2005.00035.x (2005).

10 Kobetic, R., Triolo, R. J. & Marsolais, E. B. Muscle selection and walking performance of multichannel FES systems for ambulation in paraplegia. *IEEE Trans Rehabil Eng* **5**, 23-29 (1997).

11 Zeilig, G. *et al.* Safety and tolerance of the ReWalk() exoskeleton suit for ambulation by people with complete spinal cord injury: A pilot study. *J Spinal Cord Med* **35**, 96-101, doi:jscm-d-11-00102 [pii]

10.1179/2045772312Y.0000000003 (2012).

12 Carhart, M. R., He, J., Herman, R., D'Luzansky, S. & Willis, W. T. Epidural spinal-cord stimulation facilitates recovery of functional walking following incomplete spinal-cord injury. *IEEE Trans Neural Syst Rehabil Eng* **12**, 32-42, doi:10.1109/TNSRE.2003.822763 (2004).

13 Herman, R., He, J., D'Luzansky, S., Willis, W. & Dilli, S. Spinal cord stimulation facilitates functional walking in a chronic, incomplete spinal cord injured. *Spinal Cord* **40**, 65-68, doi:10.1038/sj.sc.3101263 (2002).

14 Harkema, S. *et al.* Effect of epidural stimulation of the lumbosacral spinal cord on voluntary movement, standing, and assisted stepping after motor complete paraplegia: a case study. *Lancet* **377**, 1938-1947, doi:S0140-6736(11)60547-3 [pii]

10.1016/S0140-6736(11)60547-3 (2011).

15 Nightingale, E. J., Raymond, J., Middleton, J. W., Crosbie, J. & Davis, G. M. Benefits of FES gait in a spinal cord injured population. *Spinal Cord* **45**, 646-657, doi:3102101 [pii]

10.1038/sj.sc.3102101 (2007).

16 Graupe, D. & Kohn, K. H. Functional neuromuscular stimulator for short-distance ambulation by certain thoracic-level spinal-cord-injured paraplegics. *Surg Neurol* **50**, 202-207, doi:S0090-3019(98)00074-3 [pii] (1998).

17 Brissot, R. *et al.* Clinical experience with functional electrical stimulation-assisted gait with Parastep in spinal cord-injured patients. *Spine (Phila Pa 1976)* **25**, 501-508 (2000).

18 Thrasher, T. A. & Popovic, M. R. Functional electrical stimulation of walking: function, exercise and rehabilitation. *Ann Readapt Med Phys* **51**, 452-460, doi:S0168-6054(08)00092-5 [pii]

10.1016/j.annrmp.2008.05.006 (2008).

19 Kobetic, R. *et al.* Development of hybrid orthosis for standing, walking, and stair climbing after spinal cord injury. *J Rehabil Res Dev* **46**, 447-462 (2009).

20 Marsolais, E. B. & Kobetic, R. Implantation techniques and experience with percutaneous intramuscular electrodes in the lower extremities. *J Rehabil Res Dev* **23**, 1-8 (1986).

21 Farris, R. J., Quintero, H. A. & Goldfarb, M. Preliminary evaluation of a powered lower limb orthosis to aid walking in paraplegic individuals. *IEEE Trans Neural Syst Rehabil Eng* **19**, 652-659, doi:10.1109/TNSRE.2011.2163083 (2011).

22 Suzuki, K., Mito, G., Kawamoto, H., Hasegawa, Y. & Sankai, Y. Intention-based walking support for paraplegia patients with Robot Suit HAL. *Advanced Robotics* **21**, 1441-1469, doi:10.1163/156855307781746061 (2007).

23 Herr, H. Exoskeletons and orthoses: classification, design challenges and future directions. *J Neuroeng Rehabil* **6**, 21, doi:1743-0003-6-21 [pii]

10.1186/1743-0003-6-21 (2009).

24 Mushahwar, V. K. & Horch, K. W. Proposed specifications for a lumbar spinal cord electrode array for control of lower extremities in paraplegia. *IEEE Trans Rehabil Eng* **5**, 237-243 (1997).

25 Mushahwar, V. K. & Horch, K. W. Selective activation and graded recruitment of functional muscle groups through spinal cord stimulation. *Ann N Y Acad Sci* **860**, 531-535 (1998).

26 Bamford, J. A., Putman, C. T. & Mushahwar, V. K. Intraspinal microstimulation preferentially recruits fatigue-resistant muscle fibres and generates gradual force in rat. *J Physiol* **569**, 873-884, doi:jphysiol.2005.094516 [pii]

10.1113/jphysiol.2005.094516 (2005).

27 Lau, B., Guevremont, L. & Mushahwar, V. K. Strategies for generating prolonged functional standing using intramuscular stimulation or intraspinal microstimulation. *IEEE Trans Neural Syst Rehabil Eng* **15**, 273-285, doi:10.1109/TNSRE.2007.897030 (2007).

28 Prochazka, A., Mushahwar, V. & Yakovenko, S. Activation and coordination of spinal motoneuron pools after spinal cord injury. *Prog Brain Res* **137**, 109-124 (2002).

29 Gaunt, R. A., Prochazka, A., Mushahwar, V. K., Guevremont, L. & Ellaway, P. H. Intraspinal microstimulation excites multisegmental sensory afferents at lower stimulus levels than local alpha-motoneuron responses. *J Neurophysiol* **96**, 2995-3005, doi:00061.2006 [pii]

10.1152/jn.00061.2006 (2006).

30 Saigal, R., Renzi, C. & Mushahwar, V. K. Intraspinal microstimulation generates functional movements after spinal-cord injury. *IEEE Trans Neural Syst Rehabil Eng* **12**, 430-440, doi:10.1109/TNSRE.2004.837754 (2004).

31 Yakovenko, S., Mushahwar, V., VanderHorst, V., Holstege, G. & Prochazka, A. Spatiotemporal activation of lumbosacral motoneurons in the locomotor step cycle. *J Neurophysiol* **87**, 1542-1553 (2002).

32 Mushahwar, V. K., Collins, D. F. & Prochazka, A. Spinal cord microstimulation generates functional limb movements in chronically implanted cats. *Exp Neurol* **163**, 422-429, doi:10.1006/exnr.2000.7381

S0014-4886(00)97381-3 [pii] (2000).

33 Mushahwar, V. K. & Horch, K. W. Selective activation of muscle groups in the feline hindlimb through electrical microstimulation of the ventral lumbo-sacral spinal cord. *IEEE transactions on rehabilitation engineering : a publication of the IEEE Engineering in Medicine and Biology Society* **8**, 11-21 (2000).

34 Bagshaw, E. V. & Evans, M. H. Measurement of current spread from microelectrodes when stimulating within the nervous system. *Exp Brain Res* **25**, 391-400 (1976).

35 Yeomans, J., Prior, P. & Bateman, F. Current-distance relations of axons mediating circling elicited by midbrain stimulation. *Brain Res* **372**, 95-106, doi:0006-8993(86)91462-9 [pii] (1986).

36 Mazurek, K. A. *et al.* Feed forward and feedback control for over-ground locomotion in anaesthetized cats. *J Neural Eng* **9**, 026003, doi:10.1088/1741-2560/9/2/026003 (2012).

37 Guevremont, L., Norton, J. A. & Mushahwar, V. K. Physiologically based controller for generating overground locomotion using functional electrical stimulation. *J Neurophysiol* **97**, 2499-2510, doi:01177.2006 [pii]

10.1152/jn.01177.2006 (2007).

38 Halbertsma, J. M. The stride cycle of the cat: the modelling of locomotion by computerized analysis of automatic recordings. *Acta Physiol Scand Suppl* **521**, 1-75 (1983).

39 Lavoie, S., McFadyen, B. & Drew, T. A kinematic and kinetic analysis of locomotion during voluntary gait modification in the cat. *Exp Brain Res* **106**, 39-56 (1995).

40 Shen, L. & Poppele, R. E. Kinematic analysis of cat hindlimb stepping. *J Neurophysiol* **74**, 2266-2280 (1995).

41 Macpherson, J. M. Strategies that simplify the control of quadrupedal stance. I. Forces at the ground. *J Neurophysiol* **60**, 204-217 (1988).

42 Tepavac, D. & Field-Fote, E. C. Vector coding: a technique for quantification of intersegmental coupling in multicyclic behaviors. *Journal of Applied Biomechanics* **17**, 259-270 (2001).

43 Field-Fote, E. C. & Tepavac, D. Improved intralimb coordination in people with incomplete spinal cord injury following training with body weight support and electrical stimulation. *Phys Ther* **82**, 707-715 (2002).

44 Goswami, A. A new gait parameterization technique by means of cyclogram moments: Application to human slope walking. *Gait Posture* **8**, 15-36, doi:S0966636298000149 [pii] (1998).

45 Mazurek, K. et al. Locomotion Processing Unit. Proceedings of IEEE Biomedical Circuits and Systems Conference (BIOCAS), Paphos, Cyprus (2010).

46 Mazurek, K. A. & Etienne-Cummings, R. Implementation of Functional Components of the Locomotion Processing Unit. *Proceedings of IEEE Biomedical Circuits and Systems Conference (BIOCAS), San Diego, California USA* (2011).

47 Stein, R. B., Aoyagi, Y., Mushahwar, V. K. & Prochazka, A. Limb movements generated by stimulating muscle, nerve and spinal cord. *Arch Ital Biol* **140**, 273-281 (2002).

48 Vanderhorst, V. G. & Holstege, G. Organization of lumbosacral motoneuronal cell groups innervating hindlimb, pelvic floor, and axial muscles in the cat. *J Comp Neurol*

382, 46-76, doi:10.1002/(SICI)1096-9861(19970526)382:1<46::AID-CNE4>3.0.CO;2-K [pii] (1997).

Chapter 4: Real-time control of walking using recordings from dorsal root ganglia

Introduction

Many people with paraplegia due to a traumatic spinal cord injury (SCI) have a strong desire to walk again (Widerstrom-Noga *et al.*, 1999; Brown-Triolo *et al.*, 2002). Neuroprostheses can restore some walking functionality by activating parts of the nervous system. However, neuroprostheses will not likely replace the wheelchair for mobility purposes due to high energy costs (Ragnarsson, 2008; Stein *et al.*, 2005; Thrasher and Popovic, 2008). Devices such as the Parastep (combined electrical stimulation and leg bracing) that electrically activate motor nerves to produce contractions in paralyzed muscles can restore limited walking function (Graupe and Kohn, 1998). One of the main limitations of the Parastep is its inability to adapt to perturbations in the environment through sensory feedback. The control of natural walking within the spinal cord utilizes a combination of descending control, sensory feedback and intrinsic timing modulated by a central pattern generator (Pearson, 1995; McCrea and Rybak, 2008; Prochazka *et al.*, 2002a; Rossignol *et al.*, 2006). Mimicking the control mechanisms within the spinal cord has been the most successful approach to restore walking and has highlighted the importance of sensory feedback (Yakovenko, 2011; Mazurek *et al.*, 2012; Guevremont *et al.*, 2007; Yakovenko *et al.*, 2004).

Foot drop stimulators are neuroprostheses that have successfully used sensor feedback since the 1960s to improve walking performance in people with reduced ability to voluntarily contract ankle flexor muscles (Liberson *et al.*, 1961). These devices use sensory feedback to time electrical stimulation of the common peroneal nerve during the swing phase of the gait cycle causing ankle dorsiflexion. In the 1960s, Liberson used a force transducer (or foot switch) placed in the heel of the shoe to detect contact with the ground (Liberson *et al.*, 1961). However, the heel switch can perform unreliably (with different shoes or when patients accept most of the weight on the ball of the foot). Some modern foot drop stimulators use a tilt sensor, EMG sensing, or recordings from peripheral nerves to detect gait events (Dai *et al.*, 1996; Taylor *et al.*, 1999; Graupe *et al.*, 1983; Burridge *et al.*, 2007).

Where foot drop stimulators use one or two sensors to control a single joint, neuroprosthetic systems for restoring walking may require a larger number of sensors to control the coordinated action of many joints. Recent advances in sensor manufacturing have resulted in the creation of small, low power, and accurate sensors for a variety of sensing modalities (e.g., accelerometers, gyroscopes; Analog Devices, Norwood, MA, USA). Even with their small size, the external sensors may be cumbersome to don and difficult to place correctly for accurate measurements (Webster, 1992).

Natural control of walking also requires large amounts of accurate sensory information (Rossignol *et al.*, 2006). Sensory afferents convey information about a variety of modalities (e.g., position, pressure) to the locomotor networks in the spinal cord. The cell bodies from these sensory afferents are located in the dorsal root ganglia (DRG) just outside the spinal cord for each spinal level. Action potentials can be recorded extracellularly from the DRG and decoded to provide sensory information (Loeb and Duysens, 1979; Stein *et al.*, 2004a; Stein *et al.*, 2004b). There are many algorithms for decoding sensory information such as linear decoding, Kalman filters or Bayesian-modified Kalman filters (Carmena *et al.*, 2005; Stein *et al.*, 2004b; Li *et al.*, 2009; Li *et al.*, 2011). Although there is still some debate, the majority of the information is contained within the firing rate (action potentials/second) of action potentials recorded from single neurons (single units) rather than within multi-unit activity or local field potentials (Mehring *et al.*, 2003; Stark and Abeles, 2007; Cunningham *et al.*, 2009). Therefore, single units may produce the highest prediction accuracy (Bansal *et al.*, 2012). As early as the 1970s, it was shown that long term recordings of single sensory cells could be decoded during awake walking in chronically implanted cats (Prochazka *et al.*, 1976; Loeb *et al.*, 1977).

The recent development of high density silicon recording arrays (e.g., Utah electrode arrays) has enabled the simultaneous extracellular recording from 100 electrodes (Nordhausen *et al.*, 1996; Branner and Normann, 2000). The ability to record simultaneously from populations of neurons has allowed new decoding methods to extract a wide range of neural information, from the motor commands in the cerebral cortex to bladder pressure levels in the spinal cord (Velliste *et al.*, 2008; Patil *et al.*, 2004; Bruns *et al.*, 2011).

Stein et al. demonstrated the first implantation of a Utah array into the DRG to record simultaneously from many sensory afferents in anaesthetized cats (Stein *et al.*, 2004b). They post-processed recordings made during passive limb movements and decoded hind limb position from collections of neurons in the DRG. To implement DRG feedback in a walking device, decoded predictions of hind limb state will need to be calculated in real time. Recently, limb location from DRG recordings were predicted in real time and used to control intramuscular stimulation patterns in cats (Bauman *et al.*, 2011). The algorithm moved the leg sequentially to one of four quadrants based on predicted limb location.

The present study used a novel form of functional electrical stimulation (FES) called intraspinal microstimulation (ISMS) to elicit walking-like movements. ISMS does not fatigue the muscles as quickly as intramuscular stimulation, and is, therefore, a better candidate to be implemented in an eventual neuroprosthesis (Lau *et al.*, 2007; Bamford *et al.*, 2005; Mushahwar and Horch, 1998). ISMS uses an array of fine wires to electrically stimulate motor neuron pools in the ventral horn of the lumbar spinal cord which can selectively activate individual muscles (Mushahwar and Horch, 1997, 2000). The motor neuron pools are interconnected by interneurons that are responsible for the activation of synergistic muscles producing multi-joint movements (Mushahwar and Horch, 2000; Prochazka *et al.*, 2002b; Saigal *et al.*, 2004; Mushahwar *et al.*, 2002).

The combination of ISMS and DRG feedback completely internalizes the neural interfaces for a walking prosthetic. Together, they can be implanted in a small region along the spinal cord (approximately 5 cm in humans) that can be accessed through one surgical site. Unfortunately, the close proximity of the intraspinal stimulation electrodes (within 2 cm) to the recording arrays can cause stimulation artifacts that can overwhelm the action potentials (Weber *et al.*, 2007). Recording in the DRG during peripheral stimulation (e.g., intramuscular stimulation) is less susceptible to artifacts due to a greater distance between the stimulation site and the recording arrays. However, the current amplitude levels are much lower for ISMS which may at least partially offset the smaller distance separating the stimulation and recording sites. Additionally, contamination of recordings by biopotentials (such as electromyographic activity) can be prevented by placing shielding around the recording array (Clark *et al.*, 2011).

This study provides a proof-of-principle for using continuous real time predictions of limb state based on sensory afferent firing in the DRG to control walking. Combining this form of internally-derived feedback with a form of stimulation that is delivered through the spinal cord could eventually lead to a fully implantable neuroprosthetic system for walking. The system was tested by using the limb state predictions in combination with a previously developed walking control algorithm, to limit backward extension in response to varying perturbations (Mazurek *et al.*, 2012). We also tested a number of factors affecting prediction quality, including the type of external sensor used for training, the frequency of retraining, the number of neurons required for an accurate model, and the effect of stimulation artifacts on prediction quality.

METHODS

IMPLANTATION

All experimental procedures were approved by the University of Alberta's Animal Care and Use committee. A total of 5 intact cats (3.6-5.7 kg) were used in acute, one day-long, non-recovery experiments. Anesthesia was initially induced with isoflurane (5%), and subsequently replaced with sodium pentobarbital under which the animals were maintained throughout the implantation procedures and data collection (induction: 25mg/kg intravenously; maintenance: 1 in 10 dilutions of the anesthetic). A laminectomy was performed to expose spinal cord segments L4-S1 and the right side L6 and L7 DRG (figure 1). A fine-wire array consisting of 12 electrodes (Pt-Ir 80-20%, 50µm diameter, 4 µm polyimide insulated, 0.1mm deinsulated tip) was implanted in the right side of the spinal cord for stimulation. The fine-wire array was fixed to the L3 spinous process using dental acrylic. The electrodes were implanted in the right side of spinal cord with their tips targeting the ventral horn of the gray matter. Maps of the motor neuron pools were used to target regions that produce hip flexion, ankle flexion, knee extension and a full limb extensor synergy in the ipsilateral hind limb when activated through ISMS (3 electrodes per function)(Saigal *et al.*, 2004; Yakovenko *et al.*, 2002; Vanderhorst and Holstege, 1997). The stimulation return electrode was a 9-strand stainless steel wire (AS632, Cooner Wire Inc., Chatsworth, CA, USA) deinsulated for approximately 2 cm at its tip. To fix the return wire in place, the end of the wire was tucked along the left side of the spinal cord between the cord and the spinal canal in the center (rostal-caudally) of the stimulation array (figure 4-1, center). To record from the DRG, Utah electrode arrays were implanted into the right L6, L7 or both dorsal root ganglia with a high speed pneumatic inserter. Each Utah array consisted of either 4x10 (L6) or 5x10 (L7) electrodes with an electrode shank length of 1.5 mm (Blackrock Microsystems, Salt Lake City, UT, USA). The recording ground electrode consisted of a deinsulated band of braided stainless steel wire approximately 3 mm wide and curved around the dorsal spinal cord between the stimulation and recording locations. The recording reference wires were placed proximally and as close as possible to their respective arrays (figure 4-1, center).

ELECTRICAL STIMULATION

The 8 electrodes producing the best response to ISMS in the ipsilateral limb were selected and connected to a custom 16 channel current controlled stimulator that delivered trains of charge balanced, biphasic pulses (up to 120 μA, 290 μs pulse width, 62 Hz). Stimulation was modified in real-time by a controller capable of adapting an intrinsic timing cycle with sensory feedback (Mazurek *et al.*, 2012). The step cycle had a duration of 1.5 s and consisted of four sequential controller states (1 flexion and 3 extension states, E1, E2, and E3) each accounting for 20%, 20%, 20%, and 40% of the step cycle respectively (See Mazurek et. al for details).

External sensors

Testing of walking was performed on an instrumented walkway (Cats A, B, C) or split-belt treadmill (Cats D, E). Motion tracking markers were fixed to the right hind limb to record two-dimensional kinematics using a camcorder with lens parallel to the walking plane (120 fps, JVC Americas Corp., Wayne, NJ, USA). Markers were placed on the iliac crest, and the hip, knee, ankle and metatarsophalangeal (MTP) joints. Marker positions were digitized with custom Matlab software written by Dr. Douglas Weber (University of Pittsburgh, Pittsburgh, PA, USA). Hind limb segment length was defined as the distance between the hip and MTP marker (referred to as: distance). Hind limb segment angle was defined as the angle between the hip-MTP segment and horizontal (referred to as: tilt) (figure 4-1, bottom). Force transducers mounted within the walkway and treadmill captured supportive forces (vertical) of the right hind limb. A gyroscope was fixed to the right foot and was continuously integrated to provide a measure of angle of the foot with respect to horizontal. The gyroscope was reset during the end of the flexion phase to eliminate the build-up of error due to drift. Force and gyroscope signals were sampled using a Cerebus data acquisition system (Blackrock Microsystems, Salt Lake City, UT, USA) at 1 kHz and filtered in Matlab (The MathWorks Inc., Natick, MA, USA) with a moving average filter of 120 ms.

Neural signals

The neural signals from the DRG were also recorded and processed with the Cerebus system and Central software (v. 6.01.00.00). After filtering with a Butterworth filter (250 Hz - 7.5 kHz), the signals that crossed a manually set amplitude threshold were identified as action potentials of interest or "spikes". Spike sorting based on time-voltage windows was used to distinguish the signals of multiple neurons on one recording electrode (channel). The time-voltage windows for all channels were set during passive manipulation of the hind limb. All sensor data and timestamps of action potentials were streamed into Matlab.

Artifact Rejection

Artifact rejection ensured that information recorded from the DRG consisted of natural sensory afferent signals rather than waveforms artificially created by the electrical stimulation in the spinal cord. Artifacts were rejected using two software filters, one based on the timing and the other on the amplitude of the artifact. Unlike action potentials which may appear on one or few neighboring channels, an artifact appeared across almost all recording channels concurrently as it conducted through the tissue. Therefore, if a synchronous event was detected across at least 60% of the channels, the following 1 ms window was rejected to discard the artifact. Additionally, artifacts were discarded based on their amplitudes. Often artifacts were much larger in amplitude (sometimes an order of magnitude) than action potentials. So when either the positive or negative phase of a waveform exceeded ± 600 μV, it was assumed to be an artifact and was discarded.

Prediction Algorithm

The controller developed models for real time predictions of external sensor signals using neural recordings from the DRG. The first phase, called the *training phase*, compared signals from external sensors (distance and tilt from video recordings, foot angle from gyroscope signal, and forces) with the firing rates of DRG neurons after a recorded trial. The result of the training phase was a set of multivariate linear equations which used the firing rates of selected units to predict the signal of an external sensor. During the second phase, the *testing phase*, the model was used to create a real time prediction of an external sensor signal and in some trials, use that prediction for closed loop control.

TRAINING

The objective of the training process was to build a multivariate linear model to predict the signals from external sensors based on the weighted firing rates of selected units within the DRG. Prediction models could be created using any recorded external signals. Training was performed on 20 seconds of stepping produced by ISMS under open loop control, during which neural signals and external sensor signals were simultaneously captured. Filtered gyroscope and force plate signals were resampled to the frequency of the video recordings (1/120 s). Video recordings required further processing before they could be used for training. The marker locations were digitized and the tilt and distance of the vector connecting the hip to the limb endpoint was calculated. The first derivatives for all external sensory signals were also calculated. Methods are similar to the offline training algorithm described in Stein et al. (2004) and Weber et al. (2007) (Stein *et al.*, 2004b; Weber *et al.*, 2007).

First, the discrete timestamps were converted into a continuous firing rate (f_i) for each unit:

$$(1) \quad f_i = \frac{1}{\Delta t}\sum_j \left(1 - \frac{|t_i - t_j|}{\Delta t}\right)$$

where Δt is the sampling interval (1/120s), t_i is the current sample time indexed by i, and t_j is the jth spike in the interval between the preceding and the following samples $[t_i - \Delta t, t_i + \Delta t]$. Both the firing rates and the external sensor signals were then filtered with a critically damped, 2nd order, low-pass filter with a time constant of 50 ms to prevent any time shifting (Stein *et al.*, 2004a).

Next, the firing rate of each unit was correlated with an external sensor signal and its derivative. The units were ranked according to correlation and two separate groups of units, those best correlated with the signal and those best correlated with the derivative, were selected. The groups could contain any combination of different or similar units. A pre-determined number (selected by the operator) of the most highly correlated units were included in the prediction model (10 units was the default). Then the linear model was trained using least squares regression to find an optimal set of coefficients (c_k) to relate the firing rates to the external sensory signal:

$$(2)\quad \hat{q}_i = c_0 + \sum_{k=1}^{N}(c_k \cdot f_{i,k})$$

where $\hat{q}_i$ is the estimated value of state variable q at time i. The estimate is derived from a weighted summation of firing rates of N neurons and $f_{i,k}$ is the firing rate of neuron k at time i. c_0 is a bias term in the regression model.

After the model was generated, the firing rates (previously used to generate the model) were used as inputs to create a prediction of the external sensor signal. The error between signal and prediction (expressed as variance accounted for (VAF), see below) served as a measure of the training quality. Since some sensory afferents contain both the measurement and its first derivative (for instance: position and velocity), the final stage in the training process optimally weighted the prediction of the signal with its prediction of the derivative to best match the external sensory signal. For the weighting, a number (w) between 0 and 1 was created representing the proportion of the signal to the derivative. The algorithm systematically combined the signal and derivative at 0.01 proportional increments from w =0 to w=1 according to:

$$(3)\quad \tilde{q}_i = w \cdot \left(\hat{q}_{i-1} + \frac{d\hat{q}_i}{dt} \cdot \Delta t\right) + (1 - w) \cdot \hat{q}_i$$

where $\tilde{q}_i$ is the new estimate using a weight of w for the ith sample time. The first derivative $\frac{d\hat{q}_i}{dt}$ is integrated to provide an independent estimate of the prediction.

The optimal weight maximized the variance accounted for (VAF) between the weighted prediction and the external sensor signal. This procedure was repeated for all selected external sensors and resulted in an independent model to predict each external sensor signal.

TESTING

The testing phase used the model weightings created during the training phase to predict external sensor signals in real time using only streaming neural recordings. Several external sensor signals can be simultaneously predicted due to the low computational demand of the prediction models. The predictions were updated every 31 ms (the frequency of the controller). Only timestamps from the lists of highly correlated units selected by the models were processed. The timestamps (which occurred since the previous prediction) were converted into continuous filtered firing rates using the same calculations from the training phase. By solving equation (2), the prediction of both the external sensor signals and its first derivative ($\hat{q}_i$) were calculated from the firing rates ($f_{i,k}$) using the trained model.

Then the predictions of the external sensor signal and its first derivative were proportionally combined according to the weighting coefficient in equation (3). The final weighted prediction ($\tilde{q}_i$) was then recorded and fed into the IF-THEN rule base for closed loop control. For Cats A, B and C, tilt and distance were predicted. For Cats D and E gyroscope and force plate predictions were added.

Experimental Procedure and Test Protocol

After implantation of ISMS microwires and DRG recording arrays, the cats were transferred to an instrumented walkway (Cats A, B, C) or a split-belt treadmill (Cats D, E) and partially suspended in a sling and maintained under anaesthesia. The walkway had a cart that supported the sling (which in turn supported the head, fore limbs, trunk and abdomen) while the hind limbs freely stepped on the two tracks with embedded force transducers. The distance walked over the walkway was 2.9 m. Appropriate ISMS amplitudes were established for producing movements in the ipsilateral limb that corresponded to the four controller states (flexion, E1, E2, and E3) during initial setup trials. Because unilateral stepping could not produce continuous motion, the cart was pulled forward at constant velocity. During treadmill walking the belt speed was set to match the step cycle (about 0.15 m/s). All walking trials were 25 s long.

At set intervals open loop trials were conducted to retrain the prediction algorithm. There were no more than four consecutive test trials without retraining (except during the "longevity test", which tested the stability of predictions over time). Halfway through the experiment, the thresholds and time-voltage windows for spike sorting were adjusted to account for minor variations in waveform shape and amplitudes. Furthermore, the sensory afferents were characterized according to their modality (e.g. muscle spindles, skin receptors, etc.) by passively manipulating the leg following the methods described in (Aoyagi *et al.*, 2003). Waveform snippets (approximately 1.6 ms duration, sampled at 30 kHz) of action potentials were collected during manual stimulation of the receptor to compare with the units used in the prediction models (for Cats D and E only).

The experiment involved three types of trials: manual stepping and stepping produced by ISMS with open loop control and closed loop control. During passive stepping trials, an operator moved the foot of the cat in a stepping-like pattern and applied force against the walking surface during the stance phase (both movement and force ranges were consistent with stepping produced by ISMS). The operator minimized contact with the foot during passive movements. During open loop trials the progression of controller states was based on timing only. Open loop trials were used to test the number of units required for prediction. The prediction algorithm was trained using 3, 5, 10 or 15 units and then tested for 2 trials each. The stability of the predictions over time was tested in longevity tests, during which 8 consecutive testing trials were performed without retraining the model. To evaluate the effect of ISMS stimulation frequency on prediction accuracy, the number of channels and stimulation frequency were reduced from the standard of 8 channels at 62 Hz to 4 channels at 31 Hz. In order to maintain similar kinematic and kinetic properties of walking during these trials, stimulation amplitudes were increased by about 80%. During closed loop trials, the effect of activating a stance-to-swing phase transition was tested. Swing was initiated if the hind limb segment angle crossed a threshold (rotation clockwise with respect to forward horizontal) to limit backward hyperextension. Rule activation was tested by walking at different belt speeds (0.10, 0.15, and 0.20 m/s) during the training and testing trials.

Data Analysis

Data analysis was performed on the middle 15 seconds of the trial (between 5-20 s) to reduce the effects of starting and stopping the cart on the walkway. For consistency, analysis of the treadmill trials was also limited to the middle 15 seconds of a trial. The trials were parsed into steps by taking the touchdown of the foot on the force plate as beginning of each step. Stepping parameters were averaged across a trial.

The accuracy of the predictions against their simultaneously recorded external sensor signals was evaluated with percentage variance accounted for (VAF%). VAF% is a measure of the proportion of explained variance between the external sensory signal and the predicted values.

VAF% was calculated by:

$$(4)\quad VAF\,\% = 100\% \cdot \left(1 - \frac{variance(q - \tilde{q})}{variance(q)}\right)$$

where $q$and $\tilde{q}$ are, respectively, the actual and estimated state variables. A Chi-Square goodness of fit test was used to test the distribution of the frequencies of the identified unit types. A one-way ANOVA was used to test differences in population means between sensor types. Differences between population means between the two stimulation frequencies (32 Hz and 62 Hz) were tested using the t-test when all statistical assumptions were met. A P value ≤ 0.05 was considered significant. All values are shown as *mean* ± *standard deviation*.

RESULTS

OPEN LOOP STEPPING

Five experiments in five cats produced a total of 72 open loop trials and 71 closed loop trials with default parameters (62Hz stimulation, 10 units selected for training and trained within four trials; see table 4-1). Table 4-1 shows the average kinematic parameters and vertical forces per cat across unilateral stepping trials produced with ISMS using open loop control. Peak distance appeared to be greater for the cats tested on the treadmill (224 to 235 mm) than for those on the walkway (191 to 206 mm); similarly peak tilt appeared to be greater on the treadmill (129 to 134 °) than on the walkway (110 to 118 °). The moving belt of the treadmill probably resulted in greater backward extension of the hind leg. The mean peak ground reaction forces (%body weight) were similar for the cats tested on the walkway (6 to 8.2%) and those tested on the treadmill (6.4 to 8.9%).

Afferents used in prediction

A Utah electrode array was implanted in the L7 DRG in cats A and B, in the L6 DRG in cat D, and in L6 and L7 DRG in cat C and E (table 4-2). The arrays recorded from a total of 158 afferents (units) during passive manipulation of the hind limb in the five cats. For the majority of these afferents, the location (e.g., skin, muscle) and sensory modality (e.g., pressure, touch, stretch) could be identified (89%). The number of recordable units per array was quite variable and depended on the success of the array injection procedure in the DRG. The largest number of recordable units with one array was 37 (with a 4x10 array in L6 in cat D). There was no significant difference between the number of cutaneous (41%) and muscle (48%) afferents identified ($P=0.31$). Based on location, the likely number of units to be selected as predictors (out of 10) during training is shown in table 4-2. A large number of the units used as predictors were not identified (45%). All predictions (regardless of sensor type) used more muscle units than cutaneous units ($P<0.01$).

Prediction during Passive Movements

Real time predictions of all external sensor signals during a single trial are shown in figure 4-**2**. During this trial, the limb was passively moved in a stepping-like pattern with realistic levels of force applied during the stance phase. Therefore, it illustrates the capabilities of the real time prediction algorithm without the presence of stimulation artifacts.

For prediction of kinematics, the prediction of tilt (VAF: 95%) was more accurate than the prediction of distance (VAF: 67%). The gyroscope did not provide a usable signal during passive movements because its integration had to be reset at precise times within the step cycle to eliminate drift (VAF: 33%). The resets were pre-set in the controller and were likely asynchronous with the passive movements. Force prediction was the second most accurate with a VAF% of 82%. The force (artificially applied pressure to mimic the stance phase) reached an average peak value of 18±0.9% body weight (BW) across steps. This was somewhat higher than forces produced during ISMS stepping in our experimental setup.

Artifact Rejection

Stimulation artifacts contaminated recordings of neural signals and degraded the accuracy of the prediction based on those signals. Figure 4-**3** shows neural recordings before and after the implementation of artifact rejection filters in software on a single trial. The first section shows neural recordings during an ISMS-driven stepping trial without any artifact rejection. The patterned stimulation was applied from approximately 3 to 23 seconds into the trial. In panel **A**, multiple action potentials from a single identified unit are overlaid. In addition to the identified unit, large magnitude artifacts were also misidentified as the unit. In panel **B**, a histogram of the interspike intervals (ISI) is plotted. Based on a stimulation frequency of 62 Hz, the intervals between stimulation artifacts was approximately 16 ms. In the histogram, defined peaks were visible at the stimulation frequency and its harmonics (32 ms, 48 ms, etc.). A large number of events occurring at these frequencies implied that the detected spikes were likely caused by stimulation artifacts instead of neural signals. Panel **C** shows a raster plot of time of each identified spike per electrode for the trial. The spike marks (small vertical lines) are colored according to the unit (gray: discarded waveforms, other colors: accepted action potentials). During stimulation, large numbers of events were continuously detected on all electrodes and appeared as a solid block. All of these stimulation artifacts, which were recorded across all electrodes, are colored blue indicating that they were identified as neural signals because their waveforms crossed the time-amplitude window(s). In panels **D**-**F**, artifact rejection filters were activated during recording of an otherwise similar stepping trial (recorded consecutively). Even with the same stimulation parameters, the recordings consisted of clean neural signals with few visible artifacts on the same electrodes. The waveform of the identified unit shown in panel **D** did not contain any large amplitude artifacts and the ISI histogram (panel **E**) did not have the characteristic peaks at the stimulation frequencies. In the raster plot (panel **F**), the solid block of stimulation events was mostly eliminated by the artifact rejection code and phasic firing of spikes was distinguishable. With artifact rejection during an ISMS stepping trial, the average number of spikes per recording electrode was reduced from over 1800 to approximately 250 spikes.

PREDICTION DURING ISMS

With the stimulation artifacts rejected, the real time prediction of external sensor signals can be applied during stepping produced by ISMS. Figure 4-**4** shows real time predictions generated during a single trial of ISMS stepping. The layout is similar to figure 4-**2**. The prediction accuracy (shown in red) was again high for both distance (VAF: 93%) and tilt (VAF: 90%). The average backward tilt was 132±0.6 °and was slightly more than during passive manipulations (126±2.5 °). The gyroscope prediction of foot angle was much better (VAF: 75%) than during the passive trial. The higher accuracy was likely attributed to the synchronized gyroscope resets to the step cycle. Force profiles displayed a steep decrease during the stance phase due to some backward slipping caused by the moving treadmill belt. However, peak force was slightly less (9±1.8 %BW) than in the passive trial and the prediction was less accurate (VAF: 53%). Overall, by rejecting stimulation artifacts, the controller predicted kinematics and kinetics accurately based on streaming neural signals.

Figure 4-**5** shows the units used to predict tilt during the above mentioned trial and their consistency between training and testing trials. The left column describes data from the training phase during ISMS stepping. The first plot shows the overlap between the measured and calculated tilt as a measure of fit of the model (VAF: 96%). The panels below show the firing rates of the five most highly correlated units that were used in the prediction, in order of decreasing correlation to the external sensor signal (tilt). Real time prediction using the trained model had a VAF of 90%. The firing rates of the same five units are also shown during the testing trial (same trial as figure 4-**4**; middle column). The firing rates were well modulated to the stepping pattern during training. During testing, the firing rates were similar magnitudes and were still well modulated.

The right column contains the waveform plots recorded during the training and testing trials for each corresponding unit. The waveform shapes did not change appreciably and were likely recorded from the same unit in both trials. The two units that were best correlated with tilt during the training phase were muscle spindles (gastrocnemius and posterior biceps). Two units were identified as cutaneous afferents and one was unknown.

EFFECTS OF SYSTEM SETTINGS

SENSOR TYPE

We first evaluated which external sensor signal could be predicted most accurately. Figure 4-**6** shows a bar graph of the average VAF for each external sensor signal for all stepping trials with open loop ISMS. Distance models (VAF: 60±21%) had significantly worse prediction accuracy than tilt models (VAF: 66±17%, $P<0.001$) although both had reasonable accuracy. The gyroscope model provided the most accurate prediction of the external sensor signal (VAF: 73±8%). The force prediction was the least correlated to actual force measurements (VAF: 48±13%). Force prediction was significantly worse than distance, tilt and gyroscope predictions ($P<0.001$). In summary, predictions of kinematics were the most accurate; the prediction accuracy of force was lower.

NUMBER OF TRAINED UNITS

Next, we identified the best number of single units required for prediction. Figure 4-**7** shows prediction quality of each model after having been trained with 3, 5, 10, or 15 units. Each point includes an average of two ISMS-driven trials per cat with open loop control. All external sensor signals showed a peak in VAF when 10 units where used for training (VAF range: 53%-76%). The use of more or less units in the prediction model resulted in a lower prediction accuracy for all sensors. Prediction accuracy was the lowest when the models (except for distance) were trained with 3 units (VAF range: 32%-65%).

TIME DURATION

Another factor influencing prediction quality was the time elapsed after the training phase because the neural signals recorded with a Utah electrode array change over prolonged periods of time (hours). Figure 4-**8** shows the prediction accuracy averaged across cats (Cat B was not included due to technical issues) for up to eight successive walking trials without retraining. Linear regression was performed on these trials to determine if there was a significant relationship between trial number and prediction accuracy. Tilt prediction accuracy was the only prediction that did not show a significant correlation to time ($p=0.18$, $r^2=0.03$). Initial prediction accuracy for distance was VAF: 70% and decreased to 46% (a decrease of 34%, $p<0.01$, $r^2=0.73$). The gyroscope prediction accuracy decreased by only 8% over trials ($p<0.05$, $r^2=0.65$). Force prediction was more variable over time but still showed a significant negative relationship between trial number and prediction accuracy ($p<0.05$, $r^2=0.06$). Linear trend lines fitted to the VAF values plotted over time showed that force prediction had the steepest rate of decay (4.0%/trial), while the gyroscope prediction had least decay (1.3%/trial). With this rate of decay, and assuming an acceptable prediction accuracy of VAF > 50%, retraining would be required approximately every 20 trials for the gyroscope.

STIMULATION FREQUENCY

Lastly, prediction accuracy with two different stimulation frequencies (31Hz and 62Hz), causing different amounts of artifacts, was compared to that of passive stepping (no stimulation artifacts). The effect of two stimulation frequencies and varying numbers of stimulation electrodes were tested. Stimulation frequency of 62 Hz through eight electrodes resulted in the greatest number of artifacts that would possibly be encountered in an ISMS-based neuroprosthesis. To study the prediction in the presence of the minimal amount of stimulation artifacts, unilateral stepping was produced with four channels of stimulation at a reduced frequency of 31 Hz. This is the minimal number of channels and the minimal frequency needed to produce walking in one leg. However, the stimulation amplitudes were increased by ~ 80% to maintain a similar walking pattern. In figure 4-**9**, the prediction accuracy for each external sensor (averaged across cats during open loop trials) is shown for passive, 31 Hz and 62 Hz ISMS conditions. The poor gyroscope prediction during passive movement was previously addressed and was due to the asynchronous resetting of the integration. Gyroscope prediction improved during ISMS stepping when the resetting was synchronized to the step cycle (31Hz: VAF of 69±11%, 62Hz: VAF of 73±8%). Tilt prediction accuracy was the highest during passive movements (VAF: 81±10%). Also, force prediction accuracy was the highest during passive movements (VAF: 84±4%). For force, the prediction accuracy for 31 Hz was significantly higher than 62 Hz ($P<0.001$). For distance and tilt, the difference between 31 Hz and 62 Hz was not significant, $P=0.11$ and $P=0.22$, respectively. Even at the highest frequency tested (62Hz), the prediction quality of kinematic sensors still averaged VAF>60% while the force prediction had VAF>45% suggesting that predictions can be made in the presence of ISMS.

CLOSED LOOP PERFORMANCE

The predictions of external sensor signals were used for triggering a closed loop rule base controller for walking using ISMS. When an external sensor signal (or its prediction) crossed a rule activation threshold, an IF-THEN rule was activated immediately changing the walking state to reduce undesirable stepping behaviour. During the closed loop trials shown in figure 4-**10**, a single rule designed to limit backward hyperextension (by changing states: propulsion to swing) was triggered based on real-time predictions of hind limb segment angle.

The activations of the E3-F transition rule are shown in figure 4-**10** during two consecutive trials with different thresholds. The predicted tilt (red) was used to trigger the rule while the recorded tilt (blue) was plotted to illustrate the prediction accuracy. Crossing the threshold (horizontal dashed line) in the positive direction activated the rule. Gray vertical bands highlight the time window within the step cycle for possible rule activation. If the prediction of tilt exceeded the threshold within the activation window, the rule activated (shown by a vertical black line at time of triggering) and the controller immediately entered the swing phase. In the upper panel, the threshold limited tilt to 135 °and since the prediction did not reach threshold, the rule did not activate. In the bottom panel, all settings were the same except that the threshold was lowered to 129 °. Since the prediction already exceeded the threshold at the onset of the activation window during the first five steps, the rule activated immediately. During the next four steps, the triggering occurred when the prediction crossed threshold. In the second last step, the rule failed to trigger because the prediction did not cross the threshold within the activation window. By causing an early transition to the swing phase, the rule decreased the step duration by an average of 180 ms and consequently sped up the stepping. Overall, the rule limited backward hyperextension by reducing tilt from 133±0.6 ° to 131±1 °. Simultaneously, the rule also reduced the range of motion in hip, knee and ankle joints from 33±2, 43±4, 58±2 to 27±2, 31±3, 40±8 °, respectively.

Adaptation to Treadmill Belt Speed

Next we showed how the E3-F transition rule adapted the stepping to different treadmill belt speeds. The transition threshold was held constant across a set of three trials with various treadmill belt speeds. The walking speed used in these experiments (0.15 m/s) best matched the preprogramed timings in the step cycle (1.5s step duration; 20%, 20%, 20% and 40% for F, E1, E2 and E3 phases, respectively). In addition belt speed was decreased to 0.10 m/s and increased to 0.20 m/s. Due to the time elapsed between changing belt speed, tilt prediction models were retrained at each speed to ensure that prediction quality was controlled and only treadmill speed was variable. Figure 4-**11** shows the three trials plotted with a similar format to figure 4-**10**. The upper panel (slow belt: 0.10 m/s) has no rule activations since the leg did not hyperextend before the swing phase began. The average measured backward tilt was 124±1.1 °. The middle panel (normal: 0.15 m/s) showed six steps that triggered rule activation which limited the measured backward tilt to 128±2.1 °. The fastest belt speed (0.20 m/s) in the lower panels had 12 steps trigger rule activation (every step) and the measured tilt was 130±1.5 °. For each of the speeds, the measured tilts were limited by a threshold of 129 °. As the belt speed increased, the leg was extended farther backwards (increased tilt) during the stance phase and increased the chance of transitioning to swing due to triggering from predicted sensory feedback.

Rule Triggering Performance

Rule triggering performance (based on a real time prediction) was compared to the hypothetical triggering from the recorded external sensor signal for each step (table 4-3). A rule triggering was successful when both the prediction and the recorded external sensory signal crossed the threshold within the activation window or neither crossed. When both signals crossed, the time delay was measured between the crossing of the prediction and the recorded sensor signal. A false positive was reported if the prediction crossed the threshold but the recorded sensor signal did not. Conversely, false negatives were reported when the recorded sensory signal crossed the threshold but the prediction did not. Tilt and gyroscope prediction models were successful for a similar proportion of steps (59.7% and 60.9%, respectively). When successful, the tilt sensor had the lowest timing error (29.9±56.3 ms). The gyroscope prediction model had the highest timing error (57.6±80 ms). The force prediction model produced the highest number of successful activations at 96.3% of the 108 total steps and the lowest average timing error with 15.3±65.6 ms. All sensors produced more false positives than false negatives.

Discussion

The main objective of the study was to develop an algorithm that could use real time sensory information from neurons within the DRG as feedback for a future neuroprosthetic walking device. Overall, the real time prediction accuracy was similar to original work from our lab using offline prediction algorithms (Weber *et al.*, 2007). Previously, only offline predictions of distance and tilt were calculated.

Artifact rejection

Stimulation artifacts from ISMS in close proximity to the recording site degrade prediction performance by masking action potentials on most recording channels. Previous offline artifact rejection methods were successfully applied in real time during ISMS stepping (Weber *et al.*, 2007). Recorded artifacts were rejected using two forms of software filters previously mentioned: synchronous events and amplitude rejection. Based on the waveforms of the recorded units and their ISI histograms, we determined that most artifacts were successfully blocked. There were no non-physiological looking waveforms and events did not arrive at intervals of the stimulation frequency.

Sensor Type

Overall, the best predicted sensor model for the closed loop unilateral stepping approach used in this study was tilt. It was the only prediction that did not show a significant negative correlation with time (trial number), thus requiring less retraining. Also, video-based segment angle prediction (tilt) had less timing error than gyroscope-based foot angle prediction (gyroscope) during successful closed loop rule activations (while maintaining a similar percentage of successful activations). The main limitation to training a tilt prediction model would be the space required for a video recording system and its lack of portability. Potentially, a complementary filter combining an accelerometer and gyroscope to accurately predict leg tilt could be used to train a prediction model in a smaller space while still providing reasonable prediction accuracy (Lovse *et al.*, 2012).

Force prediction had the lowest accuracy, possibly due to the lack of force or pressure sensory afferents. We expected force prediction to utilize more of the pressure receptors in the foot. Instead, based on identified units, force prediction was probably being trained with a correlated limb position rather than cutaneous pressure and force. The force prediction provided the highest percentage of successful activations of the closed loop rule even though it had poor prediction accuracy. The hind limb angle threshold for activating the transition rule coincided with a large change in signal (the change from full load-bearing to almost nothing might have partially contributed), so it was easy to cross the threshold. Other signals had smaller variations at the point of threshold crossing, which made it more difficult to correctly trigger the rule.

Time Duration

The only sensor prediction that did not show a significant degradation over time was tilt. Retraining the prediction model was required throughout the experiment to maintain the quality of prediction of all other prediction models. Highly specific receptor fields of units can also result in changes in firing rates caused by variability in stepping. For instance, if force is applied to the lateral border of the paw during stance and then, due to paw placement, force is applied more medially, a lateral pressure sensory afferent may not be activated. It is possible that sometime after eight trials the prediction decay would reach a study plateau, but this was not tested.

Chronic implantation of Utah arrays should reduce the variability of the recorded units and decrease the frequency of retraining. Previously, chronic recordings from neurons within the DRG were consistent for up to 21 days (Weber *et al.*, 2006, 2007). In the present study, units were sorted using manually set time-voltage windows. There are a few approaches for sorting spikes online, most of which are based on clustering (Franke *et al.*, 2010). Changes in distance between electrodes and neurons causes neural signals to change their waveform over an experiment (Cham *et al.*, 2005). With online adaptive sorting, minor changes in waveform amplitude or shape would not affect unit sorting (Franke *et al.*, 2010). Continuous online training algorithms would eliminate the need for retraining. This would improve the feasibility of the technology for a neuroprosthetic device.

Number of Trained Units

The number of units required for best prediction was 10 for all sensory prediction models. This agreed with previous work by Stein et al., which suggested 6-8 units were optimal for prediction and also noted a decline in prediction accuracy if more, poorly correlated units were added (Stein *et al.*, 2004b). More (15) or less (5) units resulted in decreased prediction accuracy. Note that we used the best 10 correlated units out of 20 or 30 units recorded in a given experiment. Adding poorly correlated units likely adds noise to the prediction. Thus, it is still best to record a large number of units so that an adequate number of well correlated units is available for a given variable. Predictions from multiple units also may be more robust to changes in the firing characteristics of individual units over time and the appearance or disappearance of recorded units.

Stimulation Frequency

Predictions of distance and tilt during passive movements were better than during ISMS-driven stepping. Additionally, a reduction in stimulation frequency resulted in an increased prediction quality, but the trend was only significant for force. The greater the frequency or the number of stimulation channels, the more artifacts are recorded in the

DRG. Even though these artifacts are rejected in software, nerve action potentials occurring during the artifact are lost, which degrades the quality of the prediction. Using ISMS, bilateral walking could be restored using as few as four channels per side at 31 Hz but would likely require eight channels per side (Holinski *et al.*, 2012). The prediction algorithm was tested using similar stimulation conditions (in terms of number of stimulation pulses) that would be required for restoration of bilateral walking (8 channel, 62Hz condition). In this condition, if the duration of an artifact was about 1 ms long, over half of the recording time would be discarded. A neuroprosthetic device with DRG feedback should use the lowest stimulation frequency with the fewest number of stimulation channels possible to restore walking.

Closed loop Performance

The predictions activated an IF-THEN rule to transition from stance into the swing phase to reduce backward hyperextension in the presence of an external perturbation. As treadmill belt speed increased, the frequency of rule triggering increased as well, limiting backward hyperextension. All sensor predictions were capable of triggering a rule within the appropriate activation window during the walking cycle, with varying performance. Setting thresholds accurately is critical for proper operation of the rules and adaptive thresholding might provide better performance (Mazurek *et al.*, 2012). Interestingly, there appeared to be no correlation between prediction accuracy and the number of successful activations of the transition rule. This implies factors other than prediction quality, such as threshold location, rule design and sensor behaviour, may be important as well.

Issues and improvements

Prediction accuracy may be improved with advanced decoding models. Stein et al. have shown that prediction gains can be made by using a second-order model; however, higher order models show minimal further benefits (Stein *et al.*, 2004a). Other models have used individual representations of each sensory afferent resulting in an increased performance when decoding certain parameters such as limb length distance but were unable to improve prediction of limb tilt (Weber *et al.*, 2011).These models require more computational effort and predictions were made offline. With increasing computational power in small devices, more complex models could become feasible for real time prediction. Prediction accuracy also increased with two implanted arrays. The availability of larger amounts of neural information would be advantageous to any device relying on prediction.

Future directions

In the future, the algorithms should be tested with bilateral over ground walking. Although substantial ground reaction forces were produced during both walkway and treadmill stepping, better prediction accuracy might occur during self-propulsion. A chronic implantation might also increase the recording stability of the units over time if biocompatibility issues can be overcome. This would allow for less retraining and better prediction accuracy over a longer duration.

FIGURES

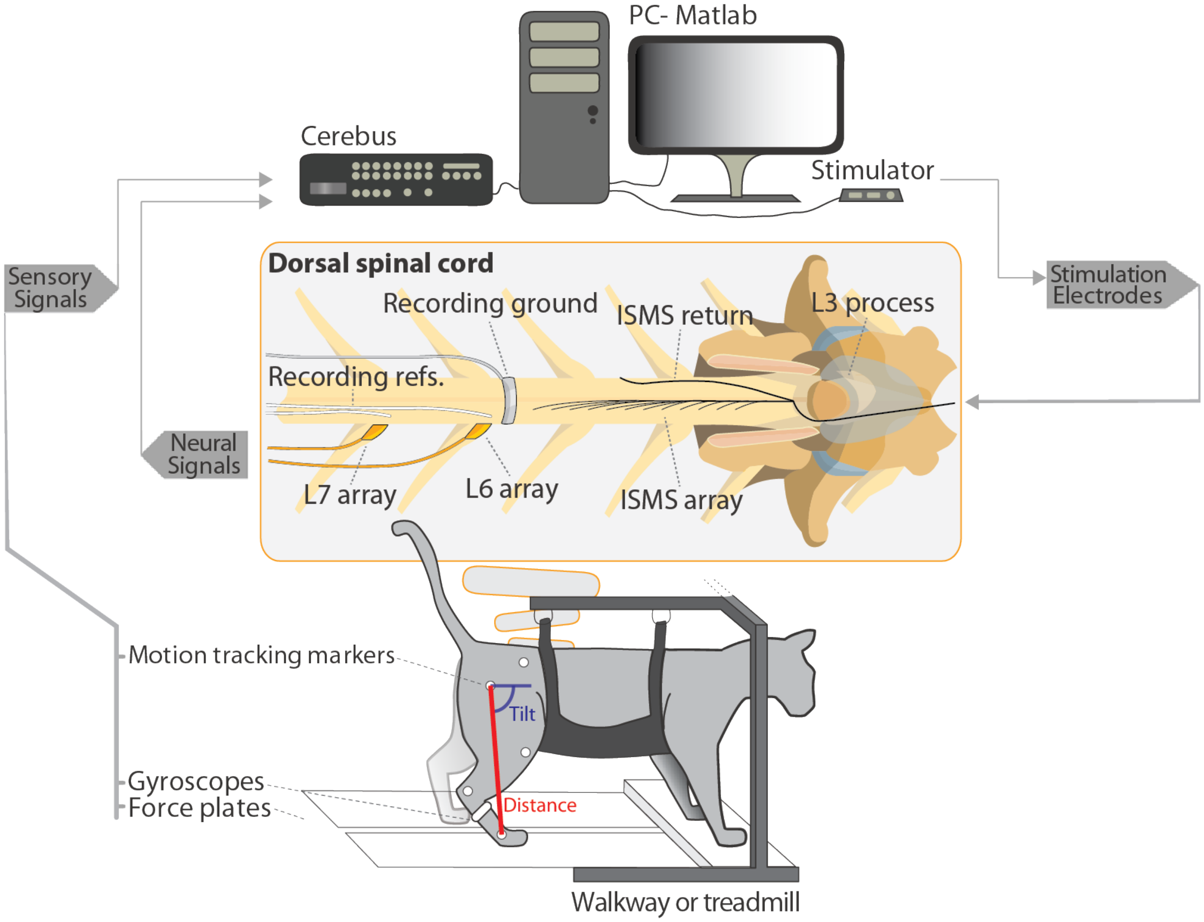

Figure 4-1: Experimental set up overview. Sensory signals recorded from video recordings of the hind limb and from gyroscopes and force plates are recorded by the Cerebus. Within the spinal cord, Utah arrays are implanted the dorsal root gangia and an ISMS array is implanted. Sensory recordings from the Utah arrays are sorted and recorded by the Cerebus. Training and real time prediction was done in Matlab from streaming recordings from the Cerebus. The Matlab algorithm controlled an ISMS stimulator to produce unilateral stepping-like movements. Distance and tilt parameters are shown overlaid on the hind limb.

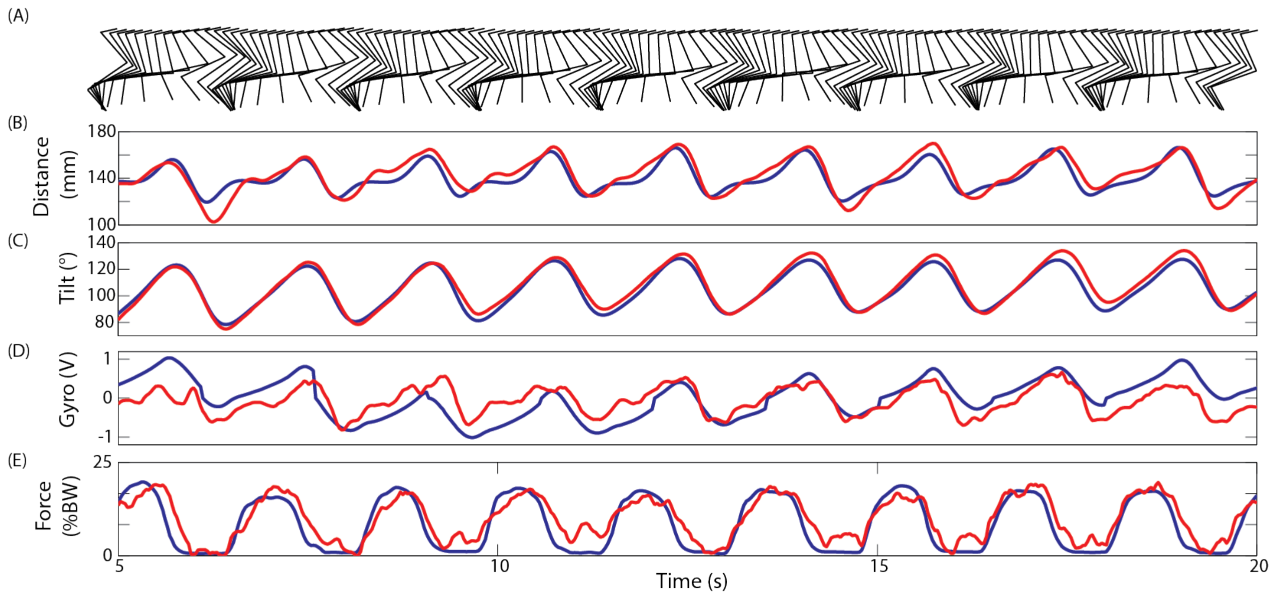

Figure 4-2: Single trial predictions during passive stepping-like movement. Recorded signals are in blue and real time predictions of the signal are in red. A) Motion capture of the right hind limb every 120 ms. B) Distance from the hip to the limb endpoint. C) Angle of the vector connecting hip to limb endpoint (measured clockwise from horizontal forward). D) Integrated gyroscope signal. E) Supportive force in % body weight. Predictions of external sensor signals are possible using recordings from the dorsal root ganglia.

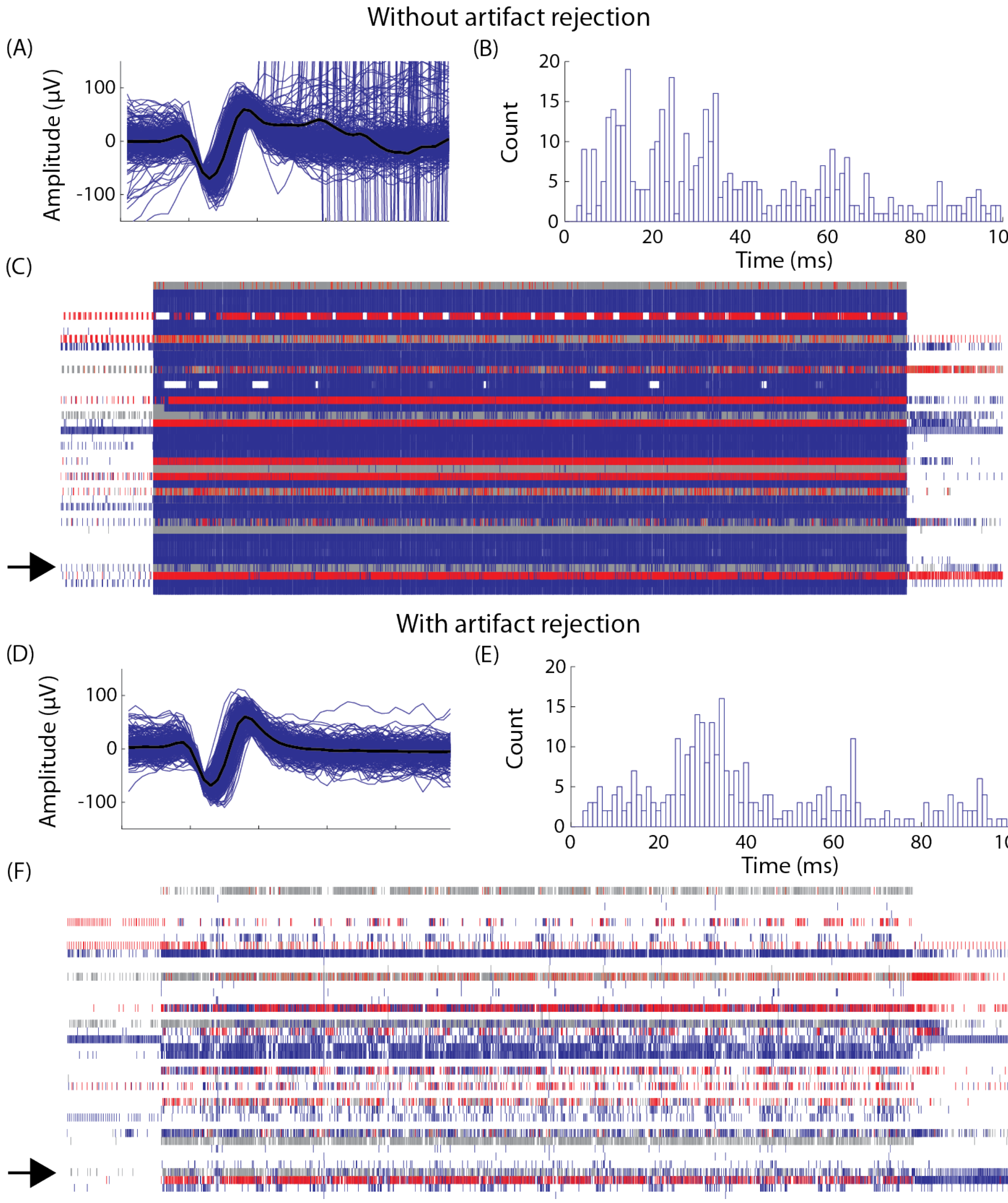

Figure 4-3: Single neuron recordings without and with artifact rejection. Without artifact rejection: A) Multiple waveforms identified as a single unit are overlaid with the average waveform shown in black. Large amplitude stimulation artifacts are also erroneously identified as the single unit. B) A histogram of interspike intervals (ISI) shows large numbers of events occurring at harmonics of the stimulation frequency (16ms). C) A raster plot of all channels with neural data. Each channel is plotted on a unique

horizontal line. Each small vertical line represents detection of an action potential on an electrode. Gray lines are unsorted units while colored lines represented signals accepted for processing. Due to stimulation artifacts so many events are accepted that it appears as a blue block. The channel of the single unit shown in A) and B) is highlighted with an arrow. D), E), and F) are similar except show the same single unit with artifact rejection. Artifacts have been successfully removed from the waveform, ISI histogram and the raster plot and are not accepted into the prediction algorithm.

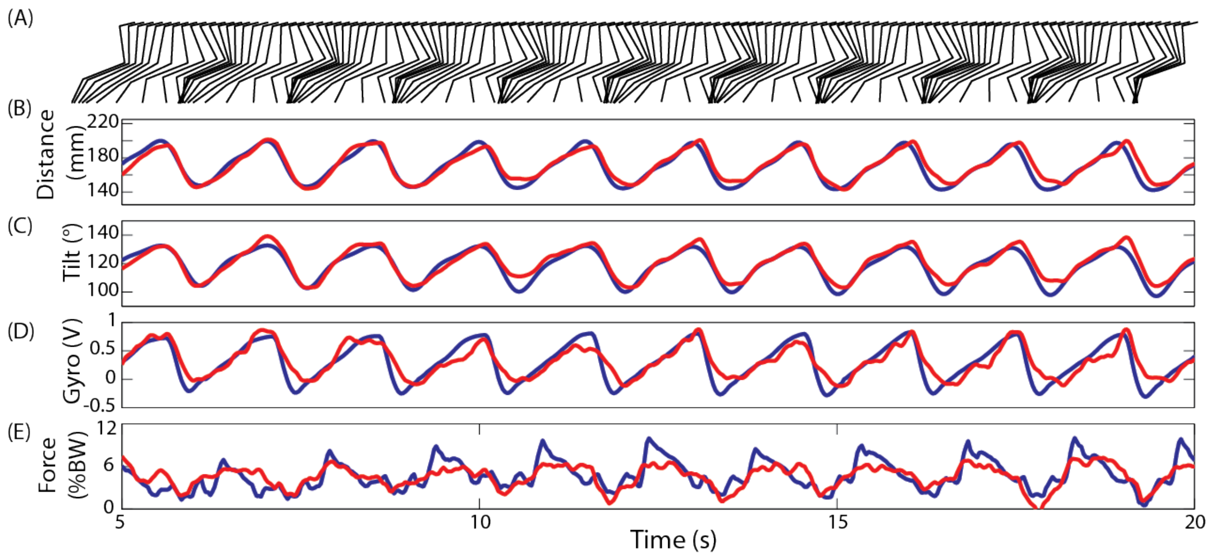

Figure 4-4: Single trial predictions during ISMS stepping. Recorded signals are in blue and real time predictions of the signal are in red (similar format to Figure 2). All external sensor signals can be predicted in the presence of ISMS.

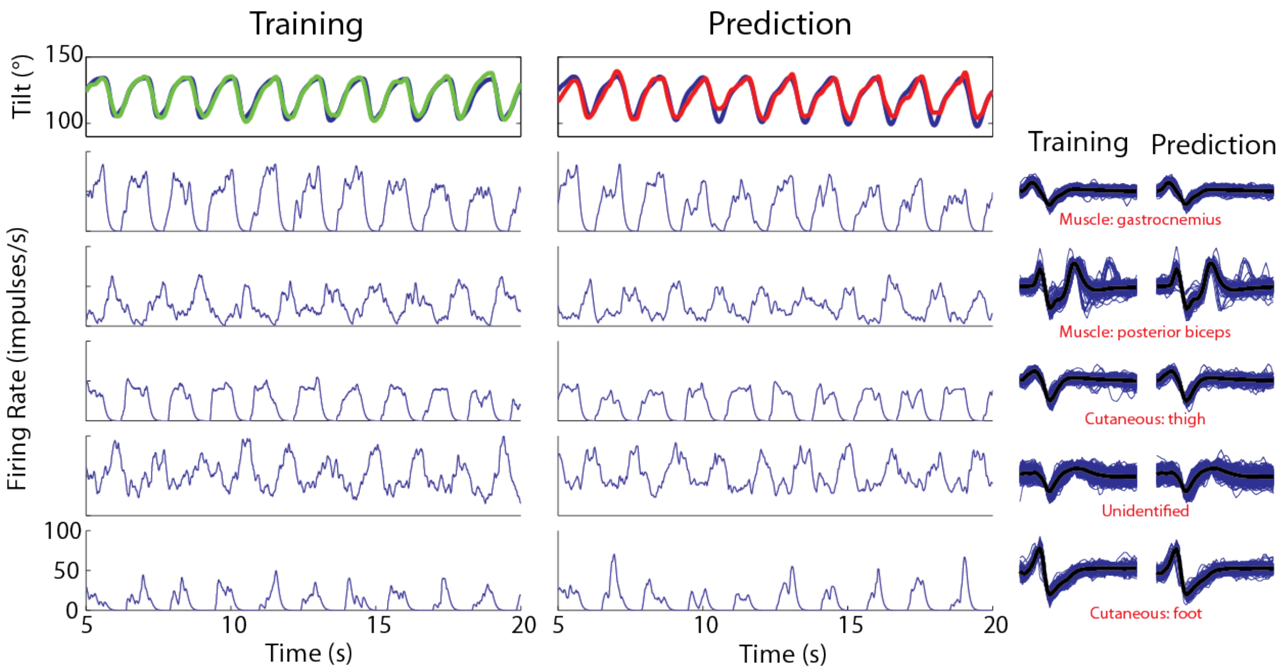

Figure 4-5: The individual single units used in a prediction of limb tilt. The first column shows the recorded tilt during the training trial (blue) and the training fit (green). Below are the firing rates of the five most correlated units used in the prediction. The 2nd column shows the recorded tilt (blue) and the real time prediction (red) from the same trial as Figure 4. Again, firing rates for the same units are shown for the prediction trial. The third and fourth columns show the waveforms during training and prediction of the selected units. Functionality of each unit is listed under the waveform and was determined during a separate identification process. From training to prediction waveforms and firing rates are stable.

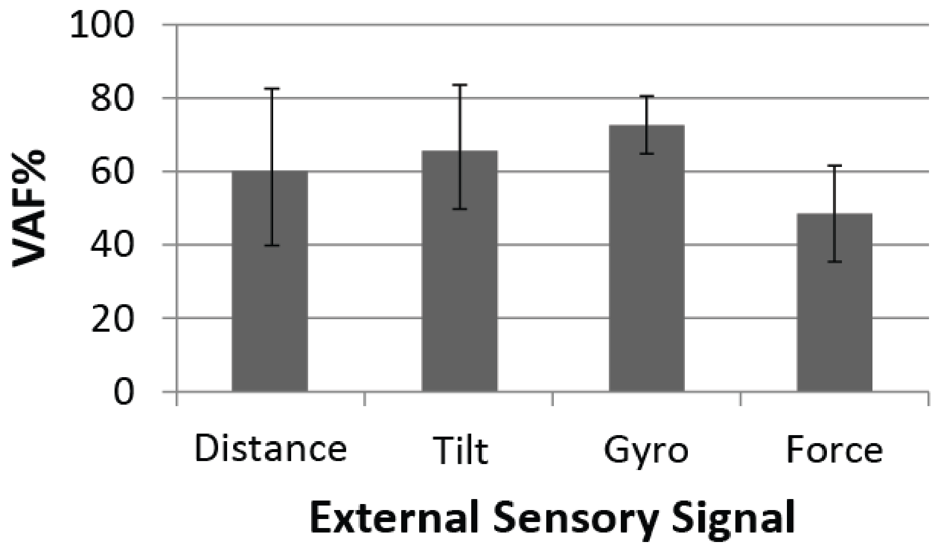

Figure 4-6: The average VAF% of the prediction of each external sensor signal during open loop trials. Bars represent the standard deviation of the predictions. N: distance, tilt=47; gyro, force=34.

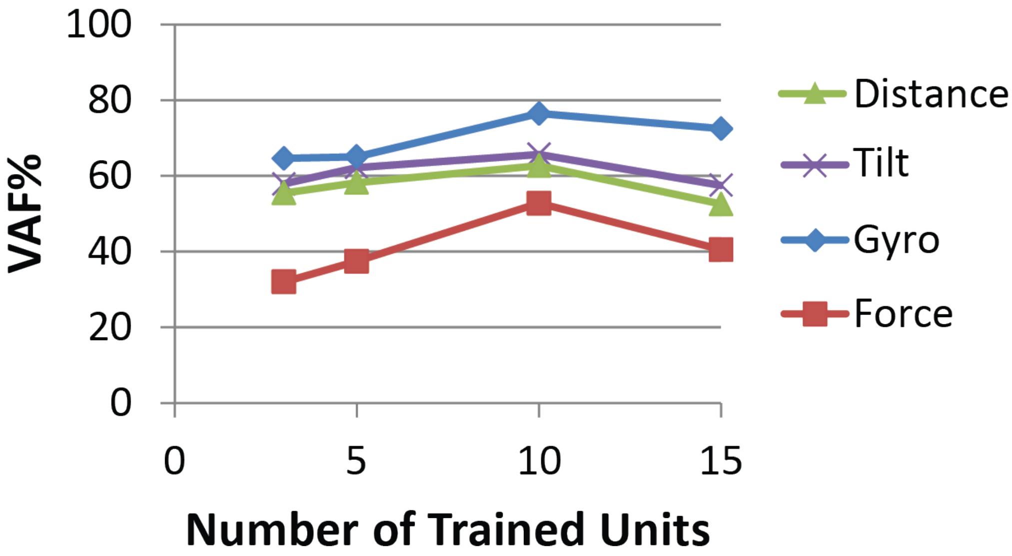

Figure 4-7: The prediction quality (VAF%) of each external sensor signal using various numbers of units. Each sensor signal is shown in a different color using 3, 5, 10 and 15 units for prediction.

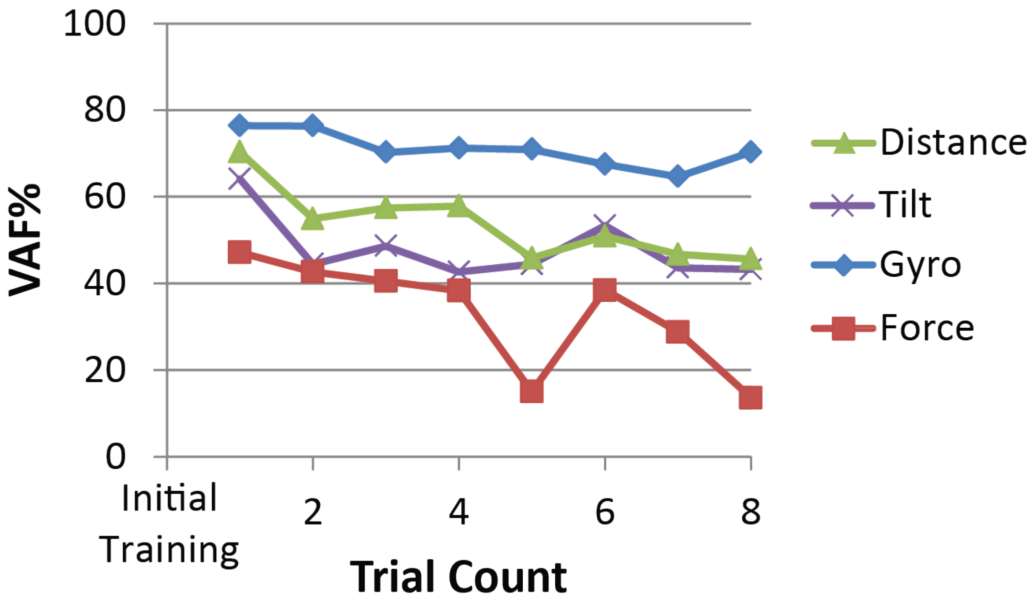

Figure 4-8: The prediction quality (VAF%) of each external sensor signal over time after initial training. Each sensor signal is shown in a different color from 1 to 8 trials after training.

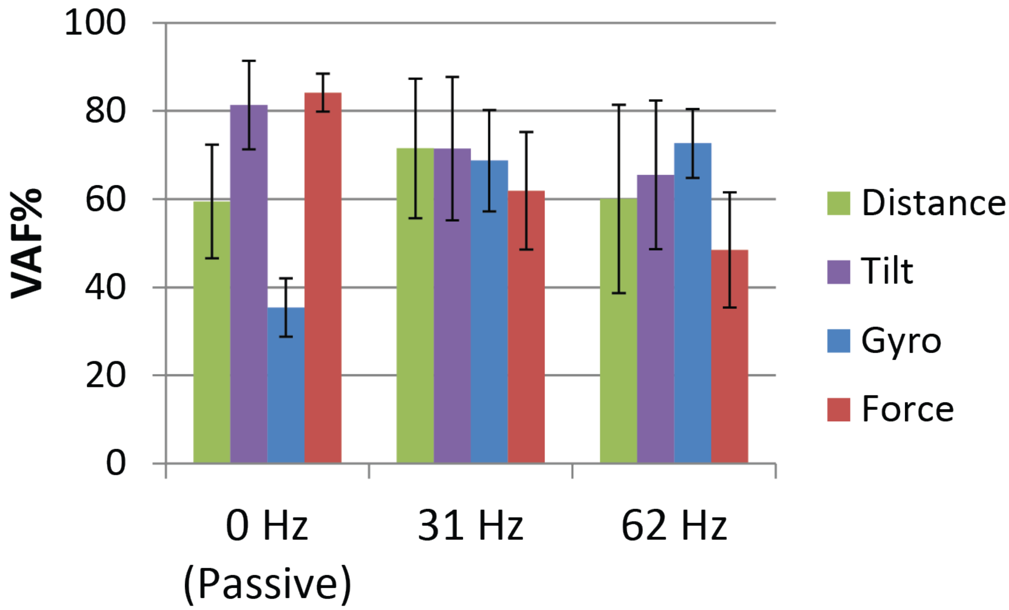

Figure 4-9: The effect of stimulation frequency on prediction quality (VAF%) for each sensory signal during open loop trials. Bars represent the standard deviation of the predictions. 0 Hz is passive movement of the hind limb, 31 Hz is the minimum stimulation frequency tested and 62 Hz is the highest stimulation frequency. Passive distance and tilt: N=16, gyro: 7, force: 11; 31 Hz distance and tilt: N=13, gyro and force= 15; 62 Hz distance and tilt: N=47, gyro and force= 34.

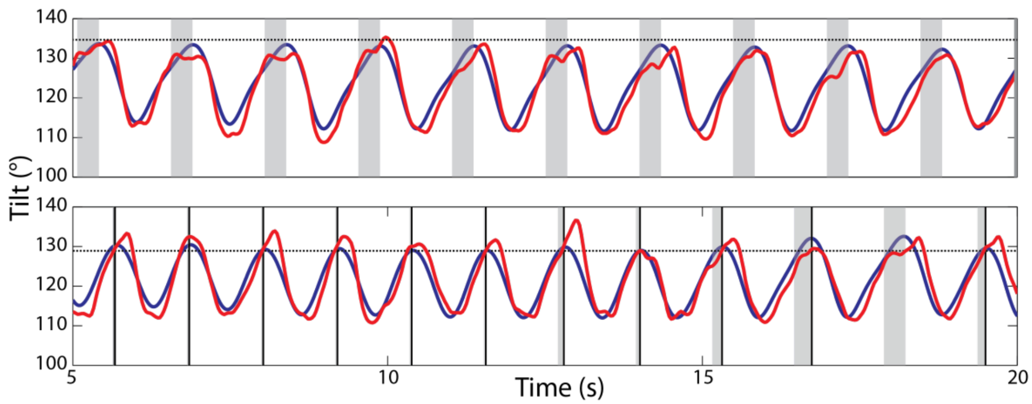

Figure 4-10: Activation based on predicted sensory input of a closed loop rule to limit backward hyperextension. Recorded hind limb tilt is shown in blue and the real time predicted tilt is shown in red. The activation threshold of the rule is shown with a black horizontal dashed line. Shaded gray vertical regions represent times within the step cycle when the rule can activate if the threshold is exceeded (activation windows). For the top panel, the prediction (red) did not exceed the threshold during the activation windows. The bottom panel shows that a lower threshold causes many activations of the rule. The solid vertical line marks a rule activation and subsequent state transition to swing.

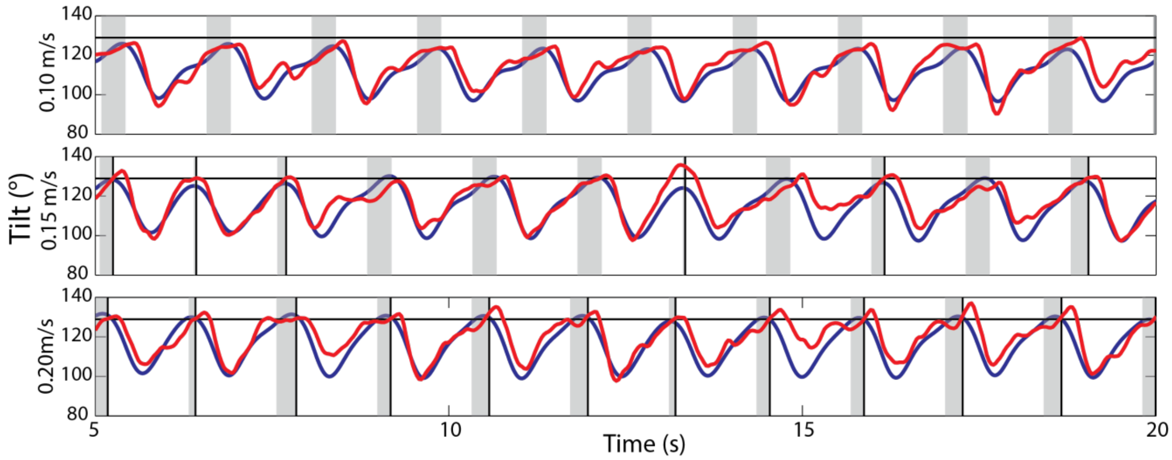

Figure 4-11: The effect of treadmill speed on backward hyperextension rule activation. Each panel is in a similar format as Figure 10. Each panel shows a trial at a different belt speed: 0.1 m/s (slow), 0.15 m/s (medium), 0.20 m/s (fast). The faster the belt speed the more the limb hyperextends and the more likely the rule will activate and begin the swing phase. Note that the threshold level was constant between belt speeds.

	Cat A		Cat B		Cat C		Cat D		Cat E	
Sex	M		M		M		F		M	
Weight (kg)	5.7		5.0		3.6		4.8		5.0	
Surface	W		W		W		T		T	
Trials										
OL	9		10		11		22		20	
CL	4		7		6		20		34	
Kinematics										
Peak Distance (mm)	191	± 4.1	206	± 9.0	205	± 7.5	224	± 2.9	235	± 3.9
Peak Tilt (°)	110	± 2.4	118	± 5.3	118	± 4.3	129	± 1.7	134	± 2.2
Hip Range (°)	19	± 1.2	29	± 2.5	26	± 5.5	21	± 2.3	40	± 5.5
Knee Range (°)	12	± 0.9	26	± 2.8	18	± 6.8	22	± 3.3	47	± 3.9
Ankle Range (°)	32	± 5.5	16	± 2.9	19	± 6.1	59	± 4.2	77	± 11.1
Kinetics										
Peak Force (%BW)	8.2	± 2.5	7.9	± 1.4	6.0	± 1.2	6.4	± 1.8	8.9	± 1.5

Table 4-1: Summary of experimental parameters and average stepping parameters for each cat. M=male, F=female; W= walkway, T=treadmill. Kinematic ranges and kinetics are shown as: *mean* ± *standard deviation*.

	DRG	Units identified		Predictor Units			
			Count	Distance	Tilt	Gyro	Force
Cat A	L7	*Muscle*	7	1.3	1.0		
		Cutaneous	10	1.0	0.8		
		Unclassified	9	1.3	2.5		
		Unknown		6.5	5.75		
		Total	26	10	10		
Cat B	L7	*Muscle*	9	2.6	2.9		
		Cutaneous	8	2.1	2.2		
		Unclassified	0	0.0	0.0		
		Unknown		5.3	4.9		
		Total	17	10	10		
Cat C	L6, L7	*Muscle*	28	5.7	0.8		
		Cutaneous	15	0.4	0.4		
		Unclassified	5	0.5	0.2		
		Unknown		3.4	8.6		
		Total	48	10	10		
Cat D	L6	*Muscle*	15	4.3	4.8	4.4	4.2
		Cutaneous	20	1.7	3.5	2.2	2.1
		Unclassified	2	0.5	0.1	0.0	0.0
		Unknown		3.4	1.5	3.4	3.7
		Total	37	10	10	10	10
Cat E	L6, L7	*Muscle*	17	5.3	7.3	0.5	6.6
		Cutaneous	11	1.4	1.3	0.7	1.2
		Unclassified	2	0.0	0.0	0.0	0.0
		Unknown		3.3	1.3	8.8	2.2
		Total	30	10	10	10	10

Table 4-2: Recorded sensory afferents used in predictions. Cats were implanted with either one or two recording arrays in dorsal root ganglia (DRG) locations L6 and/or L7. Count shows the total number of each unit type identified and total of all units identified per cat. Predictor units show the average number of each sensory afferent type used by each sensor. Unclassified units were units found during identification but their function could not be ascertained. Unknown units were not found during identification. A total of 10 units were used for each prediction.

	Trials	Steps	Successful	%	Jitter (ms)	FP	FP%	FN	FN%
Tilt	43	464	277	59.7	29.9 ± 56.3	141	30.4	46	9.9
Gyroscope	11	115	70	60.9	57.6 ± 80.0	24	20.9	21	18.3
Force	9	108	104	96.3	15.3 ± 65.6	3	2.8	1	0.9

Table 3: Rule triggering performance for each external sensor signal. Total number of closed loop trials and steps are shown. Number and percentage of successful steps are shown for each sensor. Jitter represents the *mean* ± *standard deviation* of time delay between the recorded and predicted signal threshold crossings. FP=false positive (prediction crossed the threshold but recorded signal did not), FN= false negative (recorded signal crossed the threshold but prediction did not).

References

Aoyagi Y, Stein R B, Branner A, Pearson K G and Normann R A 2003 Capabilities of a penetrating microelectrode array for recording single units in dorsal root ganglia of the cat *J Neurosci Methods* **128** 9-20

Bamford J A, Putman C T and Mushahwar V K 2005 Intraspinal microstimulation preferentially recruits fatigue-resistant muscle fibres and generates gradual force in rat *J Physiol* **569** 873-84

Bansal A K, Truccolo W, Vargas-Irwin C E and Donoghue J P 2012 Decoding 3D reach and grasp from hybrid signals in motor and premotor cortices: spikes, multiunit activity, and local field potentials *J Neurophysiol* **107** 1337-55

Bauman M J, Bruns T M, Wagenaar J B, Gaunt R A and Weber D J 2011 Online feedback control of functional electrical stimulation using dorsal root ganglia recordings *Conf Proc IEEE Eng Med Biol Soc* **2011** 7246-9

Branner A and Normann R A 2000 A multielectrode array for intrafascicular recording and stimulation in sciatic nerve of cats *Brain Res Bull* **51** 293-306

Brown-Triolo D L, Roach M J, Nelson K and Triolo R J 2002 Consumer perspectives on mobility: implications for neuroprosthesis design *J Rehabil Res Dev* **39** 659-69

Bruns T M, Gaunt R A and Weber D J 2011 Estimating bladder pressure from sacral dorsal root ganglia recordings *Conf Proc IEEE Eng Med Biol Soc* **2011** 4239-42

Burridge J H, Haugland M, Larsen B, Pickering R M, Svaneborg N, Iversen H K, Christensen P B, Haase J, Brennum J and Sinkjaer T 2007 Phase II trial to evaluate the

ActiGait implanted drop-foot stimulator in established hemiplegia *J Rehabil Med* **39** 212-8

Carmena J M, Lebedev M A, Henriquez C S and Nicolelis M A 2005 Stable ensemble performance with single-neuron variability during reaching movements in primates *J Neurosci* **25** 10712-6

Cham J G, Branchaud E A, Nenadic Z, Greger B, Andersen R A and Burdick J W 2005 Semi-chronic motorized microdrive and control algorithm for autonomously isolating and maintaining optimal extracellular action potentials *J Neurophysiol* **93** 570-9

Clark G A, Ledbetter N M, Warren D J and Harrison R R 2011 Recording sensory and motor information from peripheral nerves with Utah Slanted Electrode Arrays *Conf Proc IEEE Eng Med Biol Soc* **2011** 4641-4

Cordo P J, Flores-Vieira C, Verschueren S M, Inglis J T and Gurfinkel V 2002 Position sensitivity of human muscle spindles: single afferent and population representations *J Neurophysiol* **87** 1186-95

Cunningham J P, Gilja V, Ryu S I and Shenoy K V 2009 Methods for estimating neural firing rates, and their application to brain-machine interfaces *Neural Netw* **22** 1235-46

Dai R, Stein R B, Andrews B J, James K B and Wieler M 1996 Application of tilt sensors in functional electrical stimulation *IEEE Trans Rehabil Eng* **4** 63-72

Franke F, Natora M, Boucsein C, Munk M H and Obermayer K 2010 An online spike detection and spike classification algorithm capable of instantaneous resolution of overlapping spikes *J Comput Neurosci* **29** 127-48

Graupe D and Kohn K H 1998 Functional neuromuscular stimulator for short-distance ambulation by certain thoracic-level spinal-cord-injured paraplegics *Surg Neurol* **50** 202-7

Graupe D, Kohn K H, Kralj A and Basseas S 1983 Patient controlled electrical stimulation via EMG signature discrimination for providing certain paraplegics with primitive walking functions *J Biomed Eng* **5** 220-6

Guevremont L, Norton J A and Mushahwar V K 2007 Physiologically based controller for generating overground locomotion using functional electrical stimulation *J Neurophysiol* **97** 2499-510

Holinski B, KA M, DG E, RB S, R E-C and VK M 2012 Intraspinal Microstimulation for Restoring Walking *Conf Proc IFESS 2012, Banff, AB, Canada*

Lau B, Guevremont L and Mushahwar V K 2007 Strategies for generating prolonged functional standing using intramuscular stimulation or intraspinal microstimulation *IEEE Trans Neural Syst Rehabil Eng* **15** 273-85

Li Z, O'Doherty J E, Hanson T L, Lebedev M A, Henriquez C S and Nicolelis M A 2009 Unscented Kalman filter for brain-machine interfaces *PLoS One* **4** e6243

Li Z, O'Doherty J E, Lebedev M A and Nicolelis M A 2011 Adaptive decoding for brain-machine interfaces through Bayesian parameter updates *Neural Comput* **23** 3162-204

Liberson W T, Holmquest H J, Scot D and Dow M 1961 Functional electrotherapy: stimulation of the peroneal nerve synchronized with the swing phase of the gait of hemiplegic patients *Arch Phys Med Rehabil* **42** 101-5

Loeb G E, Bak M J and Duysens J 1977 Long-term unit recording from somatosensory neurons in the spinal ganglia of the freely walking cat *Science* **197** 1192-4

Loeb G E and Duysens J 1979 Activity patterns in individual hindlimb primary and secondary muscle spindle afferents during normal movements in unrestrained cats *J Neurophysiol* **42** 420-40

Lovse L, Bobet J, Roy F D, Rolf R, Mushahwar V K and Stein R B 2012 External sensors for detecting the activation and deactivation times of the major muscles used in walking *IEEE Trans Neural Syst Rehabil Eng* **20** 488-98

Mazurek K A, Holinski B J, Everaert D G, Stein R B, Etienne-Cummings R and Mushahwar V K 2012 Feed forward and feedback control for over-ground locomotion in anaesthetized cats *J Neural Eng* **9** 026003

McCrea D A and Rybak I A 2008 Organization of mammalian locomotor rhythm and pattern generation *Brain Res Rev* **57** 134-46

Mehring C, Rickert J, Vaadia E, Cardosa de Oliveira S, Aertsen A and Rotter S 2003 Inference of hand movements from local field potentials in monkey motor cortex *Nat Neurosci* **6** 1253-4

Mushahwar V K, Gillard D M, Gauthier M J and Prochazka A 2002 Intraspinal micro stimulation generates locomotor-like and feedback-controlled movements *IEEE Trans Neural Syst Rehabil Eng* **10** 68-81

Mushahwar V K and Horch K W 1997 Proposed specifications for a lumbar spinal cord electrode array for control of lower extremities in paraplegia *IEEE Trans Rehabil Eng* **5** 237-43

Mushahwar V K and Horch K W 1998 Selective activation and graded recruitment of functional muscle groups through spinal cord stimulation *Ann N Y Acad Sci* **860** 531-5

Mushahwar V K and Horch K W 2000 Selective activation of muscle groups in the feline hindlimb through electrical microstimulation of the ventral lumbo-sacral spinal cord *IEEE transactions on rehabilitation engineering : a publication of the IEEE Engineering in Medicine and Biology Society* **8** 11-21

Nordhausen C T, Maynard E M and Normann R A 1996 Single unit recording capabilities of a 100 microelectrode array *Brain Res* **726** 129-40

Patil P G, Carmena J M, Nicolelis M A and Turner D A 2004 Ensemble recordings of human subcortical neurons as a source of motor control signals for a brain-machine interface *Neurosurgery* **55** 27-35; discussion -8

Pearson K G 1995 Proprioceptive regulation of locomotion *Curr Opin Neurobiol* **5** 786-91

Prochazka A and Gorassini M 1998 Ensemble firing of muscle afferents recorded during normal locomotion in cats *J Physiol* **507 (Pt 1)** 293-304

Prochazka A, Gritsenko V and Yakovenko S 2002a Sensory control of locomotion: reflexes versus higher-level control *Adv Exp Med Biol* **508** 357-67

Prochazka A, Mushahwar V and Yakovenko S 2002b Activation and coordination of spinal motoneuron pools after spinal cord injury *Prog Brain Res* **137** 109-24

Prochazka A, Westerman R A and Ziccone S P 1976 Discharges of single hindlimb afferents in the freely moving cat *J Neurophysiol* **39** 1090-104

Ragnarsson K T 2008 Functional electrical stimulation after spinal cord injury: current use, therapeutic effects and future directions *Spinal Cord* **46** 255-74

Rossignol S, Dubuc R and Gossard J P 2006 Dynamic sensorimotor interactions in locomotion *Physiol Rev* **86** 89-154

Saigal R, Renzi C and Mushahwar V K 2004 Intraspinal microstimulation generates functional movements after spinal-cord injury *IEEE Trans Neural Syst Rehabil Eng* **12** 430-40

Stark E and Abeles M 2007 Predicting movement from multiunit activity *J Neurosci* **27** 8387-94

Stein R B, Aoyagi Y, Weber D J, Shoham S and Normann R A 2004a Encoding mechanisms for sensory neurons studied with a multielectrode array in the cat dorsal root ganglion *Can J Physiol Pharmacol* **82** 757-68

Stein R B, Hayday F, Chong S, Thompson A K, Rolf R, James K B and Bell G 2005 Speed and efficiency in walking and wheeling with novel stimulation and bracing systems after spinal cord injury: a case study *Neuromodulation* **8** 264-71

Stein R B, Weber D J, Aoyagi Y, Prochazka A, Wagenaar J B, Shoham S and Normann R A 2004b Coding of position by simultaneously recorded sensory neurones in the cat dorsal root ganglion *J Physiol* **560** 883-96

Taylor P N, Burridge J H, Dunkerley A L, Wood D E, Norton J A, Singleton C and Swain I D 1999 Clinical use of the Odstock dropped foot stimulator: its effect on the speed and effort of walking *Arch Phys Med Rehabil* **80** 1577-83

Thrasher T A and Popovic M R 2008 Functional electrical stimulation of walking: function, exercise and rehabilitation *Ann Readapt Med Phys* **51** 452-60

Vanderhorst V G and Holstege G 1997 Organization of lumbosacral motoneuronal cell groups innervating hindlimb, pelvic floor, and axial muscles in the cat *J Comp Neurol* **382** 46-76

Velliste M, Perel S, Spalding M C, Whitford A S and Schwartz A B 2008 Cortical control of a prosthetic arm for self-feeding *Nature* **453** 1098-101

Weber D J, London B M, Hokanson J A, Ayers C A, Gaunt R A, Torres R R, Zaaimi B and Miller L E 2011 Limb-state information encoded by peripheral and central somatosensory neurons: implications for an afferent interface *IEEE Trans Neural Syst Rehabil Eng* **19** 501-13

Weber D J, Stein R B, Everaert D G and Prochazka A 2006 Decoding sensory feedback from firing rates of afferent ensembles recorded in cat dorsal root ganglia in normal locomotion *IEEE Trans Neural Syst Rehabil Eng* **14** 240-3

Weber D J, Stein R B, Everaert D G and Prochazka A 2007 Limb-state feedback from ensembles of simultaneously recorded dorsal root ganglion neurons *J Neural Eng* **4** S168-80

Webster J G 1992 Artificial sensors suitable for closed-loop control of FNS *Neural Prostheses: Replacing Motor Function After Disease or Disability* ed R B Stein, P H Peckham and D Popovic (New York: Oxford University Press)

Widerstrom-Noga E G, Felipe-Cuervo E, Broton J G, Duncan R C and Yezierski R P 1999 Perceived difficulty in dealing with consequences of spinal cord injury *Arch Phys Med Rehabil* **80** 580-6

Yakovenko S 2011 A hierarchical perspective on rhythm generation for locomotor control *Prog Brain Res* **188** 151-66

Yakovenko S, Gritsenko V and Prochazka A 2004 Contribution of stretch reflexes to locomotor control: a modeling study *Biol Cybern* **90** 146-55

Yakovenko S, Mushahwar V, VanderHorst V, Holstege G and Prochazka A 2002 Spatiotemporal activation of lumbosacral motoneurons in the locomotor step cycle *J Neurophysiol* **87** 1542-53

Chapter 5: General Discussion

The overall goal of my project was to restore walking in people with paraplegia. Specifically, we developed a proof-of-principle for a walking neuroprosthesis comprising a controller, effectors, and sensors, and tested it in an intact anaesthetized cat. In each of three projects, a component of the neuroprosthesis was developed: the controller, intraspinal microstimulation (ISMS) (effectors), and natural sensory feedback (sensors). Each of the three projects incorporated a new biologically inspired solution into the device. First, the controller was provided with a flexible software foundation to produce feedback-controlled overground walking. Next, ISMS was incorporated into the controller to produce fatigue-resistant overground walking. Finally, feedback from natural sensors controlled ISMS elicited stepping-like movements in real time. Each project resulted in a novel accomplishment and produced a deliverable that successfully worked in conjunction with previously developed components toward a neuroprosthetic system to restore walking.

Hybrid-CPG Controller

The first project developed a controller (named: hybrid-CPG controller) that utilized a combination of intrinsic timing and sensory feedback to produce overground walking. Initial work by Guevremont et al. showed that a hybrid controller had the potential to produce overground walking more effectively than either intrinsic timing or sensory feedback alone [1]. The hybrid-CPG controller successfully produced propulsive overground walking for five cats using intramuscular stimulation and sensory feedback from external sensors. The hybrid-CPG controller also produced significantly more successful steps than intrinsic timing alone produced. This study created an adaptable controller to be used with future studies.

The hybrid-CPG controller performance was limited by the accuracy of sensory input. The integrated gyroscope signal was the best signal to limit backward excursion. However, due to the artificial resetting to eliminate drift errors, the signal could not be used to limit forward excursion as well. With better sensors such as complementary filters, the performance of feedback rules could be further improved [2]. The control was also restricted to the sagittal plane and, therefore, did not account for balance or direction changes. However, three dimensional controls may not be required to create a practical walking device when the device is used in conjunction with a balancing aid (eg cane, walker).

Intraspinal Microstimulation

The second stage of the project replaced intramuscular stimulation with intraspinal microstimulation (ISMS). This was the first demonstration of ISMS-produced overground walking-like movements. The hybrid-CPG controller was adapted to control a custom ISMS stimulator in real time. ISMS produced fatigue resistant “walking” for over 800 m in two acutely implanted cats with the potential to “walk” farther. A future ISMS-based device could be implanted within a very small region of the spinal cord to produce bilateral walking (co-ordinated movements of both hindlimbs producing propulsion)[3]. This project demonstrated that ISMS could produce overground walking-like movements in a neuroprothesis.

Currently, the functional improvement ISMS produces might not offset the limitations of the technique when eventually pursued for human implantation. The array implantation is tedious and nonstandardized. It is likely that in humans, the locations of the motor pools will not be known with any greater confidence than they are known in the cat. Probably, each electrode would have to be inserted individually since the interelectrode geometries would not be known *a priori*. Implantation consists of inserting single electrodes in the spinal cord and stimulating multiple locations within the spinal cord to form an initial estimation of motor pool locations (known to be ~ 1mm in diameter; from mapping studies) [4]. This increases surgery duration and might not be acceptable for widespread adoption by neurosurgeons. To streamline implantation, a referencing system should correlate implantation locations with respect to the gross anatomy of the subject. Also, the electrodes must have adjustable lengths at the time of the implantation to target the motor pools while not protruding from the dorsal side of the spinal cord. A possible solution might be to create multiple lengths of wireless "thumbtack electrodes" in which the electronics are contained within the base of the electrodes. Each electrode could provide stimulation and be uniquely addressed through an external coil covering the lumbar-sacral region. The design of future arrays should be standardized to stringent specifications. Prompt development of an effective array design will ensure that future exploratory work in humans will be not be delayed by regulatory red tape.

Natural Sensory Feedback

The final stage replaced the external sensors with recordings from the dorsal root ganglion (DRG) to control stepping-like movements in real time. This was the first example of DRG feedback used in conjunction with ISMS. We produced accurate predictions of hindlimb proprioception even in the presence of ISMS artifacts. Sensory predictions were fully incorporated into the existing hybrid-CPG controller to activate feedback rules. Specifically, real time feedback limited the backward hyperextension of the limb in response to a variety of walking conditions. The rule performed best when predictions of limb tilt was used. The incorporation of natural sensory feedback was the final step in creating a fully implantable neuroprosthesis (although not yet implemented bilaterally).

Improved external sensing in the future might make DRG implantation less attractive. Currently, there are major difficulties in obtaining the stable long term DRG recordings that would be vital for clinical implementation [5]. While other research groups are improving the biocompatibility and stability of the recordings, the feedback algorithm should be implemented bilaterally for overground walking [6]. That will ensure that when the biocompatibility problems are solved, natural sensory feedback will be much closer to implementation in a neuroprothesis.

Conclusion

The foundation of a novel neuroprosthesis to restore some walking function after spinal cord injury was created and proved in principle in this work. It would probably be ready for clinical applications sometime between the powered exoskeletons now entering the market and biological regeneration which appears to be decades away. The FES-based device would offer more health benefits than a powered exoskeleton and could improve walking ranges. FES-based devices might use technologies adapted from powered exoskeletons such as partial DC motor augmentation or external sensors. A passive orthosis will probably still be required even with FES-based systems to provide body weight support while standing and limit the degrees of freedom. If possible, walking devices should be designed to allow at least one hand free of crutches or other supportive hardware for grasping objects. It is likely that the implantable proof-of-principle developed in this thesis will not be implemented in its entirety. Even if only certain aspects of these projects produce spin-off technologies and improve the lives of people with paraplegia, the research will be considered highly successful.

Future Directions

Certain aspects of this system would need to be improved to translate it into a marketable device. More accurate knowledge about limb location in space from better external sensors would improve closed loop control in the hybrid-CPG controller. The IF-THEN rule structure of the controller could remain the same. However, for increased safety, additional rules monitoring body weight loading would need to be added. Control software would have to be embedded into small integrated circuits that could be worn in a fanny-pack or smaller sized container.

An active orthosis should be used for balance and weight support during stance. Ankle joints should be actuated with DC motors so that only a single cane is required to maintain balance (freeing an arm for other tasks). The controller needs to be adapted to activate DC motors to augment ISMS. The motors could be smaller and more energy efficient when used in combination with FES. Further research on optimal ISMS frequencies, amplitudes, and pulse widths will produce strong forces safely. Also, mechanical stability of chronic ISMS array implantation will have to be improved (possibly through a novel array design).

Natural sensory recordings are not likely to replace external sensors in the near future due to limitations of the stability of chronic recordings. A realistic near-future walking neuroprosthesis is a stripped down exoskeleton used in conjunction with some basic ISMS activated movements to produce a hybrid-FES system with more secondary health benefits and longer walking ranges than anything currently on the market.

References

1. Guevremont, L., J.A. Norton, and V.K. Mushahwar, *Physiologically based controller for generating overground locomotion using functional electrical stimulation.* J Neurophysiol, 2007. **97**(3): p. 2499-510.

2. Lovse, L., et al., External sensors for detecting the activation and deactivation times of the major muscles used in walking. IEEE Trans Neural Syst Rehabil Eng, 2012. **20**(4): p. 488-98.

3. Mushahwar, V.K. and K.W. Horch, Proposed specifications for a lumbar spinal cord electrode array for control of lower extremities in paraplegia. IEEE Trans Rehabil Eng, 1997. **5**(3): p. 237-43.

4. Yakovenko, S., et al., Spatiotemporal activation of lumbosacral motoneurons in the locomotor step cycle. J Neurophysiol, 2002. **87**(3): p. 1542-53.

5. Weber, D.J., et al., Limb-state feedback from ensembles of simultaneously recorded dorsal root ganglion neurons. J Neural Eng, 2007. **4**(3): p. S168-80.

6. Spataro, L., et al., Dexamethasone treatment reduces astroglia responses to inserted neuroprosthetic devices in rat neocortex. Exp Neurol, 2005. **194**(2): p. 289-300.